

Hydrodynamics of a liquid-liquid-solid fluidized-bed bioreactor

Promotor:

Prof. dr. ir. J. Tramper
Hoogleraar Bioprocestechnologie

Co-promotoren:

Dr. ir. A. Rinzema
Universitair docent Sectie proceskunde

Dr. H.H. Beeftink
Universitair docent Sectie proceskunde

Promotiecommissie:

Prof. dr. ir. R.M. Boom (Wageningen Universiteit)
Dr. ir. A.J.B. van Boxtel (Wageningen Universiteit)
Dr. ir. S. Hartmans (DSM)
Prof. dr. ir. L.A.M. van der Wielen (Technische Universiteit Delft)

Erik van Zessen

Hydrodynamics of a liquid-liquid-solid fluidized-bed bioreactor

Proefschrift

ter verkrijging van de graad van doctor
op gezag van de rector magnificus
van Wageningen Universiteit,
prof. dr. ir. L. Speelman,
in het openbaar te verdedigen
op woensdag 1 oktober 2003
des namiddags te half twee in de Aula.

Erik van Zessen

Hydrodynamics of a liquid-liquid-solid fluidized-bed bioreactor

Thesis Wageningen University, The Netherlands, 2003 — with Dutch Summary

ISBN 90-5808-875-8

Contents

Chapter 1	Introduction	7
Chapter 2	Fluidized-bed and packed-bed characteristics of gel beads	15
Chapter 3	Dispersed-phase hold-up in a liquid-liquid extraction spray column	43
Chapter 4	Solid and droplet hold-ups in a liquid-liquid-solid 3-phase fluidized-bed	71
Chapter 5	Mixing of the continuous phase in a liquid-liquid-solid fluidized-bed bioreactor	99
Chapter 6	Design of liquid-liquid-solid fluidized-bed bioreactors	125
Chapter 7	General discussion	163
	References	175
	Summary	187
	Samenvatting	192
	Nawoord	197
	Curriculum vitae	199

1

Introduction

The potentials of biotechnology, the use of living organisms or parts thereof for the benefit of mankind in an economic manner, are enormous. In ancient days, water of doubtful quality was converted into beer and wine by micro-organisms to make it potable (Coutouly, 2001). For ages, micro-organisms have also been used for bread making (Coutouly, 2001). The use of micro-organisms to produce chemicals started more or less with the production of penicillin in 1943 (Coutouly, 2001). Nowadays, chemicals are produced by a number of different micro-organisms (Krab-Hüsken, 2002). Examples of commercial microbial production processes are the production of adipyl-7-ADCA at DSM (Bruggink, 2001), production of 6-hydroxy-S-nicotine at Lonza (Schmid *et al.*, 2001), or production of 5-cyanopentazamide at DuPont (Stieglitz *et al.*, 1996).

These chemicals are mostly produced in stirred tank reactors, in which the micro-organisms are suspended in an aqueous phase, in which the desired product is also present. After the biotransformation, the product is recovered from the mixture by subsequent downstream processing. Mostly, this operation strategy works satisfactorily.

This overall production strategy, i.e. batch biotransformation and subsequent downstream processing of the desired product, may result in a low overall production in some cases. These are summarized in Table 1. In case the substrate strongly inhibits the production rate, the substrate conversion within a practical reaction time is limited and consequently, a small amount of product is formed. Only after a prolonged period of time, most substrate will eventually be converted. Also for product-inhibited biotransformations the amount of product is limited: only after a long period of time, most substrate will be converted. Another type are those biotransformations that suffer from an unfavorable thermodynamic equilibrium. Substrate is only partially converted, and production halts due to the approach of thermodynamic equilibrium. A last type is a biotransformation in which the applied substrate has a low solubility; consequently, the amount of product is limited as well. For the first three types the overall production is low, unless the unconverted substrate is recycled after downstream.

So, if these biotransformations should be applied for industrial purposes, with a standard operation strategy and within a practical biotransformation time, their productivity should be enhanced. A possible solution to do so is direct removal of the product from the reaction environment (in case of product-inhibited or thermodynamically controlled biotransformations). In case of substrate-inhibited transformations (or low substrate solubility), a controlled supply of substrate to the

reaction phase can overcome the limited productivity. Supply can be arranged by using an organic solvent with dissolved substrate, or controlled supply from a solid carrier. A possible operation strategy for product-inhibited biotransformations is depicted in Figure 1. In this strategy, the product is transferred to a second phase to keep the product concentration in the reaction phase low. This phase is circulated over the extraction device. So, for the biotransformations summarized in Table 1, integration with either substrate supply or product removal may overcome the limited overall productivity. In the remaining part of this introduction we will focus on product-inhibited biotransformations. The same principles, however, can be directly used for the other types of biotransformations.

Table I. Overview of different classes of biotransformations for which productivity is limited using a standard production strategy (batch biotransformation and subsequent downstream processing), after Vermuë *et al.* (1995).

<i>Biotransformation characteristics</i>	<i>Problem</i>	<i>Possible solution</i>
Low solubility of substrate in water	Low product concentrations	Introduce a second phase (organic solvent) that acts as a large substrate reservoir
Substrate inhibition/toxicity	Low production rates	Keep aqueous substrate concentration low by its controlled supply
Product inhibition/toxicity	High product concentrations reduce the production rate	Keep aqueous product concentration low by its <i>in situ</i> removal into a second phase
Unfavorable thermodynamic equilibrium	Incomplete conversion due to the equilibrium	Postpone attainment of equilibrium by direct product removal into a second phase

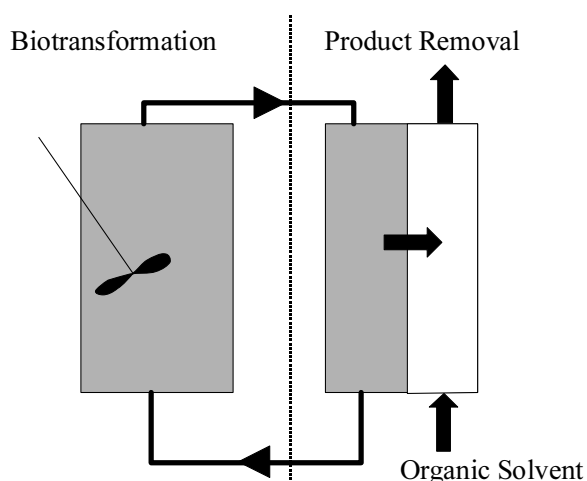


Figure 1. Operation strategy to overcome limited productivity.

True integration of the biotransformation and product removal can be realized by executing both processes in one vessel. Integration can also be achieved by physically separating the bioreactor and product removal device; the reaction mixture is continuously recirculated over the product removal device.

Various examples of this latter type of integration have been presented (e.g. Qureshi and Maddox, 1995). The product removal device can be a membrane; the reaction mixture is recirculated over the membrane, and at the other side of the membrane an organic solvent is used to collect the product (e.g. Hüsken *et al.*, 2002, who describe the production of 3-methylcatechol using octanol as the organic solvent). The product removal device can also be an adsorption column; the reaction mixture is recirculated over the column and the product is adsorbed onto a solid adsorption material. Boon *et al.* (2000), for example, described the production of oligosaccharides and their selective adsorption onto activated carbon.

From an operational point of view this recirculation type of integration may be advantageous, as both processes can be controlled and optimized independently. A disadvantage is the extra amount of equipment, and the relatively high recirculation rate between biotransformation vessel and separation device in order to keep product or substrate concentrations low. Clogging of the membrane or adsorption column by microbial cells can also be a serious problem. This latter problem can be solved by immobilizing the cells.

True integration of the biotransformation and product removal may overcome the disadvantages of dual vessel recirculation systems. Integration of both processes in a single vessel will result in a reduction in the amount of process equipment used.

Besides, transfer of product is not delayed, but takes place instantaneously. An obvious disadvantage is the higher degree of complexity, and fewer degrees of freedom for process control and optimization: the two processes have to be controlled and optimized as a single system.

Two examples of true integration of biotransformation and product removal could be:

1) The biocatalyst is immobilized in a solid carrier and another solid carrier is used for the adsorption of the reaction product. Both types of solid are fluidized in the same vessel, thus yielding a solid-solid-liquid 3-phase system. Such a design was studied extensively by Van der Wielen (1997). As a model reaction, they studied the deacylation of penicillin G.

2) A bioreactor and an extraction spray column can be integrated. Organic solvent droplets rise through the reaction mixture that contains immobilized biocatalyst particles. Such a solid-liquid-liquid 3-phase system was studied by Vermuë *et al.* (1995) for the degradation of tetratlin, and by Mateus *et al.* (1996) for the production of L-tryptophan from indole and L-serine. In both cases, the organic solvent was used as a reservoir from which an inhibitory substrate was supplied to the aqueous reaction phase. Both authors used a liquid-impelled loop reactor (Figure 2A) as a basis for their integrated system (Van Sonsbeek, 1992).

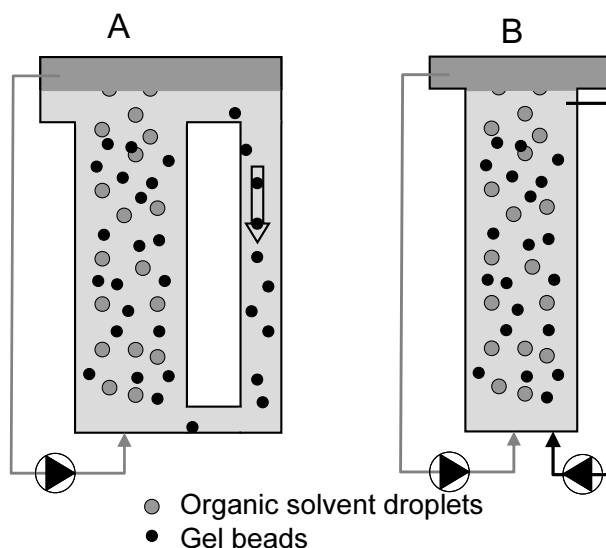


Figure 2. Liquid-impelled loop reactor (A) and 3-phase fluidized-bed bioreactor (B)

In a 3-phase reactor such as the liquid-impelled loop reactor (Figure 2A), only a single phase (the organic solvent) is recirculated in a controlled way with an external

pump. The circulation velocities of the other two phases (aqueous phase and solids phase) are not controlled directly but are dependent on the density difference between riser and downcomer. A different type of 3-phase liquid-liquid-solid bioreactor is depicted in Figure 2B. It features a stationary fluidized bed of gel beads that are not subject to (external) recirculation, with organic solvent droplets rising through this bed. In this bioreactor, two external pumps are used for recirculating a single liquid phase each: one pump recirculates the organic solvent, the other pump recirculates the aqueous phase. So, the most prominent operational difference between a 3-phase liquid-impelled loop reactor (Figure 2A) and a 3-phase fluidized bed (Figure 2B) is the way in which the aqueous phase is recirculated: a 3-phase fluidized bed features an extra external pump, thus offering an additional control option.

Performance of a bioreactor is dependent on its hydrodynamics. Also for 3-phase bioreactors mass transfer, phase hold-ups, and mixing characteristics are largely determined by the velocities of both liquids. In a liquid impelled loop reactor, the velocity of the organic phase influences directly the circulation velocity of the aqueous phase (Van Sonsbeek, 1990). In a 3-phase fluidized bed, both liquid velocities may be chosen independently of each other, as two external pumps are applied. Hence, for a 3-phase fluidized bed more control and optimization possibilities are available with respect to the hydrodynamics. Optimization of the hydrodynamics in relation to the overall production of the desired product will result in a maximal performance of the bioreactor.

A 3-phase fluidized-bed bioreactor was studied by Davison and Thompson (1993) for the production of butanol from glucose, and they reported an increase of 50-90% in the butanol production rate. Gas production and subsequent slugging necessitated the use of a tapered column to prevent wash-out of the gel beads, and to obtain stable operation of the fluidized bed. These authors focused on the biotransformation. Hydrodynamics of this 3-phase system were not studied.

Objective

The objective of the study presented in this thesis is the physical behavior of a liquid-liquid-solid 3-phase fluidized-bed bioreactor. It focused on the hydrodynamic behavior of the 3-phase system, i.e. hold-up and mixing. As a basis, the

hydrodynamics of the constituent 2-phase systems were studied: a liquid-solid fluidized bed and a liquid-liquid droplet spray column. Another objective was to identify the conditions for which this new type of bioreactor would perform superior to a conventional bioreactor.

Outline

In Chapter 2, the fluidization behavior of different types of gel beads is presented for a 2-phase liquid-fluidized bed. In Chapter 3, the droplet hold-up in a 2-phase liquid-liquid extraction spray column is reported on for different sparger lay-outs, and for co-current and counter-current operation. The results of hold-up experiments in a 3-phase liquid-liquid-gel bead (solid) fluidized bed are presented in Chapter 4. Continuous phase mixing in the 3-phase fluidized bed is discussed in Chapter 5. In Chapter 6, the preceding results are combined into a design for a 3-phase liquid-liquid-gel bead (solid) fluidized-bed bioreactor. Performance of this 3-phase fluidized bed is compared to its 2-phase counterpart. The thesis concludes with a general discussion on the current status of the newly developed 3-phase fluidized-bed bioreactor.

2

Fluidized-Bed and Packed-Bed Characteristics of Gel Beads

Abstract

A liquid-fluidized bed or packed bed with gel beads is attractive as an immobilized-cell bioreactor. The performance of such bioreactors is influenced by the physical behavior of these beads. Three different but related aspects involving the drag force between particle and flowing liquid were studied for 5 types of gel beads, differing in diameter and density. These aspects were the terminal settling velocity of a single gel bead, pressure drop over a packed bed and voidage in a liquid-fluidized bed. For gel beads the same trends and characteristics of these aspects were observed as for conventional solids. However, these aspects were not correctly predicted by established models. Though, the model of Grbavcic *et al.* (1991) predicts the voidage well.

It is concluded that the drag force between gel bead and flowing liquid is lower than that for conventional solids. Two hypotheses are suggested to explain this lower drag force. The first one attributes the drag reduction to small amounts of dissolved polymer. The second one attributes the smaller drag force to the nature of the gel beads; gel beads contain over 95% of water and can in that sense be regarded as 'rigid' water droplets. Hence, the gel bead surface might show waterlike properties.

We modeled the drag coefficient of a single gel bead in a packed bed or a fluidized bed, using the equation of Foscolo *et al.* (1983). The drag coefficient of a single gel bead, whether present in a packed bed or liquid-fluidized bed, was well described.

This opens to a better design and understanding of a packed bed and fluidized bed of gel beads.

Submitted for publication

Introduction

A packed bed or liquid-fluidized bed has attractive characteristics for application as an immobilized-cell bioreactor (Gòdia and Solà, 1995; Willaert *et al.*, 1996). Cells can be easily immobilized in solid particles, making a high biocatalyst concentration possible in a bioreactor (Wijffels *et al.*, 1996). An elegant way of immobilization is to embed the catalyst in beads of natural gels, like κ -carrageenan, alginate or agar (Hulst *et al.*, 1985). These beads, applied in fluidized-bed bioreactors, can be used for typical bio-processes like the production of ethanol (Gòdia *et al.*, 1987), or lactic acid (Wang *et al.*, 1995).

As little is known in literature on the hydrodynamics of a liquid-fluidized bed of gel beads as well as the hydrodynamics of a packed bed of gel beads, we studied the behavior of these systems. Gel beads differing in diameter and density were used.

In a packed bed upward liquid velocities up to the minimum fluidization velocity can be applied. This velocity is determined by the fact that pressure drop equals specific buoyant weight of the bed. In this paper pressure-drop experiments with different kinds of gel beads are described. We will show that pressure drop over a packed bed of gel beads is much lower than the pressure drop over a packed bed of conventional solids, like lead shot, glass pearls, etc., with the same diameter and voidage. Consequently, the pressure drop equations in literature, e.g. the Ergun equation or the equation of Foscolo (Foscolo *et al.*, 1983), cannot be applied to predict the minimum fluidization velocity.

A liquid-fluidized bed can exist between the minimum fluidization velocity and the terminal settling velocity of a single particle. The solids hold-up, ranging ca. 0.7 for the packed-bed to zero for wash out of particles, is determined by the equilibrium between the buoyancy force and the drag force experienced by a single particle in such a fluidized bed. The solids hold-up for different kinds of gel beads was determined as a function of the superficial velocity. To predict this gel bead hold-up several models are available in literature. It will be shown that the empirical model of Wilhelm and Kwauk (1948) with parameters according to Richardson and Zaki (1954) does not correctly predict the gel bead hold-up between minimum fluidization velocity and terminal settling velocity. However, the data can be well predicted with the model of Wilhelm and Kwauk (1948) with parameters obtained by fitting. The more fundamental model of Grbavcic *et al.* (1991), using independently determined parameters, predicts the data correctly.

The terminal settling velocity of different kinds of gel beads was also measured. Many models predicting this terminal settling velocity for more conventional solids are available in literature, but all these models underestimate the terminal settling velocity for gel beads.

The common feature of pressure drop over packed bed, solids hold-up in a fluidized bed and terminal settling velocity, is the fact that their magnitude is reigned by the drag force experienced by a particle. Gel beads experience a smaller drag force than conventional particles with the same diameter and density. Two hypotheses are suggested to explain this feature. In the first one it is considered that drag reduction occurs by small amounts of dissolved polymer. In the second one it is hypothesized that the observed feature results from a different surface structure of the gel beads: in a sense they can be regarded as 'rigid' water droplets.

Materials and Methods

Different gel beads and salt solutions were used. Such salt solutions are needed to prevent the elution of counter-ions from the gel beads. Using plain tap water without any salt addition would result in the dissolution of the gel beads. Table I gives an overview of the different gel beads used, and the applied molarity of the salt solutions.

All κ -carrageenan gel beads were produced using a resonance nozzle as described by Hunik *et al.* (1993). The specific aqueous κ -carrageenan (Genugel 0909 Copenhagen Pectin Factory) solution, kept at 35 °C, was pressed through a nozzle. The drops were collected in a 80 mM KCl-solution for hardening of the beads. To obtain spherical beads a butyl-acetate (Aldrich-Chemie) layer was brought upon the hardening solution. After hardening for approximately two hours, the beads were stored in a KCl-solution. The alginate beads filled with yeast were prepared with a conventional dripping method (Hulst *et al.*, 1985).

The temperature in each experiment was equal to the ambient temperature, 26±2 °C.

Table I. Different particles used for fluidization, pressure drop and terminal settling velocity experiments.

	Gel bead	Salt solution
A	3% κ -carrageenan	10 mM KCl
B	3% κ -carrageenan	10 mM KCl
C	3.25 % κ -carrageenan filled with 5% Celite™	30 mM KCl
D	3.25 % κ -carrageenan filled with 10% Celite™	30 mM KCl
E	8 % alginate filled with yeast cells 25 v %	50 mM CaCl ₂

Characterization of the beads

Diameter

The diameter was determined with image-analysis (CCD-camera with a Nikon macro objective 50 mm). The image of the particles was digitized and analyzed with the software package Genius (Applied Imaging). For a higher contrast the fluid surrounding the beads (a 10 mM KCl-solution) was colored with blue dextran (Pharmacia Biotech, $M_w=2,000,000$ g mole⁻¹). The coloring of the surrounding liquid

was used for gel beads A and B, κ -carrageenan beads without any additions, as they are transparent.

Volume and Density

Gel beads, as a consequence of their nature, do have a certain amount of water attached that cannot be removed by simply sieving. In all experiments that rely upon the exact volume of the gel beads used, this amount of water attached, has to be accounted for. The following procedure was used for determining this amount. Simultaneously the bead density can be calculated. A calibrated flask was weighted ($=M_{\text{flask}}$) and partly filled with a blue dextran solution and weighted again ($=M_1$). Sieved gel beads were added, and the flask was again weighted ($=M_2$). Next the flask was filled with the blue dextran solution up to the calibrated volume of the flask; again the flask was weighted ($=M_3$). After shaking for over 2 hours, the adsorption of the supernatant and the adsorption of the original blue dextran solution were determined with a spectrophotometer (Ultrospec 2000, Pharmacia Biotech) at 280 nm. The next equations show how from this procedure the exact volume of the gel beads can be determined:

$$V_{\text{water added}} = \frac{M_1 - M_{\text{flask}} + M_3 - M_2}{\rho_{\text{water(T)}}}$$

$$V_{\text{water total}} = V_{\text{water added}} \cdot \frac{\text{Abs}_{\text{solution}}}{\text{Abs}_{\text{supernatant}}} \quad 1$$

$$V_{\text{gel beads}} = V_{\text{flask}} - V_{\text{water total}}$$

The density of the gel beads is calculated with the next equations:

$$M_{\text{water adhering}} = (V_{\text{water total}} - V_{\text{water added}}) \cdot \rho_{\text{water(T)}}$$

$$M_{\text{gel beads}} = M_2 - M_1 - M_{\text{water adhering}} \quad 2$$

$$\rho_{\text{gel beads}} = \frac{M_{\text{gel beads}}}{V_{\text{gel beads}}}$$

Diffusion of blue dextran into the gel beads was not observed after incubating the solids in a blue dextran solution for 48 hours.

Terminal settling velocity

The split-times at different heights of a particle falling in a glass column with a 6 cm inner diameter, and a total height of 1 m filled with a salt solution were measured. A vertical distance of 50 cm from the liquid interface was used to allow a constant velocity to be attained. The terminal settling velocity of the beads followed from the slope between time and height. This slope was determined with linear regression. Wall effects might become important as the particle to column diameter ratio is not extremely large. Therefore the terminal settling velocity of bead A was also determined in a rectangular vessel with dimensions of 43.5 x 29.5 x 100.5 cm (l x b x h).

Pressure drop of a packed bed of gel beads

A packed bed of gel beads was formed in a column with an inner diameter of 2.56 cm, and a total length of 120 cm. The first 5 cm of the column was filled with glass beads to provide a good flow distribution. The pressure difference over a vertical distance was measured with a Validyne DP103 pressure transducer together with a CD23 digital transducer indicator (maximum pressure difference 140 Pa). In each set of pressure measurements the pressure transducer was calibrated; a liquid manometer filled with water and octanoic acid ($\rho=903 \text{ kg m}^{-3}$) was used for this calibration. Flow rates were measured with a calibrated rotameter (Sho-rate, Brooks). To check whether wall effects are important, pressure drop experiments were also done for bead D in a 6 cm inner diameter column.

Fluidization of gel beads

Experiments were carried out in a glass column with an inner diameter of 6 cm and a total height of 3 m. Figure 1 shows the experimental lay-out. Liquid was pumped from a storage vessel to the glass column. The first 10 cm of this column were filled with 0.8 cm glass pearls to provide a good flow distribution. The flow rate was measured with one or more calibrated rotameters (Sho-rate, Brooks). As the fluidized bed showed a quiescent behavior, the height of the bed could be determined visually. The solids hold-up followed from the bed height and the initial volume of the gel beads.

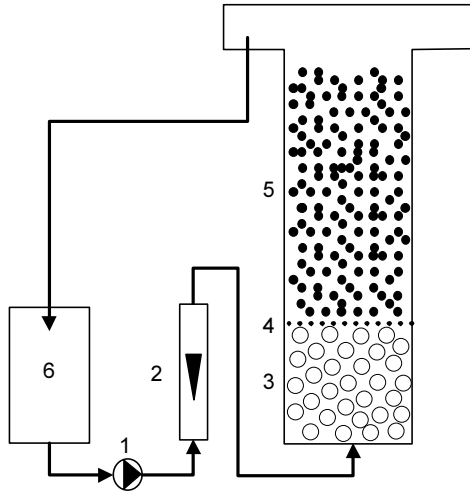


Figure 1. Experimental lay-out for the fluidization experiments. 1 pump, 2 rotameter(s), 3 bed of glass pearls, 4 sieve plate, 5 gel bead fluidized bed, 6 storage vessel

The predicting quality of a model is expressed as the average deviation (AVD) defined as:

$$AVD = \left(\sum_i \left| \chi_i^{\text{measured}} - \chi_i^{\text{model}} \right| / \chi_i^{\text{measured}} \right) / N \quad 3$$

with χ_i a model quantity, and N the number of data points.

Results

First physical parameters of the different gel beads are discussed: shape, diameter and terminal settling velocity. This settling velocity is compared with literature models. Next the data of the pressure drop experiments for a packed bed are shown and compared with literature model predictions. Thereafter, we show the results of the fluidization experiments. An empirical model (Wilhelm and Kwauk, 1948), and a more fundamental model (Grbavcic *et al.*, 1991) are tested.

Gel-bead characterization

Shape and diameter

The size and shape of the different gel beads were evaluated with image analysis. Two important chord sizes for the shape characterization of the gel bead are the object length (OL in insert of Figure 3), defined as the largest distance between two points on the perimeter of the object, and the object breadth (OB in insert of Figure 2), defined as the largest distance between two points on the perimeter of the object, perpendicular to the object length. Figure 2 shows a chord size distribution for both the object length and object breadth typical for all gel beads analyzed. This figure shows that the object-length distribution is shifted a little to higher values compared to the object-breadth distribution. This indicates that the beads were not completely spherical. This deviation from a perfect sphere was visually verified as most of the gel beads showed a droplet like shape.

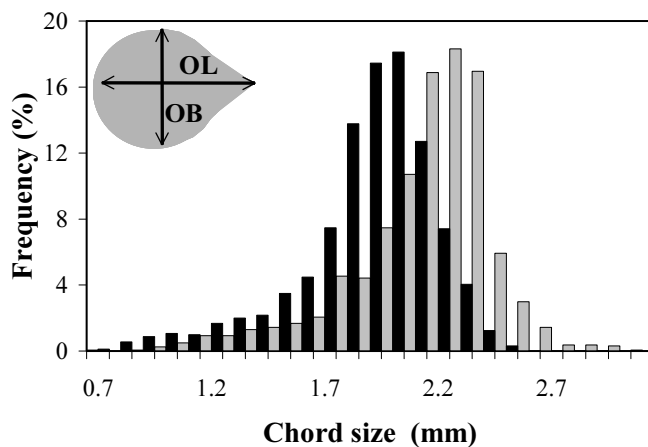


Figure 2. Object length (■) and object-breadth (■) distribution for gel bead A.

Two shape factors could be determined with the image analysis software: the elongation and the object circularity, see equation 4.

$$\text{Elongation} = \frac{\text{object length}}{\text{object breadth}}$$

$$\text{Circularity} = \frac{\text{object area}}{\text{perimeter}}$$

4

These shape factors are given in Table II together with the standard deviation. It can be concluded that the beads approach the spherical shape closely. Thus an equivalent spherical diameter, based on the measured area of the gel bead, was calculated. These diameters yielded the Sauter mean diameters in Table II.

Table II. Physical parameters of the different gel beads mentioned in Table I.

Gel bead	Size and Shape						Density kg m ⁻³
	Mean mm	(±σ)	Median mm	Sauter mean* mm	Shape factor 1*	Shape factor 2*	
A	1.90	(0.28)	1.99	1.97	1.03	1.18	1007.4
B	2.99	(0.45)	3.03	3.12	0.98	1.10	1005.4
C	3.14	(0.17)	3.14	3.16	1.01	1.06	1029.8
D	2.90	(0.42)	2.83	2.76	1.02	1.15	1065.1
E	4.25	(0.24)	4.27	4.27	1.00	1.13	1039.9

* definition of the Sauter mean $d_{32} = \frac{\sum d_i^3}{\sum d_i^2}$,

shape factor 1: circularity, shape factor 2 elongation.

Terminal Settling Velocity

The mean and median of the settling-velocity distribution for the different types of gel beads are given in Table III. As the mean and median values are almost equal, it is concluded that the distribution is symmetrical for each type of gel bead.

The terminal settling velocity is the largest liquid superficial velocity for which a fluidized bed exists. So, it is a key parameter in modeling fluidization. As the fluidization experiments were done in a 6 cm inner diameter column, the terminal-settling-velocity experiments were also done in this column. However, the ratio between column diameter and gel bead diameter is not large, and consequently wall effects will be present. In order to compare our measurements with literature models, these wall effects have to be accounted for. Therefore, the terminal settling velocity

for gel bead A was also measured in a large rectangular vessel, in which wall effects are negligible. The mean terminal velocity was equal to $1.518 (\pm 0.065) \text{ cm s}^{-1}$, the value between brackets is the standard deviation. The ratio of the terminal settling velocity with and without wall effects is equal to 0.90. This value is close to the value calculated with the correlation suggested by Richardson and Zaki (1954) to account for wall effects:

$$\frac{v_{\infty} \text{ with wall effects}}{v_{\infty} \text{ without wall effects}} = 10^{-d_p / D} = 10^{-\frac{2.02}{60}} = 0.92$$

This correlation is used to correct the measured terminal settling velocity of the other gel beads for wall effects. This corrected settling velocity is also given in Table III.

Table III. Terminal Settling velocity of the different gel beads mentioned in Table I in cm s^{-1} .

Gel bead	Mean ($\pm\sigma$)	Median	Corrected for wall effects	Model of Dallavalle
A	1.37 (± 0.08)	1.38	1.52 ¹	0.99
B	1.96 (± 0.25)	2.02	2.22	1.42
C	4.41 (± 0.17)	4.44	4.98	3.49
D	5.12 (± 0.24)	5.12	5.69	4.89
E	5.22 (± 0.11)	5.22	6.15	5.62

¹ Experimental value

The settling velocity of a single particle in a stagnant liquid can be calculated from a force balance for this particle. This force balance accounts for the gravity force, the buoyancy force and the drag force. This balance reads in dimensionless form:

$$\text{Ga} = \frac{3}{4} C_d \text{Re}_p^2 \quad 5$$

where Ga is the Galileo number, C_d is the drag coefficient for a single particle and Re_p is the particle Reynolds number, which is based on the particle dimensions. To calculate the terminal settling velocity with equation 5, a model for the drag coefficient is needed. Models relating the drag coefficient to the particle Reynolds number are abundantly available in literature (Dallavalle, 1948; Turton and Levenspiel, 1986; Hidaka *et al.*, 1994). Other models relate the Galileo number directly to the particle Reynolds number (Zigrang and Silvester, 1981; Turton and

Clark, 1987; Khan and Richardson, 1989; Hartman *et al*, 1989). All these literature models predict more or less the same terminal settling velocity. Table III shows the terminal settling velocity for the different gel beads, calculated with the equation of Dallavalle (1948), using the physical properties of the gel beads given in Table II and the physical properties of water at 24 °C (Weast, 1979). Table III shows that the calculated terminal settling velocity is considerably lower than the measured terminal settling velocity of the gel beads corrected for wall effects.

Figure 3 shows the drag coefficient calculated from the experimental values for the settling velocity (eq.5) and the drag coefficient calculated with literature models. From this figure it can be concluded that published models overestimate the drag coefficient for gel beads.

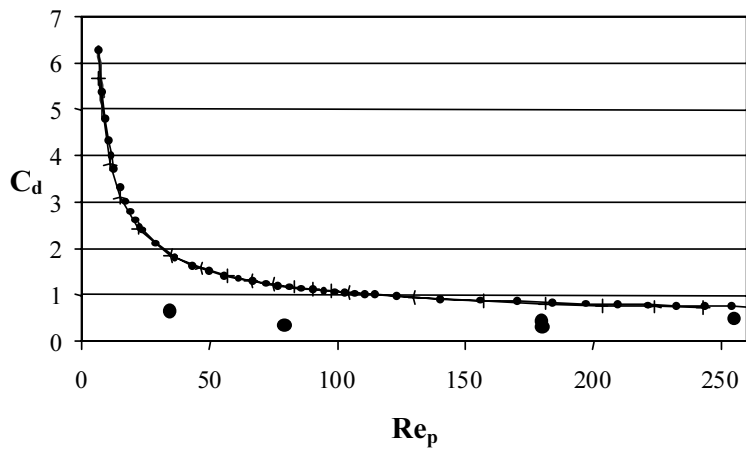


Figure 3. Drag coefficient for gel bead particles settling in stagnant water as a function of the particle Reynolds number (physical properties given in Table I). Experimental values and model predictions: ● data ; —●— model of Dallavalle, 1948; —+— Model of Turton and Clarke, 1987; — model of Silvester and Zigrang, 1981.

Packed-Bed Pressure Drop

Figure 4 shows the measured pressure drop over a fixed bed length for the different gel beads as a function of the Reynolds number ($Re = \rho U d_p / \eta$). This figure clearly shows features commonly observed in packed-bed pressure-drop experiments: pressure drop increases with an increasing Reynolds number; a smaller particle diameter gives a higher pressure drop at the same Reynolds number, and the maximum pressure drop is highest for the gel-bead type with the largest density.

A commonly used model to predict pressure drop over a packed bed is the model of Ergun (Bird *et al.*, 1960). Foscolo *et al.* (1983) revised the Ergun model by

introducing a voidage dependent tortuosity. This model predicts drag forces acting on an individual particle, either present in a packed bed or settling in a stagnant liquid. Both models overestimate the pressure drop over the packed bed of gel beads (predictions not shown).

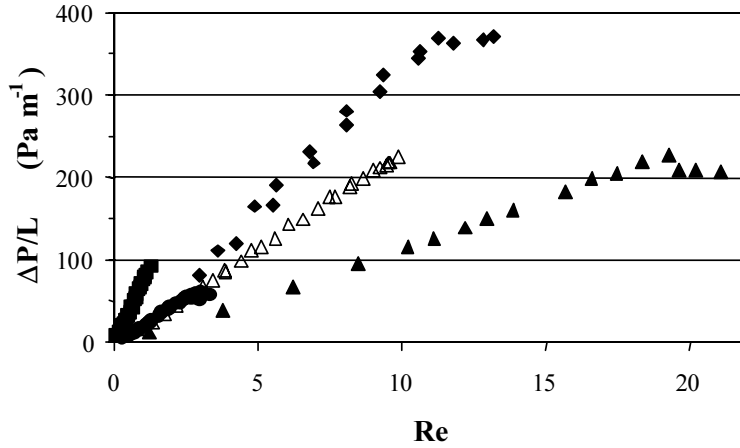


Figure 4. Pressure drop over a packed bed of gel beads as a function of the Reynolds number (see Table I for physical properties of the different gel beads). Column diameter is 2.54 cm.

■ gel bead A; ● gel bead B; △ gel bead C; ◆ gel bead D; ▲ gel bead E

The large discrepancy between measured and predicted pressure drop can be elucidated by considering the drag force experienced by a single particle in the packed bed. A good measure for this drag force is the drag coefficient. This drag coefficient can be related to the pressure drop. Appendix A gives a detailed derivation, which results in:

$$C_d = \frac{4}{3} \frac{\Delta P}{L} \left(\frac{\varepsilon^3}{1 - \varepsilon} \right) \frac{d_p}{\rho U^2} \quad 6$$

The drag coefficients derived from Ergun's and Foscolo's model are given by equation 7, see for details Appendix A:

$$\text{Foscolo } C_d = \frac{4}{3} \left(\frac{17.3}{Re} + 0.336 \right) \varepsilon^{-1.8} \quad 7$$

$$\text{Ergun } C_d = \frac{4}{3} \left(\frac{100}{Re(1 - \varepsilon)} + 1.75 \right)$$

The experimental drag coefficient for gel beads A and D, calculated with equation 6, together with the model predictions calculated with equation 7, is shown in Figure 5 as a function of the hydraulic Reynolds number ($Re_h = \frac{2}{3}(1-\varepsilon)\rho U d_p / \eta$). This figure clearly shows that the drag experienced by a single gel bead in a packed bed is smaller than the drag predicted by Ergun's and Foscolo's equations.

As the particle diameter to column diameter ratio is less than 10 for gel beads B and C, a wall effect might be expected. Therefore the drag coefficient for these gel beads is not shown in Figure 5. For gel bead A this ratio is larger than 10. For gel bead D this ratio is smaller but close to 10. Indeed, a small wall effect is observed for gel beads D; the C_d values for data corresponding with the 6 cm diameter column are a little lower than those for data corresponding with the 2.54 cm diameter column.

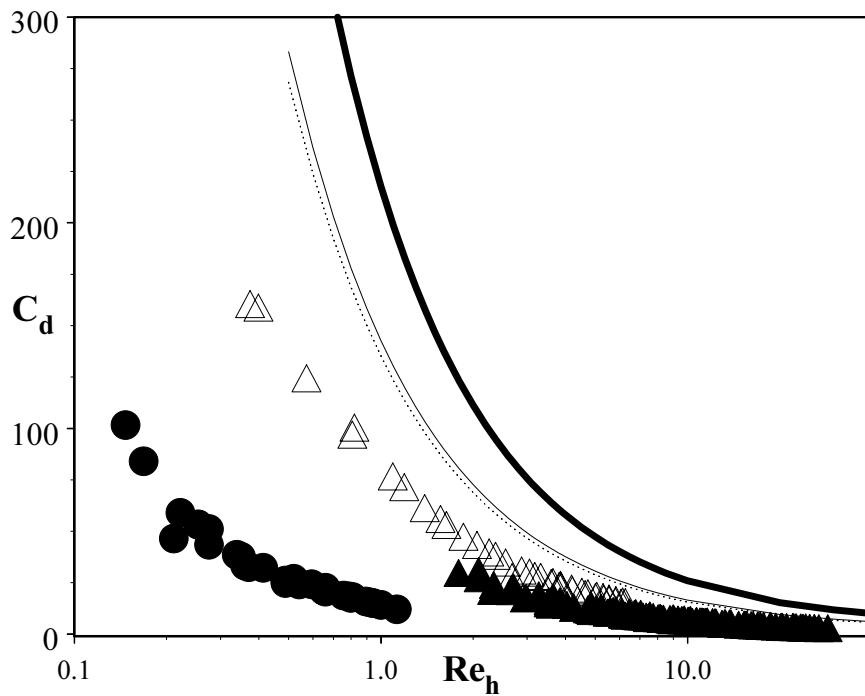


Figure 5. Drag coefficient of a single particle in a packed bed of identical particles as function of the hydraulic Reynolds number. Experimental data: ● gel bead A; ▲ gel bead D, column diameter 2.54 cm; △ gel bead D, column diameter 6 cm. Model predictions: — Foscolo, voidage is 0.25; Foscolo, voidage is 0.38; ——— Ergun.

Fluidization of gel beads

The different gel beads mentioned in Table I, were fluidized by the appropriate salt solutions. The solids hold-up as a function of the superficial velocity is shown in Figure 6.

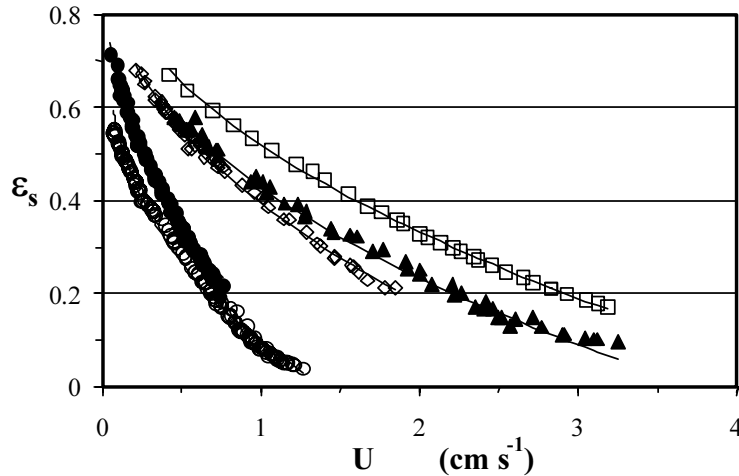


Figure 6. Gel bead hold-up in a fluidized bed as a function of the superficial velocity. Data and description with the Wilhelm and Kwauk model (for fitted parameters see Table IV).

● gel bead A; ○ gel bead B; ◇ gel bead C; ▲ gel bead D; □ gel bead E

Features commonly seen in liquid fluidization of solid particles are also observed for the fluidization of gel beads: the solids hold-up decreases with an increasing superficial liquid velocity (U); at the same U the solids hold-up is higher for gel beads with the same diameter but larger density (type C versus type B); at the same U gel beads with the highest terminal settling velocity show the highest solids hold-up.

Experimental data for particulate bed expansion were correlated by Wilhelm and Kwauk (1948) with the following empirical equation:

$$U = k\varepsilon^{-n} \quad 8$$

where U is the superficial liquid velocity, ε is the voidage, and k and n are empirical parameters. Table IV gives the parameters in equation 8 determined from fitting this equation to the experimental data. Figure 6 shows that the experimental data are well described.

Table IV. Fitted parameters in Wilhelm and Kwauk's model for liquid fluidization of different gel beads.

Gel bead	Fitted Parameters ¹		n from Rowe's model
	k	n	
A	1.31 (± 0.03)	2.29 (± 0.05)	3.06
B	1.40 (± 0.03)	3.33 (± 0.06)	2.79
C	3.16 (± 0.08)	2.29 (± 0.04)	2.61
D	3.77 (± 0.07)	2.35 (± 0.06)	2.61
E	4.67 (± 0.08)	2.10 (± 0.04)	2.55

¹ value between brackets gives the 95% confidence interval

Richardson and Zaki (1954) showed that the parameter k is equal to the terminal settling velocity and that the power n is a function of the particle Reynolds number. If we compare parameter k in Table IV with v_∞ in Table III, it is apparent that the parameter k is always smaller than the terminal settling velocity. As the voidage approaches 1, the superficial velocity should approach the terminal settling velocity, but extrapolation gives a lower value. This fact has also been reported by different authors for liquid fluidization of glass pearls (Garside and Al-Dibouni, 1977; Riba and Couderc, 1977; Grbavcic *et al.*, 1991). This kind of expansion behavior is one of the four different types of liquid-fluidized-bed expansion behavior mentioned by Di Felice (1994). The observed expansion behavior is characterized by two different regimes. For lower voidage, the voidage as a function of the ratio superficial velocity to terminal settling velocity, U/v_∞ , shows a straight line on a log-log scale, see Figure 7. Extrapolation of this straight line to $\epsilon=1$ results in a ratio U/v_∞ smaller than 1. For higher voidages, the voidage as a function of U/v_∞ shows also a straight line on a log-log scale but the slope is smaller; the extrapolation of this line to $\epsilon=1$ gives a ratio equal to 1, see the dotted line in Figure 7. In our data this second regime is hardly present. We did not do experiments at higher voidages, because the bed height could not be clearly determined.

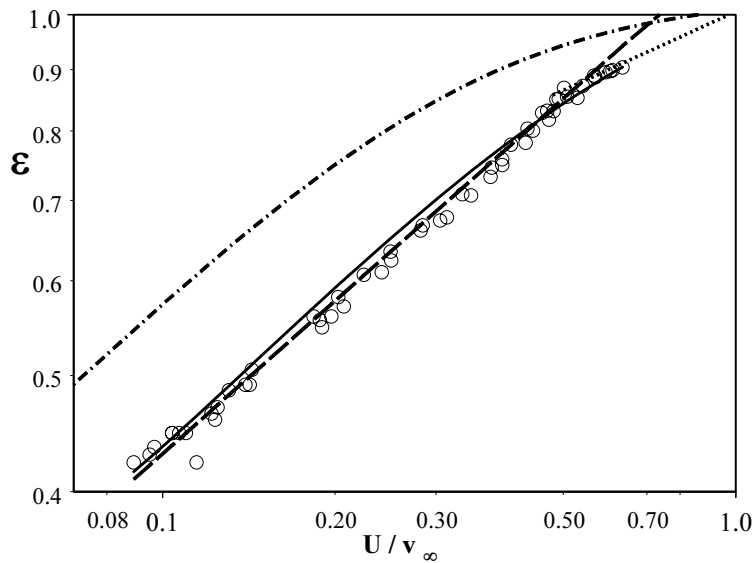


Figure 7. Voidage for gel bead D as a function of the dimensionless velocity. The superficial velocity (U) was divided by the terminal settling velocity of gel bead D (v_{∞}). O experimental data,
— model of Grbavcic, 1991 ($U_{mf} = 0.358 \text{ cm s}^{-1}$, $v_{\infty} = 5.12 \text{ cm s}^{-1}$, $\varepsilon_{mf} = 0.38$),
--- model of Wilhelm and Kwauk, 1948 with fitted constants.
- . - model of Grbavcic 1991 conventional solid
($U_{mf} = 0.18 \text{ cm s}^{-1}$, $v_{\infty} = 4.4 \text{ cm s}^{-1}$, $\varepsilon_{mf} = 0.38$, $d_p = 2.76 \text{ mm}$, $\rho_s = 1065 \text{ kg m}^{-3}$).

Table IV shows the fitted parameter n in equation 8, and parameter n calculated with a well-established model from literature (Rowe, 1987):

$$n = \frac{4.7 + 0.4112 \cdot \text{Re}_p^{0.75}}{1 + 0.175 \cdot \text{Re}_p^{0.75}} \quad 9$$

For all gel beads, except type B, the fitted parameter n is smaller than the calculated parameter. So, the parameter n in equation 8 cannot be estimated from literature models in order to predict the gel bead hold-up.

The relationship between voidage and superficial velocity as described by equation 8 does predict our data satisfactorily, provided the empirical constants are known. However, in the preceding paragraphs it was demonstrated that these constants cannot be determined from literature models.

An alternative to the Wilhelm and Kwauk approach (eq.8) is the more fundamental model of Grbavcic *et al.* (1991). These authors describe a model predicting the voidage in liquid fluidized beds without any adjustable constants. As parameters this model uses only the minimum fluidization velocity (U_{mf}), the

voidage at the onset of fluidization (ε_{mf}) and the terminal settling velocity; parameters that are easy to measure. The equation is:

$$U = U_{mf} \left(\frac{\varepsilon^3 (1 - \varepsilon)}{\varepsilon_{mf}^3 (1 - \varepsilon_{mf})} \frac{C_{d,mf}}{C_d} \right)^{0.5} \quad 10$$

The drag coefficient ratio is given by:

$$\frac{C_d}{C_{d,mf}} = 1 - c_2 + \frac{1}{\lambda} \cdot \left[1 - \left(\lambda \left(\frac{\varepsilon - \varepsilon_{mf}}{1 - \varepsilon_{mf}} \right) + c_1 \right)^2 \right]^{0.5} \quad 11$$

The constants, c_1 , c_2 , and λ , in equation 11 are functions of the minimum fluidization velocity, the voidage at the onset of fluidization, and the terminal settling velocity, see Nomenclature for the corresponding correlation.

An interesting aspect of this model, equations 10 and 11, is the fact that it uses as one parameter a single particle characteristic, the terminal settling velocity. The other two parameters are packed bed characteristics: packed bed voidage at the onset of fluidization and the minimum fluidization velocity, which is equal to the maximum velocity through a packed bed. The packed bed voidage has to be determined experimentally, regardless of the kind of particles used. Literature models are abundantly available for adequately predicting v_∞ and U_{mf} for conventional solids. However, as shown in preceding paragraphs, these models fail to predict v_∞ and U_{mf} for gel beads. These parameters, however, can be easily determined.

The predicting quality of this model, equations 10 and 11, expressed as the AVD (eq.3), is given in Table V for the different gel beads mentioned in Table I. This table also gives the minimum fluidization velocity, the voidage at this velocity, the terminal settling velocity of the different gel beads, and the corresponding constants c_1 , c_2 , and λ . As a typical example, Figure 7 shows the measured voidage, and the voidage predicted by equations 10 and 11 with the constants given in Table V, as a function of the ratio of superficial velocity to v_∞ for type D gel beads. Considering that the AVD of all gel beads in Table V is less than 0.05, we can conclude that the model of Grbavcic *et al.* (1991) predicts the experimental data well. This conclusion is supported by Figure 7.

Two models, equation 8 and Grbavcic's model, were used to describe the gel bead hold-up as a function of the superficial liquid velocity. Figure 7 shows that both models describe the experimental data well, although Grbavcic's model slightly overestimates the voidage in the intermediate regime. The advantage of equation 8 over Grbavcic's model is the less complicated mathematical functionality. However, fluidization data are necessary to get the empirical constants. For application of Grbavcic's model estimates of terminal settling velocity, minimum fluidization velocity and the voidage at this velocity suffice.

Table V. Constants for calculating the voidage in a liquid fluidized bed as described by equation 10 and 11, together with its predicting quality expressed as the average deviation (AVD).

Gel bead	Bead Characteristics			Constants in equation 11			AVD
	ε_{mf}	U_{mf}	U_t	$10C_1$	$-100C_2$	-10λ	
A	0.25	0.065	1.38	9.90	16.4	8.50	0.040
B	0.35	0.080	2.02	9.99	3.8	9.63	0.050
C	0.31	0.216	4.44	9.96	8.6	9.18	0.019
D	0.38	0.358	5.12	9.96	9.5	9.10	0.022
E	0.32	0.40	5.22	9.83	23.1	7.98	0.018

ε_{mf} : voidage at minimal fluidization velocity

U_{mf} : minimal fluidization velocity cm s^{-1}

U_t : measured terminal settling velocity cm s^{-1}

General Discussion

In this section we show that the drag coefficient for a gel bead in a fluidized bed is smaller than that of conventional solid with the same density and diameter. Next it is concluded that a smaller drag coefficient is observed in three related aspects, terminal settling velocity, pressure drop over a packed bed, and voidage of a liquid fluidized bed. Two hypotheses are discussed to explain the difference between gel beads and conventional solids. This section ends with the derivation of a model to predict the drag coefficient of an individual gel bead either present in a packed-bed or a fluidized bed of identical gel beads.

The drag force experienced by a particle in a fluidized bed of identical particles depends on the voidage in such a fluidized bed. Appendix A shows how the drag coefficient is related to the voidage:

$$C_{\text{drag}} = \frac{4}{3} \frac{\rho_s - \rho}{\rho} \frac{\varepsilon^3}{u^2} d_p g \quad 12$$

So, to compare the drag coefficient for a gel bead and a more conventional solid particle the voidage has to be known. For the gel beads we used the measured voidage. For the conventional solid particle, the voidage was calculated with the model of Grbavcic *et al.* (1991). This model is superior to all other literature models, as discussed above. As the model of Grbavcic *et al.* (1991) uses the minimal fluidization velocity, we used Foscolo's pressure-drop equation for calculating this velocity. The terminal settling velocity, the other parameter, was calculated with Dallavalle's model (1948). Figure 7 shows the voidage in the fluidized bed of conventional solids as a function of a dimensionless superficial velocity (the superficial velocity divided by the terminal settling velocity of gel bead D). Obviously, the voidage is always smaller for the gel beads at an equal velocity ratio, and consequently their drag coefficient is also smaller.

Above, it has been shown that the drag coefficient is smaller for a single gel bead settling in a stagnant liquid, see Figure 3. The same conclusion has been drawn for the drag coefficient in a packed bed, see Figure 5. Thus, for the three related aspects it is concluded that the drag coefficient for a gel bead in an array of identical gel beads is smaller than that of a conventional solid, e.g. a glass pearl. Two hypotheses are discussed below to explain this observation.

The observed difference between gel beads and conventional solids might be explained by the following hypothesis. It is known that extremely low amounts of dissolved polymer can reduce the drag force between a solid surface and a flowing liquid (Paireau and Bonn, 1999). In our experimental set-up small amounts of polymer, κ -carrageenan, will be present in the liquid. Consequently, the drag force between gel bead and flowing water is reduced.

A different hypothesis comes from considering the nature of these gel beads. Gel beads are made by dripping a solution of a natural polymer like κ -carrageenan or alginate into a salt solution; the liquid droplet transforms to a solid due to exchange of ions. Consequently, gel beads consist over 95% of water and in a sense can be considered as 'rigid' water droplets. Water streaming alongside the gel bead surface will experience a water-like surface. Consequently, the drag force is less, compared to the case in which water flows alongside a non-water-like surface.

In the next part of this section a model will be derived that describes the drag

coefficient of a gel bead in an array of other identical gel beads, whether present in a packed-bed configuration or in a fluidized bed. Most literature models do not predict the drag coefficient for gel beads correctly, except the model of Grbavcic *et al.* (1991) which predicts the drag coefficient in fluidized beds. Unfortunately, this model cannot predict the drag coefficient for a gel bead in a packed bed of gel beads.

As the drag coefficient is related to the pressure drop over a bed of particles, see appendix A, a pressure-drop relation is used to model the drag coefficient for gel beads. Pressure drop is well correlated by the Ergun equation (Bird *et al.*, 1960). In the derivation of this equation it is not required that the particles are in contact with each other. Therefore, this equation should also be applicable to a fluidized bed with a voidage ranging from the packed bed condition to the fully expanded state. Unfortunately the Ergun equation does not describe the pressure drop over a particulate fluidized bed well (Foscolo *et al.*, 1983). Foscolo *et al.* (1983) made a re-examination of the basis for the Ergun equation, which resulted in an equation describing pressure drop over a packed bed as well as a fluidized bed. Incorporating this pressure drop equation in equation 6 resulted in equation 7 for the drag coefficient. This equation does not predict the drag coefficient for gel beads correctly, see Figure 8. We used the form of this equation and introduced two unknown parameters:

$$C_d = \frac{4}{3} \left(\frac{c_3}{Re} \varepsilon^{-c_4} + 0.336 \varepsilon^{-1.8} \right) \quad 13$$

Equation 13 consists of two parts: a part describing the drag coefficient at laminar-flow conditions and a part describing this coefficient at turbulent-flow conditions. Under turbulent flow conditions the dominant contribution to energy dissipation in a bed of particles comes from the numerous expansions and contractions of the fluid streams in their passage around the particles. As fluid streams do not follow the surface of the particles strictly in the turbulent regime, we believe that in this regime the surface structure does not influence the energy dissipation. In the laminar-flow regime, however, fluid streams do follow the surface of the particles. So the structure of the surface will influence the drag force between flowing liquid and a single particle in a packed or fluidized bed. Consequently, the turbulent part of the model of Foscolo, equation 13, was used unchanged but the constants appearing in the laminar part of the model of Foscolo were fitted to the experimental data.

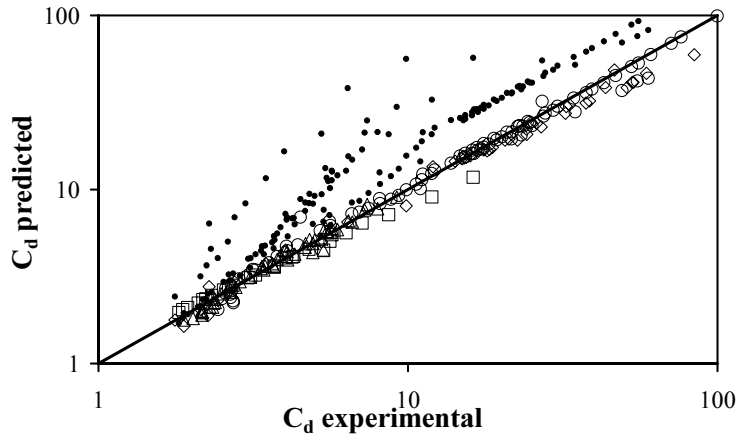


Figure 8. Parity plot for the drag coefficient of a single gel bead in a bed of identical gel beads. Model of Foscolo *et al.* (1983) with fitted constants. \diamond gel bead A; \square gel bead B; \triangle gel bead C; \circ gel bead D. \bullet Model of Foscolo *et al.* (1983) with original constants.

To find the constants c_3 and c_4 , we minimized the average deviation (AVD), equation 3, with X_i is the drag coefficient. Not only the drag coefficient calculated from the pressure-drop experiments were used, but also the drag coefficients calculated from the fluidization experiments; pressure drop over a fluidized bed is straightforwardly correlated to voidage, see also appendix A. For gel bead A pressure-drop experiments done in a small column could be used; a wall effect was not observed. In this column with a small diameter a wall effect was observed for gel beads B, C and D. So for gel beads B and C, we only used the fluidization experiments done in a 6-cm inner diameter column to fit the constants in equation 13. For gel bead D pressure-drop experiments carried out in a 6-cm inner diameter column were extended above the minimal fluidization velocity. These experiments were used also to fit the constants in equation 13. The fitted constants are given in Table VI.

Table VI shows that constant c_3 differs considerably for each gel-bead type, but constant c_4 does not differ much for gel beads A – D, especially when the sensitivity of the model for this constant is considered. For example, for gel bead B, a constant c_4 of 0.5 results in a AVD of 0.024. Therefore, a common voidage dependency was assumed for gel beads A to D. This common voidage dependency was implemented into fitting equation 13 to the experimental drag coefficient. The resulting constants are given in Table VI. Figure 8 shows that the experimental drag coefficient is well described by equation 13, and the constants from Table VI based on the common voidage-dependency. Table VI shows that constant c_3 for gel bead A is almost equal

to the value in the original model of Foscolo, equation 7, but for the other gel beads this constant is increasingly larger. The fitted constants for gel bead E are quite different from the fitted constants for gel bead A - D. We have no explanation for this difference.

For a packed bed and fluidized bed the effect of the voidage on the pressure drop is obtained by combining equations 6 and 7 for conventional solids and by combining equations 6 and 13 for gel beads A - D:

$$\begin{aligned} \text{conventional solid} &: \Delta P \sim (1 - \varepsilon) \cdot \varepsilon^{-4.8} \\ \text{gel beads A - D} &: \Delta P \sim (1 - \varepsilon) \cdot \varepsilon^{-2.43} \end{aligned} \quad 14$$

The influence of the voidage on the pressure drop is much smaller for gel beads than for conventional solids.

Table VI. Constants for equation 13 describing the drag coefficient of a single particle in a packed or fluidized bed of identical particles, as well as the average deviation (AVD) of the model from the experimental data.

Gel bead	Each gel bead type individually fitted			Common voidage dependency		
	C ₃	C ₄	AVD	C ₃	C ₄	AVD
A	16.77	0.55	0.085	16.95	0.571	0.104
B	25.45	-0.0235	0.004	33.05	0.571	0.075
C	66.19	0.85	0.041	54.46	0.571	0.051
D	92.00	0.549	0.073	95.47	0.571	0.073
E	166.96	2.84	0.079			

For gel bead E the constants given in this table are fitted on the fluidization experiments as the pressure drop experiments could not be satisfactorily fitted on equation 13.

Conclusions

Three different properties have been measured for five different types of gel beads: terminal settling velocity of a single gel bead, pressure drop over a packed bed, and voidage of a liquid fluidized bed. Although the experiments with gel beads show the same trends and characteristics as previously reported for conventional solids, pressure drop and terminal settling velocity are not correctly predicted by established models. The terminal settling velocity is higher, the pressure drop is lower. Voidage of a liquid fluidized bed is also not well predicted by the empirical

model of Wilhelm and Kwauk with parameters according to Richardson and Zaki. The more fundamental model of Grbavcic *et al.*, however, predicts the voidage well, using a measured minimal fluidization velocity and a measured terminal settling velocity.

It can be concluded that the drag coefficient for a single gel bead, whether settling or present in a packed bed or fluidized bed of other identical gel beads, is always smaller than the drag coefficient of a conventional solid having the same diameter and density.

Two hypotheses are presented to explain the features above. The first considers a lower drag coefficient by the presence of small amounts of dissolved polymer. The other considers that the difference between gel bead and conventional solid results from the difference in surface structure between gel beads and more conventional particles; a gel bead consists over 95% of water and can be regarded as a 'rigid' water droplet.

The drag force experienced by a gel bead in a liquid fluidized bed, and hence the voidage in a liquid fluidized bed, is well predicted for the different gel beads by the model of Grbavcic *et al.*, derived for more conventional solids. Unfortunately, this model is not applicable for a packed bed. So, a different model is presented for predicting the drag coefficient of a gel bead present in a packed bed or fluidized bed of other identical gel beads. This model is based on the model of Foscolo (1983) for conventional solids. The turbulent part is equal for gel beads and conventional solids. The laminar part, however, shows a different but common voidage dependency for the gel beads.

Acknowledgements

We thank Arend Mulder for supplying the alginate beads.

This work was financially supported by the Ministry of Economic Affairs, the Ministry of Education, Culture and Science, the Ministry of Agriculture, Nature Management and Fishery in the framework of a research program of the Netherlands Association of Biotechnology Centers (ABON).

Appendix A. Relationship between the drag coefficient of a single particle in packed bed or fluidized bed of other identical particles and the pressure drop

Water flows through a bed of particles. A steady-state macroscopic mechanical-energy balance from point 1 to 2 reads (Bird *et al.*, 1969):

$$\phi_m \cdot \left\{ \int_{P_1}^{P_2} \frac{dp}{\rho} + g(h_2 - h_1) + \frac{1}{2} (\langle v_2 \rangle^2 - \langle v_1 \rangle^2) \right\} - W + E_v \cdot \phi_m = 0 \quad A.1$$

This energy balance simplifies to equation A.2, as the velocity of the fluid at point 1 equals the velocity at point 2 (continuity), and no work (W) is done by the surroundings on the fluid:

$$\phi_m \cdot \left\{ \int_{P_1}^{P_2} \frac{dp}{\rho} + g(h_2 - h_1) \right\} + E_v \cdot \phi_m = 0 \quad A.2$$

with E_v the amount of mechanical energy irreversibly converted to thermal energy due to friction. Solving the integral in equation A.2 (the fluid density is supposed to be independent of the pressure) results in:

$$(P_2 - P_1) + \rho g(h_2 - h_1) + \rho E_v = 0 \quad A.3$$

The force exerted by the fluid on a single particle, is multiplied with the velocity of the fluid and the total amount of particles present; this gives the total power dissipated. This dissipated power is equal to $E_v \phi_m$ (Stammers *et al.*, 1986):

$$\begin{aligned} F_{\text{drag}} \cdot \langle v \rangle \cdot N_p &= C_{\text{drag}} \frac{1}{4} \pi d_p^2 \frac{1}{2} \rho \langle v \rangle^2 \langle v \rangle \cdot N_p = E_v \rho u A \\ N_p &= \frac{L(1-\varepsilon)A}{\frac{1}{6} \pi d_p^3} \\ u &= \varepsilon \langle v \rangle \end{aligned} \quad A.4$$

$$E_v = \frac{3}{2} C_{\text{drag}} \frac{1}{2} u^2 \frac{1-\varepsilon}{\varepsilon^3} \frac{L}{d_p}$$

Combining equation A.3 and A.4 relates the drag coefficient for a single particle in a bed of identical particles to the pressure drop:

$$P_1 - P_2 = \rho E_v + \rho g \Delta h = \frac{3}{4} C_{\text{drag}} \rho u^2 \frac{1-\varepsilon}{\varepsilon^3} \frac{L}{d_p} + \rho g \Delta h \quad A.5$$

In the set-up (Figure A.1) the pressure difference between point 1 and 2 is measured, and consequently the hydrostatic pressure, $\rho g \Delta h$, is cancelled. So equation A.5 simplifies to:

$$\frac{P_1 - P_2}{L} = \frac{3}{4} C_{\text{drag}} \rho u^2 \frac{1-\varepsilon}{\varepsilon^3} \frac{1}{d_p} \quad A.6$$

Pressure drop over a packed bed due to friction between fluid and particles can be described by the Ergun equation:

$$\frac{\Delta P}{L} = \frac{150\eta u}{d_p^2} \frac{(1-\varepsilon)^2}{\varepsilon^3} + 1.75 \frac{\rho u^2}{d_p} \frac{1-\varepsilon}{\varepsilon^3} \quad A.7$$

Pressure drop can also be described with the equation of Foscolo *et al.* (1983). These authors used the same basic elements but a porosity dependent tortuosity instead of a constant tortuosity.

$$\frac{\Delta P}{L} = \left(\frac{17.3}{Re} + 0.336 \right) \frac{\rho U^2}{d_p} (1-\varepsilon) \varepsilon^{-4.8} \quad A.8$$

At a voidage of 0.4 both models give the same pressure drop.

Equation A.6 can be combined with equations A.7 or A.8 to give an equation for the drag coefficient for a single particle in a packed bed of other identical particles:

Foscolo
$$C_d = \frac{4}{3} \left(\frac{17.3}{Re} + 0.336 \right) \varepsilon^{-1.8}$$

Ergun
$$C_d = \frac{133}{Re_h} + 2.3$$

with Re_h the hydraulic Reynolds number defined as $\frac{2}{3} \frac{(1-\varepsilon)\rho U d_p}{\eta}$.

Liquid Fluidization

The pressure drop in liquid fluidization is equal to the specific buoyant weight of the bed (Foscolo *et al.* 1983):

$$\frac{\Delta P}{L} = (1-\varepsilon) \cdot (\rho_s - \rho) g \quad A.9$$

Combining equation A.9 and A.6 gives the drag coefficient of single particle in a fluidized bed of identical particles:

$$C_{drag} = \frac{4}{3} \frac{\rho_s - \rho}{\rho} \frac{\varepsilon^3}{u^2} d_p g \quad A.10$$

Nomenclature

c_1	: constant in equation 11	$\left(1 + \left(U_{mf}^2 / (v_\infty^2 \epsilon_{mf}^3)\right)^2\right)^{-0.5}$	-
c_2	: constant in equation 11	$\left(1 - c_1^2\right)^{0.5} / \left(\left(1 - c_1^2\right)^{0.5} - c_1\right)$	-
c_3	: constant in equation 13		-
c_4	: constant in equation 13		-
C_d	: drag coefficient for a single particle		-
d_p	: particle diameter		m
g	: gravity constant		$m^2 s^{-1}$
Ga	: Galileo number	$d_p^3 (\rho_s - \rho_c) \rho_c g / \eta^2$	-
k	: constant in equation 8		-
L	: length		m
n	: constant in equation 8		-
ΔP	: pressure drop		$N m^{-2}$
Re_p	: particle Reynolds number		$\rho_c v_\infty d / \eta$ -
Re	: Reynolds number	$\rho_c U d / \eta$	-
U	: superficial liquid velocity		$m s^{-1}$
v_∞	: terminal settling velocity		$m s^{-1}$

Greek

ϵ	: voidage		-
η	: viscosity		$kg m^{-1} s^{-1}$
λ	: constant in equation 11	$\left(1 - c_1^2\right)^{0.5} - c_1$	-
ρ	: density		$kg m^{-3}$
$\Delta\rho$: density difference		$kg m^{-3}$

Subscript

mf	: at minimal fluidization conditions
s	: gel bead
c	: liquid

3

Dispersed-phase hold-up in a liquid-liquid extraction spray column

Abstract

Phase hold-ups were studied in a spray column with a water/dodecane 2-phase system, in order to support the development of an extractive fermentation process. Different sparger geometries were used. Water and dodecane were introduced in co-current and counter-current flow. Although water and dodecane fluxes were of the same order of magnitude, the water flux had a minor influence on the dodecane hold-up. The nozzle geometry, however, influenced the hold-up to a large extent; the sparger with the lowest number of nozzles showed the highest hold-up at the same dodecane flux. A model that predicts the dispersed-phase hold-up in a spray column regardless of the mode of operation is presented. This model uses the slip velocity between the continuous phase and the dispersed phase to determine the dispersed-phase hold-up. The proposed model incorporates the nozzle geometry, the physical properties of the 2-phase system and the fluxes of the continuous and dispersed phase. A Richardson and Zaki type equation is used for the slip velocity. We present a new model for the power n in the Richardson and Zaki model, in which n depends on the dimensionless drift flux. The model describes the hold-up data for the water/dodecane system well. Validation of the model was obtained with a 60 mM KCl solution/dodecane 2-phase system. This 2-phase system differs only in surface tension.

Introduction

Kinetic or thermodynamic product inhibition in bioconversion processes can be reduced by integrating the conversion with an extraction process in one apparatus, so-called *in situ* extraction. The (bio)catalyst can be freely suspended or immobilized in a solid support. The protection against direct contact with extractant droplets is an important advantage of immobilized biocatalyst systems (Vermuë and Tramper, 1995). With regard to the extraction, a choice has to be made between systems with and without moving internals. Moving internals enhance the extraction process (Godfrey and Slater, 1994), but are likely to cause inadmissible damage to the solid biocatalysts. This holds especially for solid biocatalysts immobilized in a gel matrix (Wijffels *et al.*, 1995). Therefore, columns without moving internals are more appropriate for immobilized biocatalysts.

We are currently developing a fluidized bed with extractant droplets rising through the bed of biocatalytic solids. This system can be a suitable reactor set-up for biotransformations using immobilized biocatalysts and applying *in situ* extraction. This reactor set-up can offer high biocatalyst hold-up as well as high mass transfer rates. Our first aim is to predict the hold-up of the two liquids and the solids phase in this system, as these are important variables with respect to the conversion and extraction rates. In order to understand the behavior of the 3-phase system we have studied the behavior of the spray column with two liquids (the extractor) and a fluidized bed with one liquid and suspended solids (the reactor) separately. This paper describes the work on the spray column.

Although the dispersed-phase hold-up in spray columns has been studied several times (Kumar and Hartland, 1991; Godfrey and Slater, 1994), the models resulting from these studies cannot be extended straightforwardly to models predicting the dispersed-phase hold-up in the above-mentioned 3-phase fluidized bed. We believe that the prediction of droplet hold-up in such a 3-phase system can be based on the prediction of droplet hold-up in a spray column. Such an extension of a 2-phase model to a 3-phase model predicting the dispersed-phase hold-up, has been demonstrated for the prediction of the gas hold-up in a liquid-solid-gas fluidized bed (Chen and Fan, 1990). Richardson and Zaki's model (Richardson and Zaki, 1954) for solid fluidization can be extended to predict the hold-up of the different components in a multi-component fluidized bed (Van der Wielen *et al.* 1996).

This article presents a model that predicts the dispersed-phase hold-up in a

spray column regardless of the mode of operation. This model can be easily extended to predict the dispersed-phase hold-up in a 3-phase system. The slip velocity between the continuous phase and the dispersed phase is used to determine the dispersed-phase hold-up, analogous to models presented in literature. The slip velocity is described with Richardson and Zaki's model for a fluidized system of mono-sized particles. This model uses two parameters, viz. the terminal rise velocity of a single droplet and a power n . The terminal velocity can be calculated with models from literature, but models for determining the power n in liquid-liquid 2-phase systems have not yet been published. In this paper we will propose a new model for this power n .

Theory

The dispersed-phase hold-up can be predicted according to a model presented below. A schematic overview of this model is shown in Figure 1. This figure shows how the combination of a definition of the slip velocity and a model for this slip velocity can be used to predict the dispersed-phase hold-up. This figure also shows how the various operating variables (superficial velocity of both phases and lay-out of the sparger) as well as the physical properties of the 2-phase system influence the slip velocity, and hence the dispersed-phase hold-up.

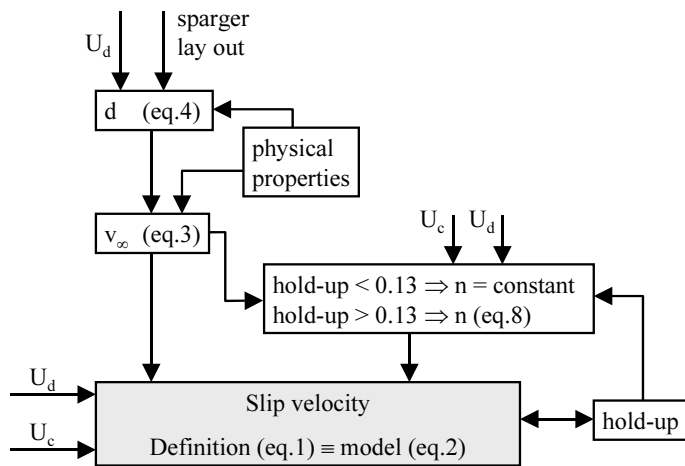


Figure 1. Schematic representation of the model for the prediction of the dispersed-phase hold-up. Droplet Hold-ups are less than 0.23. U_d : superficial velocity dispersed phase; U_c : superficial velocity continuous phase; v_∞ : terminal rise velocity of a single droplet; n : power n in equation 2; d : droplet diameter.

Slip velocity

The slip velocity (v_{12}) is defined as the difference between the velocities of both phases taking into account the direction of flow:

$$v_{12} = \frac{\vec{U}_{sd}}{\alpha} - \frac{\vec{U}_{sc}}{1 - \alpha} \quad 1$$

with U_{sd} is the superficial velocity of the dispersed phase, U_{sc} is the superficial velocity of the continuous phase and α is the dispersed-phase hold-up. Upward flow is taken as the positive direction for both flows.

The relationship between slip velocity and hold-up is implicit: the dispersed-phase hold-up is determined by the slip velocity and the slip velocity depends on the dispersed-phase hold-up. Empirical models that predict directly the dispersed-phase hold-up have been reviewed (Kumar and Hartland, 1995). However, these authors demonstrated that those empirical models are less accurate than slip velocity models.

Different relations for slip velocity can be found in literature (Kumar and Hartland, 1995; Godfrey and Slater, 1991). Godfrey and Slater state that the best equation describing the slip velocity is the equation of Kumar and Hartland (Kumar and Hartland, 1985). Godfrey and Slater (1991) also concluded that most of the equations describing slip velocity can be summed up to one equation based on Richardson and Zaki's equation for fluidized systems of mono-sized rigid particles:

$$v_{12} = v_k (1 - \alpha)^n \quad 2$$

with v_k a characteristic velocity, in most cases equal to the terminal rise velocity of a single droplet (v_∞). The power n indicates the influence of liquid flow around a droplet. To calculate the slip velocity (eq.2), models for the terminal rise velocity and power n are needed. As the terminal rise velocity depends on the droplet diameter, also a model is needed to predict this diameter (see also Figure 1).

Terminal rise velocity

Godfrey and Slater (1994) give a selection chart, based on physical properties of both phases, for choosing the best-suited terminal rise-velocity equation. The selection is mainly based on the Morton number of the 2-phase system, with the Morton-number

defined as $Mo = \frac{g \Delta \rho \eta_c^4}{\rho_c^2 \sigma^4}$. We have studied a water/dodecane 2-phase system. The surface tension between water and dodecane is high, which results in a low Morton number. Therefore, based on the selection chart, Vignes' equation was used:

$$v_\infty = \frac{d}{4.2} \left(\frac{g \Delta \rho}{\rho_c} \right)^{2/3} \left(\frac{\rho_c}{\eta_c} \right)^{1/3} \left(1 - \frac{Eo}{6} \right) \quad 3$$

where d is the droplet diameter, g is the gravity constant, $\Delta \rho$ is the density difference between water and dodecane, ρ_c is the density of the continuous phase, η_c is the viscosity of the continuous phase. Eo is the Eötvös-number defined as $\frac{g \Delta \rho d^2}{\sigma}$, representing the ratio of the buoyancy force over the resistive force defined by the interfacial tension.

Droplet diameter

Liquid droplets can be made by pumping liquid through one or more nozzles. An overview of different droplet formation mechanisms is given elsewhere (Dalingaros *et al.*, 1986). At a nozzle Weber number less than 2, single drops are formed at the tip of a nozzle, with the nozzle Weber number defined as $\frac{\rho u_{noz}^2 d_{noz}}{\sigma}$. The Weber number represents the ratio between inertial force and resistive interfacial force. At a nozzle Weber number between 2 and a critical nozzle Weber number 8.64, drops are formed by uniform break-up of the liquid jet existing in this range. Above a nozzle Weber number of 8.64 the liquid jet starts to atomize and a broad droplet-size distribution is formed. A single relation covering nozzle Weber numbers up to 8.64 has been derived by Kumar and Hartland (1996):

$$d = \frac{d_{noz}}{0.55 Eo_{noz}^{0.33} + 0.0393 We_{noz}^{0.73} \left(\frac{\rho_d g d_{noz}^2}{\sigma} \right)^{-0.315}} \quad 4$$

where d_{noz} is the nozzle diameter, Eo_{noz} is the Eötvös number based on the nozzle dimensions, ρ_d is the density of the dispersed phase, and σ is the interfacial tension between water and dodecane. This relation was used here for calculating the droplet diameter.

Power n

A model predicting the power n used in the slip velocity model (eq.2), has not yet been published for liquid-liquid 2-phase systems. It is concluded by Godfrey and Slater (1991) that this power n has a value between 0 and 4. When the interfacial tension is high, liquid droplets can be regarded as solid particles. In that case relations for the power n derived for water and solid particles can be used. An overview of different relations and their accuracy can be found elsewhere (Hartman *et al.*, 1994). However, we will show that these models for the power n do not describe the slip velocity for a water-dodecane 2-phase system accurately. As slip velocity and hold-up are closely related, see Figure 1, the dispersed-phase hold-up is also not well predicted.

In this study we will propose a new model for the power n ; for reasons of clarity this model is integrated in the Results and Discussion section. Applying the total model as given in Figure 1, i.e. the combination of equation 1 and 2, the new model for the power n , and the presented equations for droplet diameter (eq.4) and terminal rise velocity (eq.3), the experimental dispersed-phase hold-up is well described. Data from a water/dodecane 2-phase system with a different surface tension are well predicted by the model presented in Figure 1.

Materials and Methods

Wageningen tap water was used as continuous phase and n-dodecane (Aldrich, 99%+ pure) as dispersed phase. As the n-dodecane is lighter than tap water, it was introduced in all experiments at the bottom of a 2 m high and 60 mm internal-diameter column equipped with sample ports to make measurements at different heights. Tap water was introduced at the bottom of the column in co-current operation and at the top in counter-current operation. On top of this column a phase separator was placed with a diameter of 180 mm. As water and n-dodecane are highly immiscible, phase separation was easily achieved for the applied fluxes.

Co-Current Operation

Figure 2 shows schematically the experimental set-up. Both tap water and n-dodecane were introduced through a sparger at the bottom of the column. The separated phases at the top of the column were sent back to the storage vessels to allow recirculation of both liquids. As the storage vessels were jacketed, temperature could be maintained at $25\pm 1^\circ\text{C}$ by circulating water of appropriate temperature. No temperature gradient was observed between top and bottom of the column.

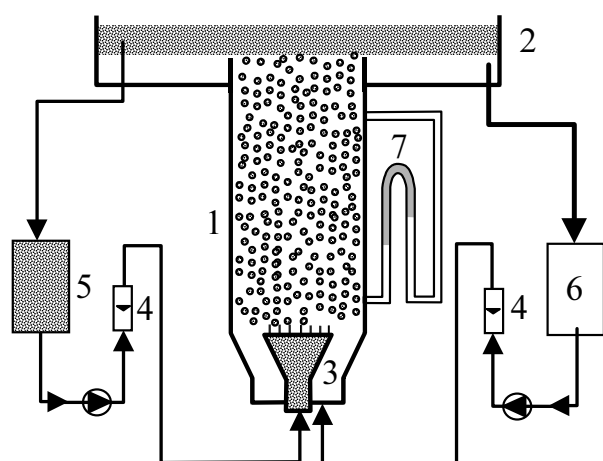


Figure 2. Experimental set-up for co-current operation. 1 column; 2 phase separator; 3 sparger; 4 rotameters; 5 dodecane storage vessel; 6 tap water storage vessel; 7 inverse water manometer

Liquid Distributor. The liquid distributor is schematically shown in Figure 3a. This distributor consisted of an inner and an outer cone. The distance between both cones was constant, with dodecane flowing through the inner cone, and the tap water through the outer one. Both cones had a 10° angle and were filled with glass beads to provide a good flow distribution. The maximum diameter of the outer cone was 60 mm, the inner cone had a 30 mm maximum diameter. On top of the inner cone a sparger was placed, which consisted of a number of nozzles. An overview of the different spargers used is given in Table I. The nozzles were made of hollow stainless-steel tube with a length of 3 cm, which were hammered through a Teflon plate. The distance between the nozzles was arranged in such a way, that the growing droplets did not touch each other. The nozzles were evenly distributed over the area of a circle with a 30 mm diameter.

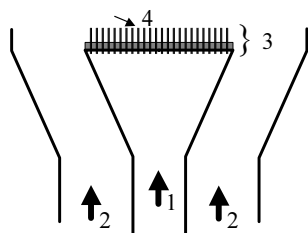


Figure 3a. Liquid distributor in co-current operation. 1 dodecane inlet; 2 water inlet; 3 sparger; 4 nozzles

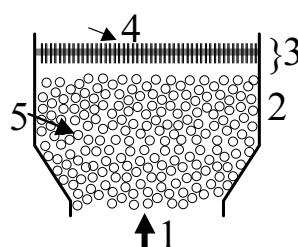
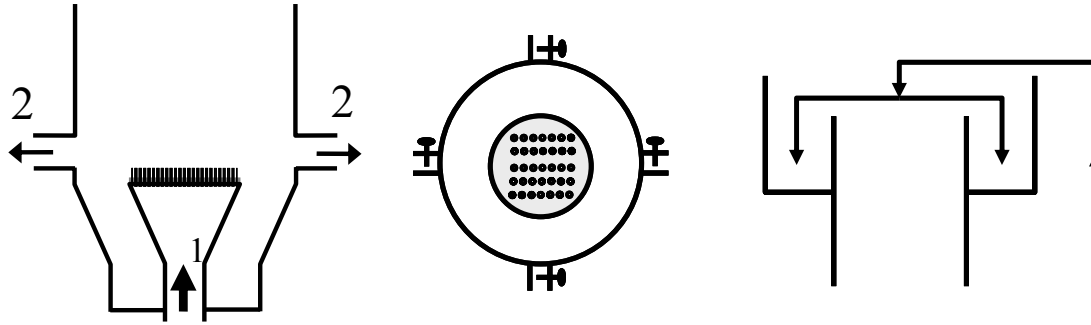


Figure 3b. Alternative liquid distributor in counter-current operation. 1 dodecane inlet; 2 water inlet; 3 sparger; 4 nozzles; 5 glass pearls.

Counter-Current Operation

The same experimental set-up was used as described in the co-current operation part, except for the introduction and recirculation of the tap water. Figure 3c gives details of the changes made in the co-current experimental set-up to make counter-current water recirculation possible. The first adaptation was made in the glass column wall, see Figure 3c1 and 3c2; the wall had four circular openings, diameter 10 mm, located in one plane at 90° relative to each other, Figure 3c2. These openings were 1 cm above the liquid distributor, Figure 3c1. The flows through these openings were adjusted with throttle valves in such a way that they equaled each other. The second adaptation was made on the tube used for the water introduction at the top of the column, see also Figure 3c3. This tube was split in two parts, and both ends were directed to the outer wall and bottom of the annulus made up between column and enlarged column, see also Figure 3c3. In this way plug flow was assured through the

column. This was visually verified by color-pulse experiments. With these color-pulse experiments a flat front was still observed at the bottom of the column. Although only the dodecane storage vessel was maintained at $25\pm 1^\circ\text{C}$ by circulating water of appropriate temperature, a temperature gradient was not observed in the column.



3c1

3c2

3c3

Figure 3c. Details on adaptations made on the co-current experimental set-up for counter-current operation

Liquid Distributor. The same liquid distributor was used for dodecane dispersal as described with the co-current operation. Also another sparger was used, see Figure 3b. This liquid distributor consisted of a sparger with 209 nozzles (5 cm length and 1 mm diameter), evenly distributed over the area of a circle with a 60 mm diameter. On top of a cone a 10 cm high glass column, diameter 6 cm, was placed. The cone had an angle of 10° and a maximum diameter of 60 mm. Both cone and column were filled with glass beads to provide a good flow distribution over the nozzles that were placed on top of the glass column.

Table I. Different spargers used in experiments.

	# nozzles	nozzle diameter (mm)
sparger 1	12	1.4
sparger 2	23	1.0
sparger 3	37	1.0
sparger 4	54	1.0
sparger 5 ¹	209	1.0

¹ only in counter-current operation

Measurements

The hold-up of n-dodecane at different flow rates of tap water and n-dodecane was determined with a reversed U-tube water manometer. To increase the accuracy, the water manometer was filled with hexanoic acid ($\rho=921 \text{ kg m}^{-3}$). These measurements were used to determine the parameters in the model for the power n. Dodecane hold-up measurements have also been done with a slightly different 2-phase system: a 60 mM KCl solution as continuous phase and the same dodecane as dispersed phase. These measurements were used to validate the new model.

The fluxes of tap water and dodecane were measured with calibrated rotameters (Sho-Rate). The flux of tap water ranged from 0 to 0.7 cm s^{-1} and the dodecane flux ranged from 0 to 1.25 cm s^{-1} .

The static interfacial tension between continuous phase and dispersed phase was determined with the Wilhelmy-plate method.

The average deviation (AVD) between measurement and model is defined as:

$$\text{AVD} = \sum \left| \frac{\alpha_{\text{meas}} - \alpha_{\text{mod}}}{\alpha_{\text{meas}}} \right| / N - 1 \quad 5$$

Results and Discussion

The dispersed-phase hold-up was measured for different sections of the column and different combinations of dodecane and water fluxes. From these data (not shown) it can be concluded that an axial hold-up profile is not significant for any of the combinations. Radial profiles may exist (Ueyama and Miyauchi, 1979). However, for the sake of simplicity, a uniform distribution of the droplets across the column diameter is assumed here.

Zero water flux

The effect of the sparger lay-out on the measured dodecane hold-up is shown in Figure 4. In this figure experimental data are shown for spargers 3, 4 and 5 at zero water flux. The same trends were observed for the co- and counter-current hold-up data. Hold-up increases with an increasing superficial dodecane velocity. Figure 4

clearly shows that the increase in hold-up is larger for a sparger with a lower number of nozzles. This holds especially at dodecane fluxes larger than 3 mm s^{-1} .

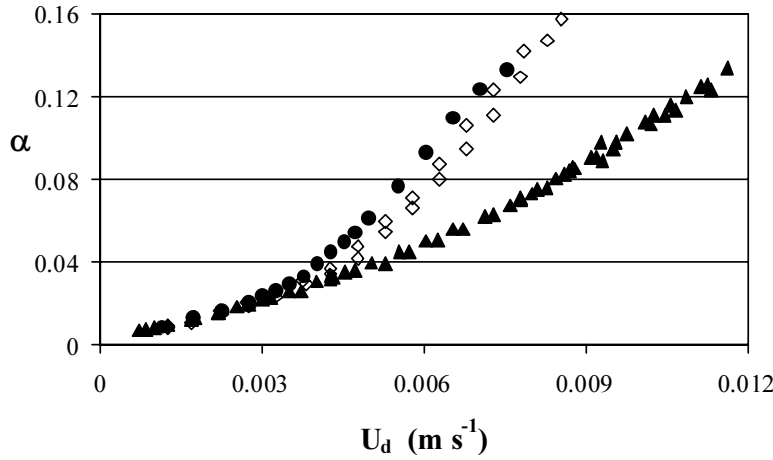


Figure 4. Dodecane hold-up versus dodecane superficial velocity for sparger 3 to 5 (Table I).

● sparger 3, 37 nozzles; ◇ sparger 4, 54 nozzles; ▲ sparger 5, 209 nozzles

The difference between these spargers can be explained by considering the one-dimensional continuity equation for the dodecane phase:

$$U_d = \alpha v_d \Rightarrow \alpha = \frac{U_d}{v_d}$$

So the dodecane hold-up (α) is defined by the ratio between the superficial velocity (U_d), and the true velocity (v_d) of the dodecane phase. If it is assumed that the droplets do not influence each other, then the true velocity equals the rise velocity of a single droplet. At an equal superficial dodecane velocity there is a difference in droplet diameters generated by the different spargers, as the diameter depends on the dodecane velocity through one nozzle (see also the section on the droplet diameter). A smaller number of nozzles per sparger will result in a higher velocity through one nozzle, and hence a smaller diameter. A smaller diameter results in a lower terminal rise velocity (eq.3) and hence a higher hold-up.

Figure 4 shows data up to a nozzle Weber number of 8.64. Above this nozzle Weber number atomization of the liquid jet starts; a broad droplet-size distribution will occur, and the slip velocity is not described by equation 2. Moreover, phase separation becomes less straightforward, as it can not be achieved by a single-stage phase-separator that is based on gravity.

Figure 5 shows data for spargers 1 and 2. In this figure, contrary to Figure 4, the superficial velocity goes beyond the velocity corresponding with the critical nozzle

Weber number. Figure 5 shows that for sparger two at each superficial dodecane velocity, the hold-up is equal or larger compared with data for sparger 1. Below the critical nozzle Weber number this is explained in exactly the same way as above: at a dodecane superficial velocity of 3 mm s^{-1} the velocity through one nozzle equals 0.459 m s^{-1} for sparger 1 (12 nozzles, with a diameter of 1.4 mm), and 0.470 m s^{-1} for sparger 2 (23 nozzles, with a diameter of 1 mm). At this superficial velocity the droplet diameters (eq.4) and terminal rise velocities (eq.3), are 3 mm and 0.123 cm s^{-1} for sparger 1, and 2.4 mm and 0.103 cm s^{-1} for sparger 2. Consequently, the hold-up is expected to be higher for sparger 2. (The physical properties used for calculating droplet diameter, and terminal rise velocity are given in Table II).

Table II. Physical Properties of the liquids applied at $25 \pm 1^\circ\text{C}$.

	Density kg m^{-3}	Viscosity Pa s	Surface tension ¹ mN/m	Surface tension ² mN/m
Tap water	998	0.00093	68-63.5	40
Dodecane	742.7	0.0012	24	

¹surface tension against water, ²surface tension between tap water and dodecane

At a zero water flux the slip velocity reduces to the true velocity, $\frac{U_d}{\alpha}$. In Figure 5 this velocity is shown as a function of the superficial dodecane velocity. The true dodecane velocity is almost constant above a certain value of the superficial dodecane velocity.

For both spargers this value corresponds with the critical superficial dodecane velocity, calculated from the critical nozzle Weber number. This Weber number is indicated by the vertical lines in Figure 5. So above the critical nozzle Weber number the true dodecane velocity is independent of the hold-up. This means that the hold-up is linearly proportional to the superficial dodecane velocity, as indicated by the dotted lines in Figure 5. Obviously the relationship between hold-up and superficial dodecane velocity becomes different above the critical nozzle Weber number.

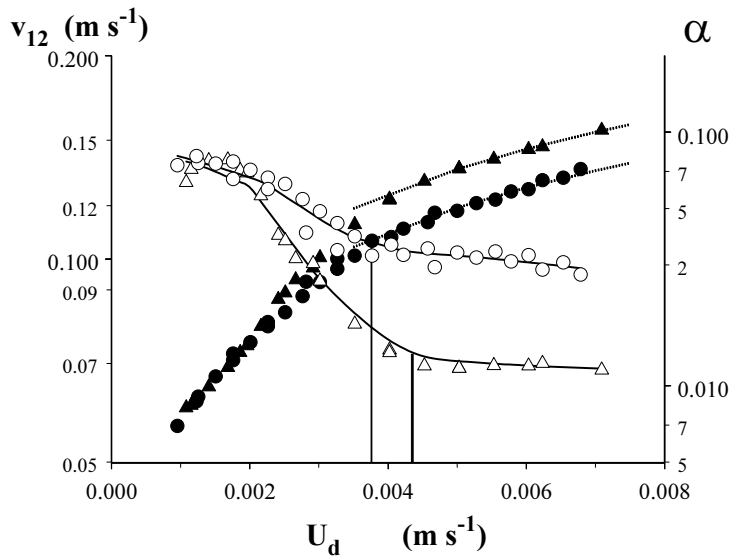


Figure 5. Dodecane hold-up (closed symbols) and slip velocity (open symbols) versus dodecane superficial velocity for sparger 1 and 2. ● sparger 1, 12 nozzles, i.e. 1.4 mm; ▲ sparger 2, 23 nozzles, i.e. 1 mm. Superficial water velocity is zero.

Co- and counter-current water flux

The above-described characteristics for dodecane hold-up at zero water flux are also observed for co- and counter current operation, when the dodecane flux is changed at a constant water flux (data not shown). At low superficial dodecane fluxes, i.e. low hold-ups, no effect of the water flux can be observed. At higher superficial dodecane fluxes, i.e. higher hold-ups, there is a small effect of the water flux. For co-current operation an increase in water flux resulted in a slightly lower hold-up at the same superficial dodecane flux, whereas for counter-current operation a slightly higher hold-up was measured. Obviously, this is straightforwardly explained by the reduction or increase of the true dodecane velocity at counter- or co-current operation, respectively.

Under the conditions tested the influence of the superficial water velocity is marginal. This can be illustrated by comparing the true water velocity with the true dodecane velocity: at a superficial water velocity of 7.51 mm s^{-1} , and a superficial dodecane velocity of 7.14 mm s^{-1} , a dodecane hold-up of 0.14 was measured in counter-current operation using sparger 4 (54 nozzles). With these values the true dodecane velocity becomes 5.8 times higher than the true water velocity:

$$\frac{U_d}{\alpha} \cdot \left(\frac{U_c}{1-\alpha} \right)^{-1} = \frac{7.14}{0.14} \cdot \left(\frac{7.51}{0.86} \right)^{-1} = 5.8$$

Dodecane hold-up can be manipulated to a large extent with the sparger lay-out and to a minor extent with the mode of operation. Less nozzles on a sparger give a higher hold-up at the same superficial dodecane flux. However, for a sparger equipped with few nozzles, the dodecane flux corresponding with a nozzle Weber number of 8.64 is lower compared with a sparger equipped with more nozzles. Under our conditions the water flux only slightly influenced the dodecane hold-up. A larger influence can be expected with increasing water flux. In counter-current operation this would yield a higher hold-up. However, at the higher applied water fluxes satellite-formation was observed. As these satellites form emulsions, and phase separation of emulsions is not straightforward, the water flux cannot be increased unlimitedly. Also, in counter-current operation, flooding will occur at a certain water flux.

Modeling droplet hold-up

The droplet hold-up can be predicted from an accurate slip velocity model (Kumar and Hartland, 1985):

$$\frac{4}{3} d g \Delta \rho (1 - \alpha) = \rho_c v_{12}^2 (1 + 4.56 \alpha^{0.73}) \cdot \left(0.53 + \frac{24 \eta_c}{d v_{12} \rho_c} \right) \quad 6$$

However, this model can not be extended easily to systems with more than two phases. A slip velocity model (eq.2), analogous to the Richardson and Zaki model (1954), can be easily extended. Figure 1 shows how from such a model the droplet hold-up can be predicted. This model, however, depends on a model for the power n , which has not been developed yet. Below a model will be proposed to predict this power n . This model holds for dispersed-phase velocities up to velocities corresponding with the critical nozzle Weber number of 8.64.

Obviously, the power n can be obtained from fitting equation 2 to the slip velocity, with this velocity determined from the experimental hold-up. However, especially at low hold-ups, the relative error in the hold-up is large, and consequently there is large scatter in the slip velocity. This scatter largely disappears when the slip velocity is transformed to a drift flux, U_{dc} (adapted from Wallis, 1969):

$$U_{dc} = \left(\frac{U_d}{\alpha} - \frac{U_c}{1 - \alpha} \right) \alpha \cdot (1 - \alpha) = v_{12} \alpha \cdot (1 - \alpha) = v_{\infty} \alpha \cdot (1 - \alpha)^{n+1} \quad 7$$

A drift flux represents the volumetric flow rate of the dispersed-phase relative to a surface moving at the volumetric average velocity ($U_d + U_c$) (Wallis, 1969). Next, the drift flux is made dimensionless by dividing this drift flux by the terminal rise velocity (eq.3). For all the spargers applied, the dimensionless drift-flux, derived from experiments for co- and counter-current operation, is shown in Figure 6 as a function of the dodecane hold-up. This figure shows that the dimensionless drift flux is virtually independent of the sparger lay-out.

Equation 7 was fitted to the dimensionless drift flux data up to a dispersed-phase hold-up of 0.13. This gave a power n of 4.00 with a 95% confidence interval of 0.07.

Up to a hold-up of 0.13 the dimensionless drift flux is well described with a constant power n . At higher hold-ups this model systematically underestimates the dimensionless drift flux, as can be seen in Figure 6. An underestimation of the dimensionless drift flux means that the power n in equation 7 is too large. It appears that the power n , derived from the measured hold-up and equations 3 and 7, decreases monotonically with the dimensionless drift-flux. So a new model is proposed for the power n :

$$n = n_0 - c_1 \left(\frac{U_{dc}}{V_\infty} \right)^{c_2} \quad 8$$

The dimensionless drift flux, defined as the drift flux divided by the terminal rise velocity of a single droplet, is shown in Figure 6. This figure shows that the dimensionless drift flux (U_{dc}^*) becomes constant for higher hold-ups. The hold-up for which U_{dc}^* becomes constant, is called $\alpha_{boundary}$, and is also shown in Figure 6. So, the new model for the power n , equation 8, is applicable for hold-ups up to $\alpha_{boundary}$.

The total model for predicting the dimensionless drift flux consists of two parts:

- for hold-ups below $\alpha_{boundary}$, the model is represented by Figure 1:
 - nozzle lay-out and physical properties of the 2-phase system determine the terminal rise velocity of a droplet;
 - a definition and a model of the slip velocity transformed to a drift flux, eq.7;
 - a model for the power n , eq.8.
- for holds-ups above $\alpha_{boundary}$, the dimensionless drift flux is constant, and equal to 0.0975 with a 95% confidence interval of 0.0004.

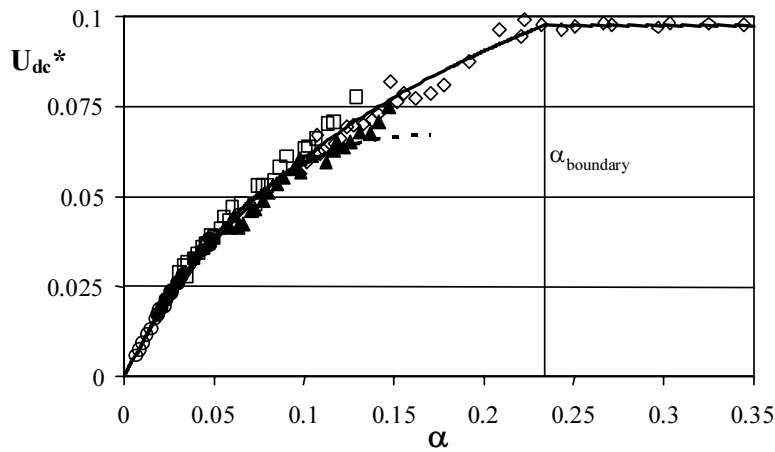


Figure 6. Dimensionless drift flux versus dodecane hold-up. O sparger 1; ● sparger 2; □ sparger 3; ▲ sparger 4; ◇ sparger 5. — total model with $n = f(U_{dc})$, ... total model with $n=4$

Both parts of the model hold at the α_{boundary} , which gives an additional equation for the coefficients n_0 , c_1 , and c_2 . Using equation 7, with the hold-up equal to α_{boundary} , and the dimensionless drift flux equal to its constant value (0.0975), a corresponding power n can be calculated: this is n_{boundary} . Substituting this n_{boundary} in equation 8, gives the following relationship between the coefficients in equation 8.

$$n_0 - n_{\text{boundary}} = c_1 \cdot 0.0975^{c_2} \Rightarrow c_2 = \ln\left(\frac{n_0 - n_{\text{boundary}}}{c_1}\right) \cdot \frac{1}{\ln(0.0975)} \quad 9$$

If coefficient c_2 is determined with equation 9 at any given n_0 , c_1 and n_{boundary} both parts of the model for the dimensionless drift flux will hold at α_{boundary} .

A clear value for α_{boundary} cannot be determined unambiguously from Figure 6. Therefore α_{boundary} has been varied on the interval 0.19...0.24. At each α_{boundary} a corresponding n_{boundary} is calculated, and the coefficients n_0 and c_1 are fitted to equations 3, 7, 8 and 9 by minimizing the residual sum of squares of measured and predicted droplet hold-up (equation 10), using a downhill simplex method (Nelder and Mead, 1965):

$$SS_{\text{res}} = \sum_i (\alpha_{i,\text{measured}} - \alpha_{i,\text{predicted}})^2 \quad 10$$

In appendix A it is shown that the parameters n_0 and c_1 cannot have an arbitrary value, but are subjected to some constraints. Applying these constraints, fitting was

successful with the next set of parameters yielding the lowest sum of squares of residuals: $\alpha_{\text{boundary}}=0.233$, $n_0=6.55$ and $c_1=33.2$. Coefficient c_2 follows from equation 9 and is equal to 0.88. It is concluded from Fig 6, which shows the dimensionless drift flux predicted with equations 3, 7, 8 and 9 and the fitted constants, as well as the experimentally determined dimensionless drift flux, that the prediction of the model is good. This is also supported by the parity plot in Figure 7.

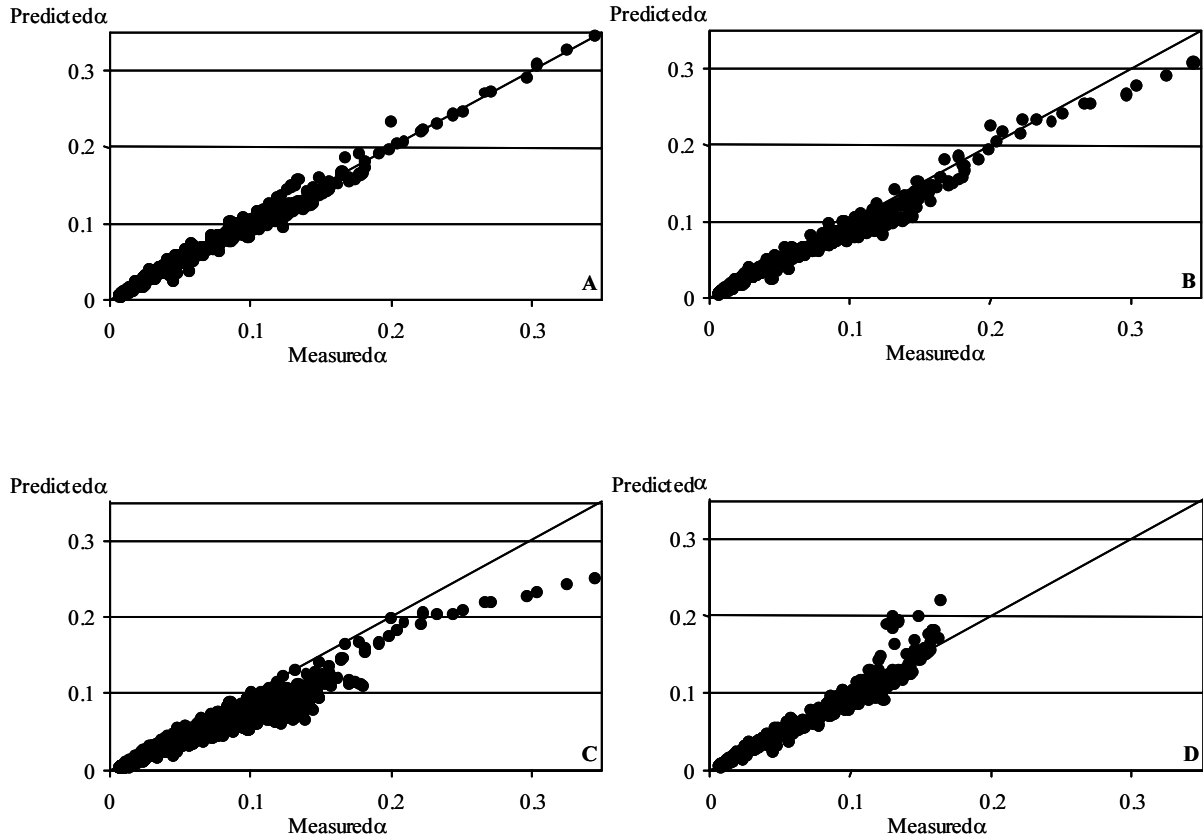


Figure 7. Parity-plot between measured and predicted dodecane hold-up for different models. A : presented model; B : slip velocity model of Kumar and Hartland 1985; C : explicit model of Kumar and Hartland 1995; D : slip velocity model with n according Richardson and Zaki 1954

A complete analysis of the confidence intervals of the fitted parameters is beyond the scope of this paper. However, to get some insight in the sensitivity of the model to its parameters, the SS_{res} was calculated at different combinations of parameters n_0 and c_1 for $\alpha_{\text{boundary}}=0.23$. The SS_{res} for the fitted parameters is equal to 0.0244. Figure 8 shows contour lines at 1, 5 and 10 % higher values than the minimal SS_{res} . This figure also shows the relation between the parameters n_0 and c_1 that resulted from the constraint

used in the fitting procedure. At the left, the end of this constraint line is (25.5; 8.5); for lower c_1 -values the constraint function does not exist. This Figure 8 ends at $c_1=60$, as for higher c_1 values the constraint is violated for the contour lines. For values of n_0 and c_1 in the area below the constraint line, the contours are continuous and smooth. For values of n_0 and c_1 in the area above the constraint line, the contours are discontinuous and behave not at all smooth. This behavior results from the constraint violation, see also appendix A. The 5 and 10% contour lines cover a broad interval for n_0 and c_1 . For n_0 the minimum and maximum values are 5.4 ($0.82 \times$ fitted value) and 11.1 ($1.71 \times$ fitted value), and for c_1 these values are 21.75 ($0.66 \times$ fitted value) and 60 ($1.81 \times$ fitted value), all referring to the 5% contour line. The large range might suggest that the model seems insensitive to its parameters. However, at a given c_1 the allowed range for n_0 is limited, as can be seen in Figure 8.

Up to a hold-up of 0.13 a constant n of 4 suffices to describe the data (see Fig 6). This is in agreement with the results of Godfrey and Slater (1991), who concluded that this power is between 0 and 4. This power n also compares well with values of n derived from literature models for liquid fluidization of solid spheres at laminar flow conditions (Richardson and Zaki (1954), $n=3.65$; Rowe (1987), $n=3.7$; Foscolo (1987), $n=3.8$; Garside and Al-Dibouni (1977), $n=4.09$). Apparently, the dodecane droplets behave as solid spheres at laminar flow conditions. At a high interfacial tension droplets indeed tend to behave like solids. The interfacial tension between water and dodecane is 40 mN m^{-1} . Such an interfacial tension is regarded as high. So the solids-like behavior of the droplets is to be expected.

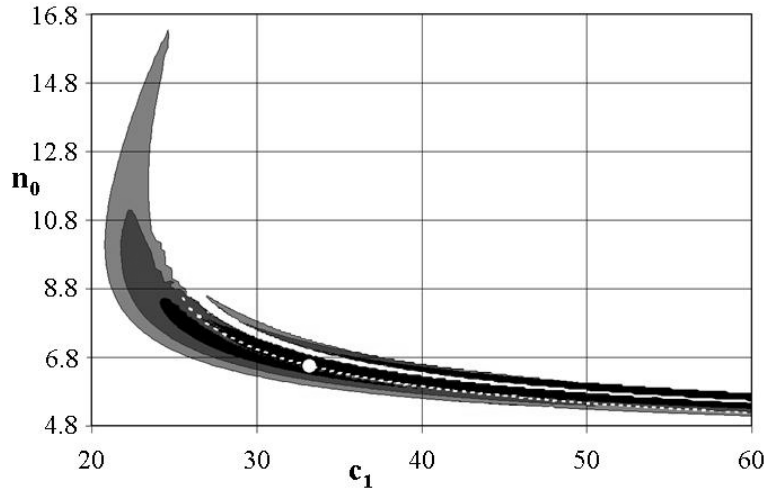


Figure 8. Sensitivity analysis for parameter n_0 and c_1 of the presented model. Contour lines of 1% (black), 5% (dark grey) and 10% (grey) higher values than the SS_{res} for $n_0=6.33$ and $c_1=33.2$ (●), --- constraint line

The transition from a constant power n of 4 to a decreasing power n might indicate a deviation from laminar flow to more turbulent flow. For this type of droplet flow, this transition corresponds with a certain dimensionless drift flux (0.065) or dispersed-phase hold-up (0.13), instead of a single Reynolds number. This is in contrast to what is suggested in literature (Wallis, 1969). To illustrate that this transition does not correspond to a single Reynolds number, but to an endless set of Reynolds numbers, we calculated the superficial dodecane velocity at different nozzle geometries, and two column diameters, that will result in a hold-up of 0.13. Figure 1 shows how this can be achieved; the results are shown in Table III. This table clearly shows that there is not a constant Reynolds number for the transition from a constant power n to a decreasing power n .

Table III. Droplet characteristics at the transition from laminar to more turbulent flow for different sparger geometries (nozzle diameter is 1 mm), and two column diameters:
D₁=6 cm, D₂=9 cm.

# nozzles	U _d (mm s ⁻¹)		v _∞ (m s ⁻¹)		d (mm)		Re	
	D ₁	D ₂	D ₁	D ₂	D ₁	D ₂	D ₁	D ₂
50 ¹	7.3	-	0.098	-	2.3	-	254	-
100	9.3	7.0	0.124	0.094	3.0	2.1	425	230
200	10.8	9.0	0.145	0.120	3.7	2.9	607	394
500	11.8	11.0	0.158	0.147	4.2	3.7	764	631

¹ for this sparger, the liquid velocity through one nozzle to obtain a hold-up of 0.13 using a column with diameter D₂ should be larger than the maximum velocity corresponding with a nozzle Weber number of 8.64. So no calculations of terminal droplet rise velocity and droplet diameter could be done.

Comparison with literature models

Different models from literature were evaluated with all the measured droplet hold-ups (N=912). Their prediction is expressed as the average deviation (AVD), as defined by equation 5. The results are given in Table IV, and parity plots for the different models are shown in Figure 7 (the physical constants used are given in Table II).

It can be concluded from Table IV and Figure 7 that, for the whole range of measured hold-ups, only the slip-velocity model (Kumar and Hartland, 1985), eq.6, predicts the measured hold-ups well. Up to a hold-up of 5% the prediction is good; at larger hold-ups the model slightly underestimates the experimental data. This model is based on a force balance around a single droplet and a hold-up dependent drag coefficient to account for the presence of other droplets. This model was derived for a large number of different 2-phase systems with a wide range of physical constants.

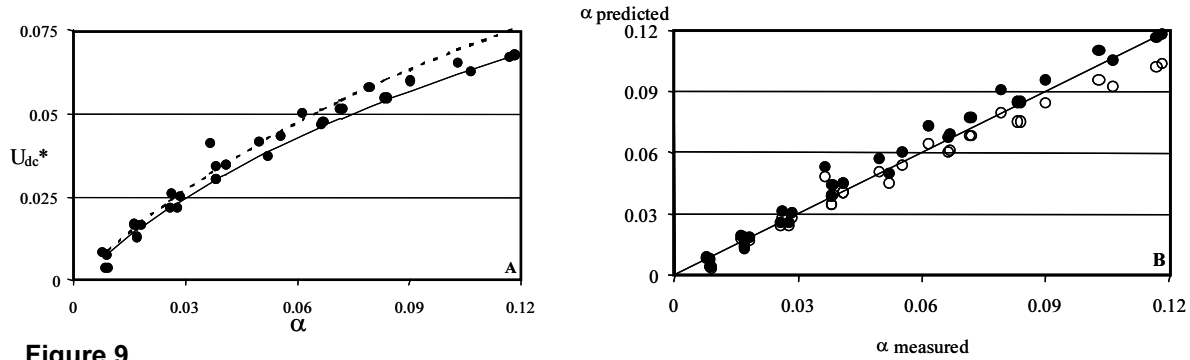
For hold-ups up to 15% the hold-up is well predicted with a slip velocity according to equation 2 and a power n according to Richardson and Zaki (1954). At higher hold-ups no solution for the hold-up is possible. The good prediction of the Richardson and Zaki model is not surprising as the power n is between 4.2 and 4.3 (the value of the power n obtained from fitting the hold-up data up to 13% is equal to 4.0).

Table IV. Comparison of measured data with models from literature. Physical constants are given in Table II.

	AVD	Remarks
<i>Droplets behave like solids</i> Richardson and Zaki (1954)	0.0728	Good prediction of the hold-up up to 15%, at higher hold-ups no solution of the model for the hold-up
<i>A slip velocity model</i> Kumar and Hartland (1985)	0.0797	Good prediction of the data, 68% of the data show a deviation less than 10%, 95% of the data has a deviation less than 20%
<i>An explicit model</i> Kumar and Hartland (1995)	0.2748	All data points are underestimated
<i>Presented model</i>	0.0750	Good prediction of the data, 72% of the data show a deviation less than 10%, 97% of the data has a deviation less than 20%

Validation of the presented model

As mentioned in the experimental part, a different 2-phase system was used to validate the newly proposed model; the continuous phase is a 60 mM KCl-solution instead of tap water and dodecane is again used as dispersed phase. The physical properties are equal to those for a tap-water/dodecane 2-phase system, except for the interfacial tension, which is equal to 29 mN m^{-1} , in contrast to 40 mN m^{-1} for the first 2-phase system. Figure 9A shows the measured dimensionless drift-flux, as well as the predictions of our proposed model, and those from Kumar and Hartland (1985), eq.6, as a function of the dodecane hold-up. Figure 9B shows the parity plot for predicted and measured droplet hold-up for both models. It can be concluded from Figure 9A-B, that both models predict the droplet hold-up well; the AVD as defined by equation 5, is 0.119 for the model of Kumar and Hartland (1985), and 0.115 for the presented model. At higher hold-ups, however, our model predicts the dimensionless drift-flux and hold-up better. At these higher hold-ups the model of Kumar and Hartland overestimates the dimensionless drift flux, and underestimates the hold-up.

**Figure 9**

A. Dimensionless drift flux versus dodecane hold-up. Continuous phase is a 60 mM KCl solution. ● : data; — : presented model; --- : model of Kumar and Hartland, 1985.

B. Parity plot between predicted and measured hold-up. ○ : model of Kumar and Hartland, 1985; ● : presented model.

Conclusion

The sparger lay-out influences the dodecane hold-up. A higher hold-up is obtained with a sparger with less nozzles and the same nozzle diameter, using the same superficial dodecane velocity. The presented hold-up model predicts well the dispersed-phase hold-up and related properties like slip velocity and drift-flux. This model uses the definition of the slip velocity and a Richardson and Zaki type equation for the slip velocity: an equation for the droplet diameter and an equation for the terminal rise velocity of a single droplet. Up to a hold-up of 0.13, or a dimensionless drift-flux of 0.065, a constant n of 4 in the slip-velocity model suffices to describe the hold-up adequately. At hold-ups higher than 0.13 the parameter n decreases with an increasing dimensionless drift-flux. A model for this parameter based on the dimensionless drift-flux is used in the hold-up model, which predicts the dispersed-phase hold-up from zero to 0.23 well. At hold-ups larger than 0.23 the dimensionless drift flux becomes constant.

Up to 0.15 the slip velocity model of Richardson and Zaki (1954) for solids predicts the data well, but for higher hold-ups this model gives no solution. The model of Kumar and Hartland (1985) is applicable for the whole range of measured hold-ups; at low hold-ups the prediction is good, at higher hold-ups the model underestimates the hold-up. The average deviation between data and model (=AVD) is for the model of Kumar and Hartland 0.080, whereas our model gives an AVD of 0.075.

Our model was validated with measured data using a different dodecane/water 2-phase system; all physical properties were the same, except for the interfacial tension (29 mN m⁻¹ for the new data versus 40 mN m⁻¹ for the old data). The new data were well predicted.

Acknowledgements

This work was financially supported by the Ministry of Economic Affairs, the Ministry of Education, Culture and Science, the Ministry of Agriculture, Nature Management and Fishery in the framework of a research program of the Netherlands Association of Biotechnology Centres (ABON).

Appendix A. Constraints applied in the fitting procedure

The equations describing the dimensionless drift flux (U_{dc}^*) are:

$$\frac{U_{dc}}{V_{\infty}} = U_{dc}^* = \alpha \cdot (1 - \alpha)^{n+1} \quad A.1$$

with n given by:

$$n = n_0 - c_1 (U_{dc}^*)^{c_2} \quad A.2$$

The parameter c_2 is given by:

$$c_2 = \ln \left(\frac{n_0 - n_{boundary}}{c_1} \right) \cdot \frac{1}{\ln(0.0975)} \quad A.3$$

with $n_{boundary}$ given by :

$$n_{boundary} = \left(\ln \left(\frac{0.0975}{\alpha_{boundary}} \right) / \ln(1 - \alpha_{boundary}) \right) - 1 \quad A.4$$

Parameter c_2 is constant at a given n_0 , c_1 and $\alpha_{boundary}$. Substituting equation A.2 into equation A.1 yields an implicit equation for U_{dc}^* . A new function f is defined by rewriting equation A.1:

$$f = U_{dc}^* - \alpha \cdot (1 - \alpha)^{n(U_{dc}^*)+1} = 0 \quad A.5$$

The constants n_0 and c_1 were fitted with a downhill simplex method as suggested by Nelder

and Mead (1969) without any constraint on the fitting procedure. It is only demanded that U_{dc}^* is smaller than 0.0975. This gave a value for n_0 equal to 4.37, and for c_1 equal to 685.

However, as shown in Figure A.1, these fitted constants do not give a good fit at higher hold-ups; U_{dc}^* decreases at higher hold-ups and is estimated far too low. At α_{boundary} a discontinuity can be observed.

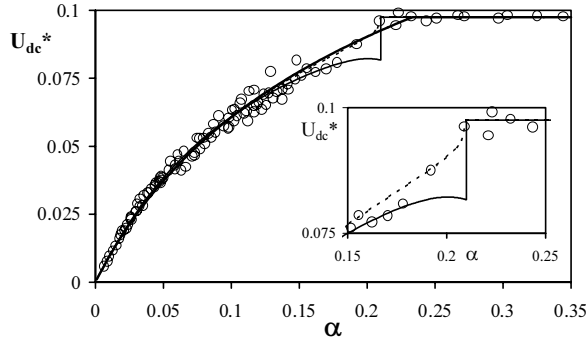


Figure A.1. The dimensionless drift flux as a function of the hold-up for different combinations of the parameters n_0 and c_1 . The add-in figure is an enlargement. — $n_0 = 685$, $c_1 = 4.37$; --- $n_0 = 69.1$, $c_1 = 5.48$; — $n_0 = 33.2$, $c_1 = 6.55$.

Figure A.2 shows f as a function of U_{dc}^* (equation A.5). This figure shows that at a given α two roots exist for U_{dc}^* that satisfy equation A.5. The smallest of both roots is taken as the correct solution of equation A.5. When α approaches α_{boundary} equation A.5 still gives two roots for U_{dc}^* . None of these roots are near the constant dimensionless drift flux. However, equation A.4 demands that the root of equation A.5 is equal to the constant dimensionless drift flux (0.0975) at α_{boundary} . This explains the discontinuity in Figure A.1.

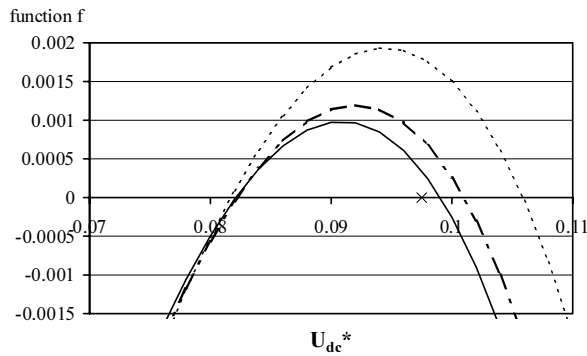


Figure A.2. Function f versus the dimensionless drift flux for different values of the hold-up — hold-up is 0.21 ; --- hold-up is 0.20; ... hold-up is 0.19; × hold-up is 0.21, $U_{dc}^*=0.0975$, $f=0$.

In order to avoid the discontinuity, we demand that the first root of the function f at α_{boundary} is equal to the constant value of the dimensionless drift flux. This means that the derivative of function f with respect to the dimensionless drift flux is less than or equal to zero.

From equation A.6 a maximum value for n_0 can be determined at a given c_1 , and α_{boundary} .

$$\left. \frac{df}{dU_{dc}^*} = \frac{d \left(U_{dc}^* - \alpha \cdot (1-\alpha)^{(1+n_0-c_1(U_{dc}^*)^{c_2})} \right)}{dU_{dc}^*} \right|_{\text{boundary}} \leq 0 \Rightarrow \quad \text{A.6}$$

$$\frac{df}{dU_{dc}^*} = 1 - \alpha(1-\alpha)^{(1+n_0-c_1(U_{dc}^*)^{c_2})} \cdot \ln(1-\alpha) \cdot \left(-c_1 c_2 (U_{dc}^*)^{(c_2-1)} \right) \leq 0$$

Equation A.1 and A.2 were fitted on the data, together with the constraint given by equation A.6. This resulted in a n_0 equal to 5.48 and $c_1=69.1$ at $\alpha_{\text{boundary}} = 0.21$. The dimensionless drift flux as a function of the hold-up is given in Figure A.1.

This figure clearly shows that the fit is much better for the higher hold-ups; see the enlargement in Figure A.1. However, around a hold-up of 0.21, the increase of the dimensionless drift flux with the hold-up is really large, and shows an inflexion point. This feature of the relationship between the dimensionless drift flux and the hold-up has no physical meaning. Our data, however, suggest a monotonic increase in drift-flux with the hold-up. To obtain a relationship between the dimensionless drift and the hold-up which does not show the sharp increase, another more severe constraint has to be applied to the fitting procedure.

An obvious constraint would be demanding that the first derivative of U_{dc}^* with respect to α is equal or larger than 0:

$$\frac{dU_{dc}^*}{d\alpha} \geq 0 \quad \text{A.7}$$

Equation A.5 shows that U_{dc}^* is an implicit function of the hold-up. To obtain the first derivative of U_{dc}^* with respect to α implicit differentiation has to be applied (equation A.8).

$$U_{dc}^* - \alpha \cdot (1-\alpha)^{n+1} = 0 \Rightarrow \frac{d(U_{dc}^*(\alpha) - \alpha \cdot (1-\alpha)^{n+1})}{d\alpha} = 0 \quad \text{A.8}$$

If the numerical operation given in equation A.8 is applied, equation A.9 is obtained (Almering, 1988) :

$$\frac{dU_{dc}^*}{d\alpha} = \frac{(1-\alpha)^{n+1} - (n+1) \cdot \alpha \cdot (1-\alpha)^n}{1 + \alpha \cdot (1-\alpha)^{n+1} \cdot c_1 c_2 \cdot U_{dc}^{*(c_2-1)} \cdot \ln(1-\alpha)} \quad \text{A.9}$$

This derivative should be larger than or equal to zero. So the nominator should be larger than or equal to zero. This leads to:

$$\alpha \leq \frac{1}{n+2}$$

This equation gives no extra information for the parameters c_1 and n_0 .

However, a maximum α_{boundary} can be derived. At the boundary the following two equations hold.

$$\alpha_{\text{boundary}} (1 - \alpha_{\text{boundary}})^{n_{\text{boundary}}+1} = 0.0975$$

$$\alpha_{\text{boundary}} = \frac{1}{n_{\text{boundary}} + 2}$$

Solving these equations gives a maximum for α_{boundary} : 0.2334. At a higher α_{boundary} $dU_{\text{dc}}^*/d\alpha$ is negative.

The first derivative should also exist; this means that the denominator should not be equal to zero. From the denominator of equation A.9 a maximum n_0 can be determined at a given c_1 , α_{boundary} , and $U_{\text{dc}}^*=0.0975$. Equation A.1 and A.2 were fitted on the data, together with the constraint discussed above (the denominator in equation A.9 equals zero). This resulted in an n_0 equal to 6.55 and $c_1=33.2$ at $\alpha_{\text{boundary}} = 0.23$. The dimensionless drift flux as a function of the hold-up, equation A.1 and A.2 with the fitted constants, is given in Figure A.1. This figure shows that the obtained constants give a good fit.

Nomenclature

c_1, c_2	: parameter in equation 6	-
d	: diameter droplet	m
d_{noz}	: diameter nozzle	m
E_o	: Eötvös number, $\frac{g\Delta\rho d^2}{\sigma}$	-
$E_{o_{noz}}$: Eötvös nozzle number, $\frac{g\Delta\rho d_{noz}^2}{\sigma}$	-
g	: gravity constant (9.8)	$m^2 s^{-1}$
N	: number of data points	-
n	: power n	-
n_0	: parameter in equation 6	-
U_{dc}	: drift flux	$m^3 m^{-2} s^{-1}$
U_{sc}	: superficial velocity of the continuous phase	$m^3 m^{-2} s^{-1}$
U_{sd}	: superficial velocity of the dispersed phase	$m^3 m^{-2} s^{-1}$
V_{dj}	: drift velocity	$m s^{-1}$
v_{∞}	: terminal rise velocity single droplet	$m s^{-1}$
v_k	: characteristic velocity	$m s^{-1}$
v_{12}	: slip velocity	$m s^{-1}$
We_{noz}	: nozzle Weber number, $\frac{\rho_d v_{\infty}^2 d_{noz}}{\sigma}$	-

Greek

α	: dispersed-phase hold-up	-
α_{meas}	: measured dispersed-phase hold-up	-
α_{mod}	: predicted dispersed-phase hold-up	-
$\Delta\rho$: density difference continuous and dispersed phase	$kg m^{-3}$
ρ_c	: density continuous phase	$kg m^{-3}$
ρ_d	: density disperse phase	$kg m^{-3}$
η_c	: viscosity continuous phase	$Nm s^{-1}$
σ	: interfacial tension	$N m^{-1}$

Solid and Droplet hold-ups in a liquid-liquid-solid 3-phase fluidized-bed

Abstract

The hydrodynamics of a 3-phase fluidized bed reactor were studied. In view of biocatalytic purposes, the reactor featured a bed of κ -carrageenan gel beads as solid phases. The bed was fluidized by a continuous aqueous phase (30 mM KCl as continuous aqueous phase), and a disperse organic phase (n-dodecane droplets) rose through the bed of particles. At different aqueous and n-dodecane velocities, the type of gel bead flow inside the 3-phase fluidized bed was characterized, and the various phase hold-ups were measured and studied. Visual observations of the 3-phase fluidized bed revealed five different flow regimes, characterized by the gel beads flow: two homogeneous flow regimes, two heterogeneous flow regimes and a region with wash-out of gel beads. Literature models for different types of 3-phase systems could not be extended to the system under study and a new model for gel bead and dodecane droplet hold-up in the fluidized bed was derived, based on stationary force balances. A drag-force model for a single gel bead and a single droplet in the 3-phase mixture was derived. All data for gel bead hold-up and for droplet hold-up up to 0.06 were well described. An empirical model was derived to describe the droplet hold-ups for the entire range of measured hold-ups.

Introduction

Gas-liquid-solid fluidized beds have been abundantly studied and are widely used in industry. Different modes of operation were classified by Muroyama and Fan (1984). Most frequently, the solids are fluidized by a rising liquid, while gas bubbles rise through the bed. The liquid analogue of these systems, i.e. a liquid-liquid-solid fluidized bed with liquid droplets instead of gas bubbles, has received little attention in literature. An overview and classification of 3-phase systems is given in Table I, of which the liquid-liquid-solid 3-phase systems are discussed in more detail below.

Application of a liquid-liquid-solid fluidized bed as extraction column was firstly studied by Roszak and Gawronski (1979) and Dakshinamurty *et al.* (1979), who studied a 3-phase system of water, organic solvent droplets, and a solid like glass beads. Roszak and Gawronski (1979) focused on mass transfer and found it to be faster than in a fluidized bed. Dakshinamurty *et al.* studied solids hold-up (1979), and mass transfer (1984). In support of Roszak and Gawronski (1979), they found the mass transfer rate to be higher than in a 2-phase droplet column. Physical aspects of a similar 3-phase system, with water as continuous phase, and with kerosene and glass pearls as disperse phases, have been reported by Kim *et al.* (1988, 1989, 1994, 1999), who also reviewed the disperse phase characteristics (Kim and Kang, 1997).

Here, we report on a different type of 3-phase liquid-fluidized bed, with water as the continuous phase, and with n-dodecane droplets and polymeric gel beads as disperse phases. This 3-phase system differs from the above described 3-phase liquid-liquid-solid system in the type of solid used; gel beads versus glass pearls. The physical characteristics (density and composition) between both types of solid differ largely. The density of gel beads is much lower, and gel beads consist over 95% percentage of water. Gel beads are an interesting type of solid, as they frequently are used to immobilize a biocatalyst, e.g. enzymes or micro-organisms, thus allowing a large amount of biocatalyst to be retained in the reactor (Wijffels *et al.*, 1996). Such a 3-phase liquid-fluidized bed may have an advantage over more conventional bioreactors, especially if the biological reaction is inhibited by toxicity of the reaction substrate or reaction product (De Bont, 1998; Collins *et al.*, 1995; Hüsken *et al.*, 2001; Marshall and Wooley, 1995; Tramper *et al.*, 1992). In a liquid-liquid-solid fluidized bed, the organic solvent droplets may serve as a substrate reservoir or a product sink. As a result of such an exchange between the liquid phases, the concentration of substrates and products are kept at sub-inhibitory levels, thus improving the reaction

rate significantly.

Application of such a liquid-liquid-solid fluidized bed as an extractive bioreactor was studied by Davison and Thompson (1993). *Clostridium acetobutylicum*, immobilized in gel beads, was used to ferment glucose to acetone and butanol, while an organic solvent was used for *in situ* removal of inhibitory butanol. A substantial increase in butanol production rate was reported. These authors, however, did not study physical aspects of the 3-phase fluidized bed.

To our knowledge these are the only 3-phase liquid-liquid-solid fluidized bed systems studied. In this paper we therefore focus on the physical aspects of such 3-phase liquid fluidized beds. To this end, a 3-phase fluidized bed reactor has been developed on a pilot scale.

This paper describes observed phenomena, like the bed stability and the type of the solids flow inside the fluidized bed. Subsequently, droplet and solids hold-ups at different velocities of water and dodecane are discussed. Hydrodynamics of our 3-phase fluidized bed have not been studied before. Since available models for the hold-ups in more or less similar 3-phase systems (gas-liquid-solid: Yu and Rittmann, 1997; liquid-solid-solid fluidized beds: Van der Wielen *et al.*, 1996a) gave an unsatisfactory description of our data, a new model was developed. The solids hold-up followed from the drag force of a single gel bead in the 3-phase mixture. For this drag force, an existing 2-phase model was successfully adopted with minor adaptations. For the droplet hold-up, an empirical model was derived from experimental data. The combination of these models gave a satisfactory description of the solid-liquid-liquid 3-phase system over a wide range of hold-up values.

Table I. Overview of different 3-phase systems

Reference	Disperse phase	Disperse phase	Continuous phase	Remarks
Muroyama and Fan, 1984	gas	solid	liquid	hydrodynamics
Hunik <i>et al.</i> , 1994	gas (air bubbles)	solid (reactive gel bead)	liquid	aerobic conversions
Roszak and Gawronski 1979, Dakshinamurthy <i>et al.</i> 1979, Kim <i>et al.</i> 1994	liquid (organic droplets)	solid (glass beads)	liquid (water)	hydrodynamics
Davison and Thompson, 1993	liquid (organic droplets)	solid (reactive gel beads)	liquid (water)	bioreaction
Van der Wielen <i>et al.</i> , 1996b	solid	solid	liquid	reaction and hydrodynamics
Michielsen <i>et al.</i> 2001	solid (substrate crystals)	solid (product crystals)	liquid (water)	reaction not performed in a packed or fluidized bed
this study	liquid (organic droplets)	solid (gel beads)	liquid	

Material and Methods

Gel beads

Celite™-enforced κ -carrageenan gel beads were used as disperse solid phase; they were produced with a resonance nozzle (Hunik and Tramper, 1993). An aqueous 3.25 % κ -carrageenan solution (Genugel 0909 Copenhagen Pectin Factory), mixed with 10 w/w% Celite™, kept at 35 °C, was forced through a 0.8-mm nozzle at 202 Hz and 1.5 bar. Drops were collected in a 80-mM KCl solution for hardening. To obtain spherical beads, butyl acetate (Aldrich) was layer upon the hardening solution. After hardening for approximately two hours, the beads were stored in a 30-mM KCl solution. The same KCl solution was used as continuous phase; it prevented the

elution of counter-ions from the gel beads. Density and diameter of the gel beads were determined as described by Van Zessen *et al.* (2001). Physical properties of the gel beads are given in Table II.

Table II. Phase properties in the 3-phase fluidized bed

		gel beads	n-dodecane	30 mM KCl
density	(kg m ⁻³)	1065	742.7	998
viscosity	(mN s ⁻¹)	-	-	0.93
diameter	(mm)	2.80	flux dependent	-
settling velocity	(cm s ⁻¹)	5.12	flux dependent	-
surface tension 30 mM KCl/ n-dodecane		(mN m ⁻¹)		40.0

Fluidized bed

The fluidized bed (Figure 1) consisted of a 2-m high and 6-cm diameter glass column. On top of it, a widened section facilitated coalescence of the organic phase droplets and separate discharge of the organic solvent (n-dodecane, Aldrich 99%+ pure) and aqueous (30 mM KCl) phases. n-Dodecane was introduced at the bottom of the column through a liquid distributor (Figure 2). It consisted of a 10 cm high glass column filled with 8 mm glass pearls for a good distribution of the flow over the flow-through column area, and with a sparger on top. The sparger consisted of 209 nozzles protruding through a Teflon plate with a diameter of 6 cm. The nozzles (5 cm length and 1 mm internal diameter), were placed sufficiently far apart to prevent contact between the growing droplets. As continuous phase, a 30-mM KCl solution was introduced through four openings in the column wall, located below the nozzles outlets (Figure 2). An equal flow rate through each of these continuous phase inlets was obtained with throttle valves; this was verified with color-pulse experiments. The storage vessels of both liquids (Figure 2) were maintained at 26 °C. A temperature gradient over the column was not observed.

Solids hold-up

Solids hold-up (ϵ_s) was calculated from the measured bed height (H_{bed} , see also Figure 1), the known total solids volume (V_s), and the known column cross-sectional area (A).

$$\epsilon_s = \frac{V_s}{H_{bed} A} \quad 1$$

Bed height was easily determined as there was a distinct transition between the 3-phase and 2-phase regions in the upper part of the column (Figure 2). Total solids volume was determined as described by Van Zessen (2001).

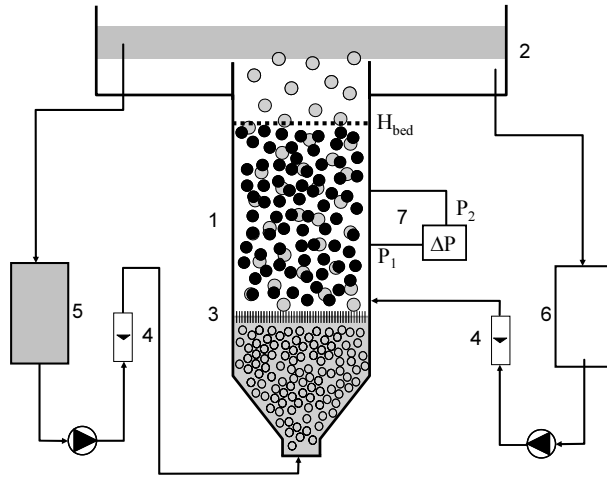


Figure 1. Experimental set-up. 1 column; 2 phase separator; 3 sparger; 4 rotameters; 5 dodecane storage; 6 30 mM KCl storage; 7 pressure measurement device. • gel beads, • droplets; H_{bed} height of the 3-phase fluidized bed

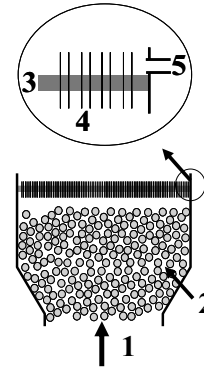


Figure 2. Sparger lay-out. 1 dodecane inlet, 2 glass pearls, 3 Teflon™ plate, 4 nozzles, 5 water inlet

Dodecane hold-up

At steady state conditions, the pressure drop (ΔP) between two points a distance Δz along the column apart is equal to the total weight per unit of cross-sectional area of the bed inbetween these points (Muroyama and Fan, 1984):

$$\Delta P = (\rho_s \epsilon_s + \rho_d \epsilon_d + \rho_c \epsilon_c) g \Delta z \quad 2$$

where ρ_s , ρ_d and ρ_c are the densities of the solid gel beads, the dodecane droplets and the continuous phase (30 mM KCl). Measurement of the pressure difference between both points involved an external loop filled with continuous phase only (Figure 1). The actually measured pressure difference (ΔP_{exp}) is therefore equal to:

$$\Delta P_{exp} = P_1 - P_2 = (\rho_s \epsilon_s + \rho_d \epsilon_d + \rho_c \epsilon_c) g \Delta z - \rho_c g \Delta z \quad 3$$

As the sum of the various phase hold-ups is unity,

$$\varepsilon_s + \varepsilon_d + \varepsilon_c = 1$$

4

the droplet hold-up follows from solving equations 3 and 4.

Pressure difference was measured over a vertical distance of 25 cm, at 24 cm and 49 cm above the sparger. A Validyne DP103 pressure transducer with a CD23 digital transducer indicator (maximum pressure difference 140 Pa) was used. For each set of measurements, the transducer was calibrated with a liquid manometer with water and octanoic acid ($\rho = 903 \text{ kg m}^{-3}$). As rising droplets lead to pressure fluctuations, the analogue signal was monitored with a personal computer and an A/D converter until a total of 1000 data points were collected that were normally distributed. The mean of this distribution was used as a measure for ΔP_{exp} .

Similar pressure measurements were also done in the 2-phase solids-free top section of the column above the 3-phase fluidized beds (positions at 175 cm and 190 cm above the sparger).

Miscellaneous

Flow rates of the KCl solution (0.58 to 2.06 cm s^{-1}) and n-dodecane (0 to 0.91 cm s^{-1}) were measured with calibrated rotameters (Sho-Rate).

Density of both liquids was measured with a pycnometer, total volume 25.00 ml. The static interfacial tension between the continuous phase and n-dodecane phase was determined by the Wilhelmy plate method (Hiemenz, 1986). Table II summarizes the physical properties of both liquids.

Values for model parameters were obtained from a Gauss-Newton algorithm that minimized the residual sum of squares.

Results

First, observations on the nature of the 3-phase fluidized bed will be described and discussed. Thereafter, the hold-ups of the different phases will be shown. It will be demonstrated that literature models for comparable 3-phase systems do not predict these hold-ups correctly. A new model describing the hold-ups correctly will be presented.

Visual Observations

A large variety in water and dodecane fluxes was applied to study the behavior of the fluidized bed. In the absence of dodecane, a minimal water flux (0.36 cm s^{-1}) was required to obtain fluidization; below this flux, the gel beads formed a packed bed. At a water flux exceeding 5 cm s^{-1} , the gel beads were washed out and a 2-phase water/ dodecane system remained. At large dodecane fluxes (not applied in our experiments), phase inversion will occur; the continuous phase will be dodecane, and the dispersed phase will be water.

Inspired by visual observations on the behavior of the 3-phase fluidized bed, five different regions were identified (Figure 3), but the transition from one region to another region was not sharp. Below, only 3-phase fluidized bed regions are briefly discussed.

Homogeneous flow pattern: mimic of a 2-phase fluidized bed (region 1)

In this region, the flow pattern of gel beads was not disturbed by the droplets. The gel bead movement did not differ from its movement in a 2-phase fluidized bed. At the top of the bed, little bead ‘eruptions’ were observed when dodecane droplets escaped. The gel beads, however, fell back in the fluidized bed, and a so-called free board was not formed.

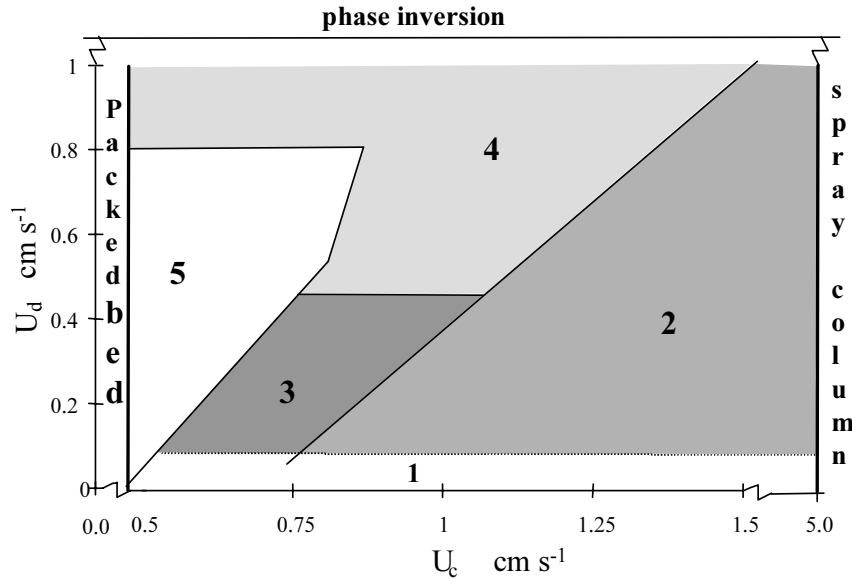


Figure 3. Flow map for a 3-phase fluidized bed with gel beads, ($\rho_s=1067 \text{ kg m}^{-3}$ and $d_s=2.8 \text{ mm}$), and dodecane droplets ($\rho_d=743 \text{ kg m}^{-3}$) in an aqueous continuous phase. 1 Homogeneous flow pattern: mimic of a 2-phase fluidized bed; 2 Homogeneous flow pattern: turbulent solids flow; 3 Heterogeneous flow pattern: structured solids flow; 4 Heterogeneous flow pattern: unstructured chaotic solids flow; 5 Droplet coalescent region: slug formation

Homogeneous flow pattern: turbulent solids flow (region 2)

Characteristic for this region is bed expansion. The height of the 3-phase fluidized bed always exceeded the 2-phase fluidized-bed. At none of the fluxes, a significant freeboard of solids was formed. Gel beads moved randomly through the fluidized bed in little groups, like aggregates. The velocity of the solid groups was much higher in the 3-phase fluidized bed as compared to a 2-phase bed; due to a continuous change in direction the group motion was much more chaotic (turbulent). The size of these groups did not alter in time. However, at higher water fluxes these aggregates became increasingly smaller, until at a water flux of $\sim 2 \text{ cm s}^{-1}$ the gel beads moved individually. The overall picture was not influenced by the dodecane flux, although the solids group flow became more pronounced for the lower dodecane fluxes.

Heterogeneous flow pattern: structured solids flow (region 3)

A clear characteristic of this region is bed contraction: the bed height of the 3-phase fluidized bed was smaller as compared with the 2-phase fluidized bed. Another characteristic for this region is the gel bead flow. The gel bead flow is characterized by repetitive waves of solids concentrations traveling through the fluidized bed

(Figure 4). Wash-out of the gel beads did not occur, and a freeboard was not formed.

This gel bead flow behavior can be explained with the droplet flow. For the dodecane fluxes in this region, dodecane droplets are released group wise from the tip of the nozzles. Such a swarm of droplets rises then through the fluidized bed and pushes the gel beads upwards (thus increasing the solids concentration). As the droplet velocity is larger than the solids velocity, the swarm of droplets passes this high-concentration area. No other swarm of droplets follows immediately, and the gel beads fall back (decrease of the solids concentration). A subsequent swarm of droplets arrives and the cycle is repeated.

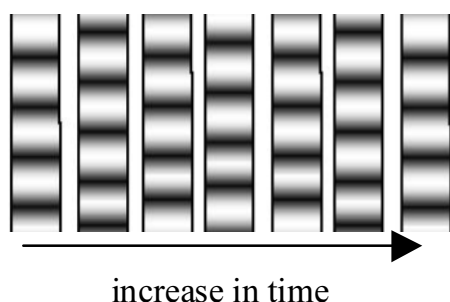


Figure 4. Schematic gel bead flow pattern through a 3-phase fluidized bed in heterogeneous flow region: structured solids flow. Dark areas represent high solids concentration, white areas are low solids concentrations.

Heterogeneous flow pattern: unstructured chaotic solids flow (region 4)

Behavior in this region could not be characterized by a single key feature. An overall characteristic, however, was the very heterogeneous axial and radial distribution of the gel beads. The flow pattern of both gel beads and droplets was random and chaotic. Locally, the solvent droplets pushed the gel beads towards one side of the column, thus creating high-voidage pockets. Droplets entering into such pockets rose very fast, and entailed some gel beads. Once gel beads approached each other closely, they stopped moving and fell back, tumbling chaotically.

At dodecane fluxes above 0.8 cm s^{-1} and water fluxes below 0.8 cm s^{-1} , droplet coalesce was observed to some extent. As opposed to full coalescence, full slug formation was not observed, as smaller slugs were rapidly disintegrated.

Droplet coalescent region: slug formation (region 5)

At the bottom of the column, dodecane droplets rose very slowly through the fluidized bed, and the droplets start to coalesce. Eventually at a certain height, dodecane slugs spanning the column diameter were formed. These slugs pushed the

full bed of gel beads upwards out of the column. In this region a fluidized bed could not exist.

Particle and droplet hold-ups

Dodecane droplet hold-up as a function of the water flux at various dodecane fluxes is shown in Figure 5a; gel bead hold-up as a function of the water flux at various dodecane fluxes is shown in Figure 5b.

Droplet hold-up

The droplet hold-up was found to increase with the dodecane flux, and to decrease with the water flux, (Figure 5a), which is in full agreement with the findings of Kim *et al.* (1999). For the higher dodecane velocities ($U_d \geq 0.44 \text{ cm s}^{-1}$), hold-ups were only measured in region 2 (homogeneous turbulent solids flow). For the lower dodecane velocities, hold-ups were measured in region 2 and region 3 (heterogeneous structured solids flow). The transition from region 3 to region 2 had no effect on the dodecane hold-up, which was found to increase smoothly with the decreasing water flux.

At dodecane fluxes above 0.36 cm s^{-1} and water fluxes below 1.25 cm s^{-1} , the 3-phase fluidized-bed is in the unstructured chaotic flow region 4 (Figure 3), and thus features prominent axial and radial distributions of solids and droplets. Consequently, hold-ups could not be measured unequivocally in this region.

Solids hold-up

The solids hold-up was found to decrease with increasing water fluxes (Figure 5b), both in 2-phase and 3-phase fluidized beds. At water fluxes above 0.75 cm s^{-1} and dodecane fluxes above 0.42 cm s^{-1} , the solids hold-up in the 3-phase system was always smaller (i.e. the bed was higher) than in a 2-phase system ($U_d=0$) at the same water flux. Similar results have been reported for a water-kerosene-glass pearl fluidized bed (Dakshinamurthy *et al.*, 1979; Kim *et al.* 1989).

At water fluxes below 0.75 cm s^{-1} the bed height decreased with the dodecane flux (bed contraction, data not shown). This phenomenon is not unique: Muroyama and Fan (1984), who reviewed gas-liquid-solid fluidization, cite various authors who observed it. Yu and Rittmann (1997), who studied a gas-liquid-solid fluidized bed with and without biofilms, also reported on bed contraction. For liquid-liquid-solid

fluidization the phenomenon was observed before by Dakshinamurthy *et al.* (1979) and Kim *et al.* (1989).

According to figure 4, at lower dodecane fluxes ($U_d \leq 0.27 \text{ cm s}^{-1}$), the bed will transform from an expanded state, $\varepsilon_s|_{3\text{-phase}} \geq \varepsilon_s|_{2\text{-phase}}$ (region 3), to a contracted state, $\varepsilon_s|_{3\text{-phase}} \leq \varepsilon_s|_{2\text{-phase}}$ (region 2), upon decreasing the water flux. This transition was indeed observed (data not shown).

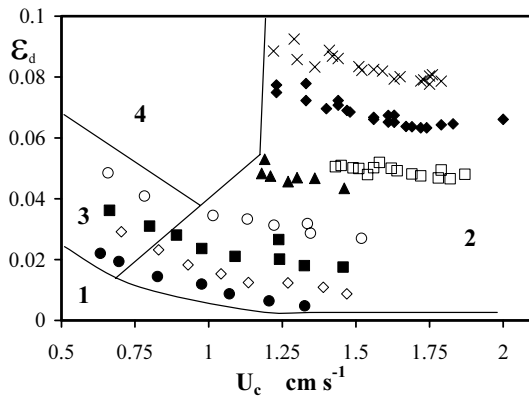


Figure 5a. Droplet hold-up as a function of water and dodecane fluxes. Numbers refer to the different flow regions.

- $U_d = 0.05 \text{ cm s}^{-1}$, $\diamond U_d = 0.10 \text{ cm s}^{-1}$,
- $U_d = 0.18 \text{ cm s}^{-1}$, $\circ U_d = 0.27 \text{ cm s}^{-1}$,
- ▲ $U_d = 0.44 \text{ cm s}^{-1}$, $\square U_d = 0.54 \text{ cm s}^{-1}$,
- ◆ $U_d = 0.73 \text{ cm s}^{-1}$, $\times U_d = 0.91 \text{ cm s}^{-1}$

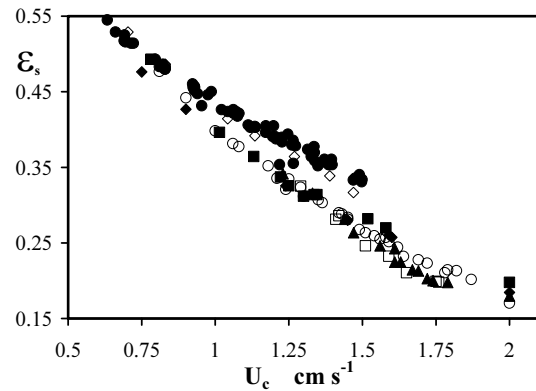


Figure 5b. Gel bead hold-up as a function of the water and dodecane flux.

- $U_d = 0 \text{ cm s}^{-1}$, $\diamond U_d = 0.10 \text{ cm s}^{-1}$,
- $U_d = 0.29 \text{ cm s}^{-1}$, $\blacklozenge U_d = 0.42 \text{ cm s}^{-1}$,
- $\circ U_d = 0.54 \text{ cm s}^{-1}$, $\blacktriangle U_d = 0.75 \text{ cm s}^{-1}$,
- $\square U_d = 0.91 \text{ cm s}^{-1}$

Figure 6 shows the dodecane hold-up and the gel bead hold-up for various dodecane fluxes. When the gel bead hold-up increased (i.e. when the water flux decreased) the dodecane hold-up increased as well. When compared to a 2-phase droplet column of dodecane in water ($\varepsilon_s=0$), the mere presence of gel beads in a 3-phase fluidized bed had a positive effect on droplet hold-up: $\varepsilon_d|_{\varepsilon_s>0} > \varepsilon_d|_{\varepsilon_s=0}$ in all cases.

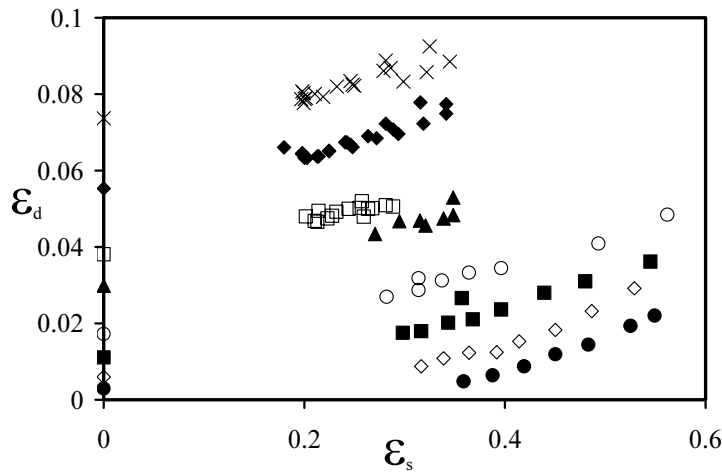


Figure 6. Droplet hold-up (ϵ_d) as a function of solids hold-up (ϵ_s) and dodecane fluxes. Points on the ϵ_d -axis are calculated from equation 14 (assuming a water flux of 2 cm s^{-1}).

- $U_d = 0.05 \text{ cm s}^{-1}$, ◇ $U_d = 0.10 \text{ cm s}^{-1}$
- $U_d = 0.18 \text{ cm s}^{-1}$, ○ $U_d = 0.27 \text{ cm s}^{-1}$
- ▲ $U_d = 0.44 \text{ cm s}^{-1}$, □ $U_d = 0.54 \text{ cm s}^{-1}$
- ◆ $U_d = 0.73 \text{ cm s}^{-1}$, × $U_d = 0.91 \text{ cm s}^{-1}$

Available models for solids and droplet hold-up

3-Phase hold-up models are available in literature, although not for liquid-liquid-solid (gel bead) fluidized beds. For gas-liquid-solid fluidized beds, Muroyama and Fan (1984) gave an extensive overview of models, which were either empirical or based on the wake model. A more fundamental model for the gas hold-up in a liquid-solid-gas fluidized bed was derived by Chen and Fan (1990). The solids hold-up was assumed to be known. Yu and Rittmann (1997) presented a model for all three hold-ups in a gas-solid-liquid fluidized bed, based on the wake model and with an empirical model for the gas hold-up. For a solid-solid-liquid 3-phase system, Van der Wielen *et al.* (1996a) presented a model for predicting all phase hold-ups.

Droplet hold-up

We tested the model of Chen and Fan (1990) and Yu and Rittmann (1997) for the droplet hold-up. Although gas bubbles differ in physical characteristics from dodecane droplets, the fundamental force balances are the same. In these calculations we used the measured solid hold-ups. It appeared that both models failed in predicting the droplet hold-up. The model of Chen and Fan largely underestimated the dodecane hold-ups below 0.03, and overestimated dodecane hold-ups above 0.06.

In the intermediate region (0.03 – 0.06), the prediction was fair. When the model parameters were fitted to our data, the description did not improve. The model of Yu and Rittmann highly overestimated all hold-ups. When the model parameters were fitted to our data, the hold-ups were well predicted (81% of all data showed a deviation less than 25%).

For a different 3-phase system, a solid-solid-liquid fluidized bed, Van der Wielen *et al.* (1996a) presented a model for all hold-ups. This model uses parameters of the individual 2-phase systems. Using these parameters, low droplet hold-ups (<0.02) were well predicted, but the higher hold-ups were largely overestimated.

Solids hold-up

When the liquid-liquid-solid model of Van der Wielen was used to predict the solid hold-up in our 3-phase fluidized bed, hold-ups up to 0.3 were well predicted, but the higher hold-ups were systematically underestimated (measured parameters of the 2-phase liquid-solid fluidized bed were used). The model of Yu and Rittmann largely overestimated the hold-up. When model parameters were fitted on our data, the description improved. However, the fitted parameters resulted in a negative wake volume, which has no physical meaning.

Table III and IV summarize the above described results.

¹ For $\varepsilon_s \rightarrow 0$ the 3-phase fluidized bed simplifies to a droplet column. Thus, this model describes the hold-up in a droplet column. Coefficient m_2 is equal to 5 for droplet hold-ups less than 0.15, as shown by Van Zessen *et al.* (2003)

² For $\varepsilon_s \rightarrow 0$ the 3-phase fluidized bed simplifies to a droplet column, and coefficient $n_d=5$, for droplet hold-ups less than 0.15 as shown by Van Zessen *et al.* (2003).

³ The average deviation (AVD) is defined as:

$$AVD = \left(\sum_{i=1..N} \left| \left(\varepsilon_{\text{measured},i} - \varepsilon_{\text{model},i} \right) / \varepsilon_{\text{measured},i} \right| \right) / N$$

10% is the percentage of data with an AVD less or equal to 10%; 25% be the percentage of data with an AVD less or equal to 25%.

⁴ The parameters in this model are fitted together with the parameter in the gel bead hold-up model based on the total gel bead drag coefficient model in Table IV.

Table III. Models for the droplet hold-up in a 3-phase fluidized bed

Droplet Hold-up					
<i>Reference</i>	<i>Equation</i>	<i>Results³</i>			<i>Remarks</i>
		AVD	10 %	25 %	
Chen and Fan 1990	$\frac{U_d}{\varepsilon_d} = \frac{U_d + U_c}{1 - \varepsilon_s} + V_{\infty,d} \left(\frac{\varepsilon_c}{\varepsilon_c + \varepsilon_s} \right)^{m_1} \left(\frac{\varepsilon_c}{\varepsilon_c + \varepsilon_d} \right)^{m_2}$ with $m_1=1.045$, $m_2=5^1$	24	32	64	Lower hold-ups are underestimated, whereas higher hold-ups are largely overestimated. In the intermediate region, $\sim 0.03 - 0.06$, the prediction is fair
with constant m_1 fitted on our data	$m_1=0.5$	26	21	54	Fitting does not improve the description: lower hold-ups are underestimated; higher hold-ups are less overestimated
Yu and Rittmann 1997	$\frac{U_d}{\varepsilon_d} = \frac{U_d + U_c}{1 - \varepsilon_s} + 0.1016 + 1.488 \left(\frac{U_d}{1 - \varepsilon_s} \right)^{0.5}$	150	0.4	1.2	all hold-ups are highly overestimated
with constants fitted on our data	$\frac{U_d}{\varepsilon_d} = \frac{U_d + U_c}{1 - \varepsilon_s} + 4.23 + 3.45 \left(\frac{U_d}{1 - \varepsilon_s} \right)^{0.5}$	14	51	81	Fitting results in a much better description. All hold-ups are well described.
Van der Wielen et al. 1996	$\frac{\rho_d - \rho_{\text{mix}}}{\rho_d - \rho_c} = \left(\varepsilon_c \left(\frac{U_d}{\varepsilon_d} - \frac{U_c}{\varepsilon_c} \right) / V_{\infty,d} \right)^{4.8/n_d} \cdot \varepsilon_c^{-3.8}$ and $\rho_{\text{mix}} = \varepsilon_d \rho_d + \varepsilon_s \rho_s + \varepsilon_c \rho_c$, $n_d=5^2$	71	6.3	16	up to 0.02 the hold-ups are well predicted. The higher hold-ups are largely overestimated.
This paper: Drag coefficient based	$\varepsilon_s \frac{\rho_s - \rho_c}{\rho_c - \rho_d} + 1 - \varepsilon_d = \left(\frac{V_{cd}}{V_{\infty,d}} \right)^{-0.06}$	16.5	34	81	The numbers in results column refer to a hold-up up to 0.06. At higher hold-ups the data are underestimated
Empirical	$\frac{V_{cd}}{V_{\infty,d}} = 5.37 U_d^{0.88} \cdot \varepsilon_d^{-0.76}$	13	55	89	All hold-ups are well described
Empirical -2 ⁴	$\frac{V_{cd}}{V_{\infty,d}} = 6.15 U_d^{0.90} \cdot \varepsilon_d^{-0.76}$	12	63	89	All hold-ups are well described

Table IV. Models for the gel bead hold-up in a 3-phase fluidized bed.

Gel bead Hold-up					
Reference	Equation	Results ¹			Remarks
		AVD	10%	25%	
Yu and Rittmann 1997	$\varepsilon_c = \left(\frac{U_c}{V_{\infty,s}} - k \frac{U_d}{V_{\infty,s}} \right)^{1/n} \cdot (1 - \varepsilon_d - k\varepsilon_d)^{1-1/n} + k\varepsilon_d$ $k = 3.5 \varepsilon_c^3 \exp(-5.08 \varepsilon_d), n=2.35, v_{\infty s}=3.77 \text{ cm/s}$	33	13	42	the gel bead hold-up is highly overestimated
with constants fitted on our data	$k = -5.01 \varepsilon_c^3 \exp(-34.17 \varepsilon_d)$	16	35	82	Fitting results in a better description of the data, but the data are still overestimated. Moreover, with the fitted constants a negative volume ratio is predicted. A negative volume ratio has no physical meaning.
Van der Wielen et al. 1996	$\rho_s - \rho_{\text{mix}} = (\rho_s - \rho_c) \cdot \left(\frac{U_c}{V_{\infty,s}} \right)^{4.8/n_s} \cdot \varepsilon_c^{-3.8}$ $\text{and } \rho_{\text{mix}} = \varepsilon_d \rho_d + \varepsilon_s \rho_s + \varepsilon_c \rho_c, n_s=2.35^2,$ $v_{\infty s}=3.77 \text{ cm/s}$	7	75	100	Hold-ups up to 0.3 are well predicted. The higher hold-ups, are systematically underestimated.
This paper drag coefficient based	$\frac{\rho_{\text{mix}} - \rho_s}{\rho_c - \rho_s} \left(\frac{V_{\infty,s}}{V_{\text{cs}}} \right)^2 = 1.24 \cdot \left(\frac{V_{\text{cs}}}{V_{\infty,s}} \right)^{-1.26} (1 - \varepsilon_d)^{-6.51}$	7.2	76.5	97.2	Hold-ups are well predicted over the whole range

None of the available models thus gave a fair description of the whole range of both solvent and solids hold-up. Consequently, a new model was derived.

New model for gel bead and droplet hold-up

As a basis to a new model for all three phase hold-ups, drag coefficients for single droplets or gel beads in a 3-phase mixture were calculated from the experimental data on hold-ups and liquid fluxes. Subsequently, a model was developed to describe these drag coefficient data. This model, finally, was used to describe the droplet and gel bead hold-up. This model was based on a steady state force balance for a single particle in a multi-component system, in which one species of particles settled at constant velocity in a fluidized bed of a second species of particles (Van der Wielen *et al.*, 1996a). It was assumed that the time-averaged velocity of the gel beads is zero.

$$F_{\text{gravity}} = F_{\text{buoyancy}} + F_{\text{drag}} \quad 5$$

where F_{drag} is the total drag force experienced by a single particle from its mixed 3-phase surroundings. This drag force is the sum of all liquid-particle and particle-particle drag forces, including the drag forces originating from like particles. As in general the contributions of both fractions cannot be distinguished, a total drag force for a single particle is used (Van der Wielen *et al.*, 1996a). The total drag force for a single particle in a 3-phase mixture is given by a general equation:

$$F_{\text{drag}} = \frac{1}{4} \pi d^2 \cdot \frac{1}{2} \rho_c v_{ci}^2 \cdot C_d(\epsilon_s, \epsilon_d) \quad 6$$

where d is the particle diameter, v_{ci} is the slip velocity between water and particle and $C_{di}(\epsilon_s, \epsilon_d)$ is the total drag coefficient for a single particle in a 3-phase mixture. Combining equations 5 and 6 and evaluating gravity and buoyancy force gives for a gel bead:

$$\frac{1}{6} \pi d_s^3 g (\rho_s - \rho_{\text{mix}}) = \frac{1}{4} \pi d_s^2 \frac{1}{2} \rho_c v_{cs}^2 C_{d,s}(\epsilon_s, \epsilon_d) \quad 7a$$

and for a dodecane droplet:

$$\frac{1}{6} \pi d_d^3 g |(\rho_d - \rho_{\text{mix}})| = \frac{1}{4} \pi d_d^2 \frac{1}{2} \rho_c v_{cd}^2 C_{d,d} (\varepsilon_s, \varepsilon_d) \quad 7b$$

The bulk density ρ_{mix} is determined by all phases (Duijn and Rietema, 1982):

$$\rho_{\text{mix}} = \varepsilon_d \rho_d + \varepsilon_s \rho_s + \varepsilon_c \rho_c \quad 8$$

The slip velocities between water/ particle or water/ droplet are defined as the velocity differences between water and particle and between water and droplet. Water and droplet flows were assumed to be strictly vertical, while the solids flow was assumed zero. Based on continuity, the slip velocities thus should equal:

$$\text{Slip velocity droplets/water} : v_{cd} = \frac{U_d}{\varepsilon_d} - \frac{U_c}{\varepsilon_c} \quad 9a$$

$$\text{Slip velocity gel beads/water} : v_{cs} = \frac{U_c}{\varepsilon_c} \quad 9b$$

The gel bead diameter (d_s) is given in Table II. The droplet diameter (d_d) is calculated with the equation of Kumar and Hartland (1996):

$$\frac{d_d}{d_{\text{noz}}} = \left(0.55 Eo_{\text{noz}}^{0.33} + 0.0393 We_{\text{noz}}^{0.73} \left(\frac{\rho_d g d_{\text{noz}}^2}{\sigma} \right)^{-0.315} \right)^{-1} \quad 10$$

and the rise velocity can be calculated with Vignes' equation (Godfrey and Slater, 1994):

$$v_{\infty,d} = \frac{d}{4.2} \left(\frac{g \Delta \rho}{\rho_c} \right)^{2/3} \left(\frac{\rho_c}{\eta_c} \right)^{1/3} \left(1 - \frac{Eo}{6} \right) \quad 11$$

The validity of equations 10 and 11 for the present case might be argued, as they were developed for a droplet column. However, the hold-up in the column section above the 3-phase bed (a droplet column equivalent) could be well predicted with equations 9a, 10, 11 and 14, assuming the droplet diameter to be the same throughout the whole column. Based on the validity of these hold-up predictions, equations 10

and 11 were adopted for the present 3-phase fluidized bed.

The total drag coefficient in a 3-phase mixture for a droplet ($C_{d,d}$) and for a single gel bead ($C_{d,s}$) were calculated from the measured hold-ups and the water and dodecane fluxes by equations 4 and 7-11.

Figure 7a shows the total droplet drag coefficient in a 3-phase mixture as a function of the dimensionless slip velocity between droplets and water, which was defined as the actual slip velocity divided by the rise velocity of a single droplet in stagnant water (equation 11); its value ranges from zero to one. Drag coefficients were classified according to the measured solids hold-up. Figure 7a reveals two interesting features. The behavior of the total drag coefficient ($C_{d,d}$) for the friction between a droplet and its surroundings (gel beads, droplets and 30 mM KCl mixture) was found to be fully accounted for by its dimensionless slip velocity v_{cd}^* . There is no influence of the solids hold-up ϵ_s other than $v_{cd}^* = f(\epsilon_s)$. In, addition the total droplet drag coefficient in a 2-phase water/dodecane droplet column follows directly the behavior of the total droplet drag coefficient in a 3-phase fluidized-bed (Figure 7a, $\epsilon_s=0$).

As opposed to the behavior of the total droplet drag coefficient $C_{d,d}$, the behavior of the drag coefficient $C_{d,s}$ for the friction between a single gel bead and its surroundings (droplets, gel beads and 30 mM KCl) was not fully accounted for by variations in v_{cs}^* (Figure 7b). Apart from $v_{cs}^* = f(\epsilon_d)$, there is an additional dependency of $C_{d,s}$ on ϵ_d : a larger droplet hold-up was found to yield a relatively high $C_{d,s}$ value.

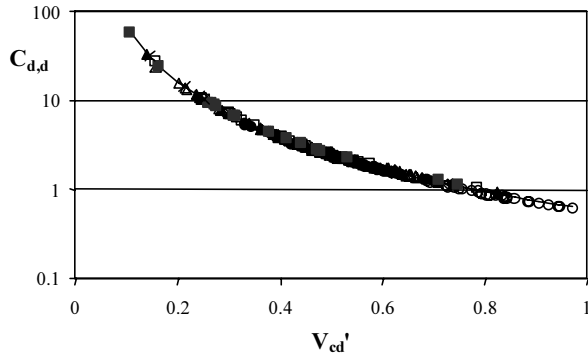


Figure 7a. Single droplet drag coefficient in a 3-phase mixture of gel beads, dodecane droplets and 30mM KCl as function of the dimensionless slip-velocity.

- | | |
|---------------------------------|---------------------------------|
| ○ $\varepsilon_s = 0$ | ● $\varepsilon_s = 0.17 - 0.20$ |
| ◇ $\varepsilon_s = 0.20 - 0.25$ | ◆ $\varepsilon_s = 0.25 - 0.30$ |
| △ $\varepsilon_s = 0.30 - 0.35$ | ▲ $\varepsilon_s = 0.35 - 0.40$ |
| □ $\varepsilon_s = 0.40 - 0.45$ | ■ $\varepsilon_s = 0.45 - 0.50$ |
| × $\varepsilon_s = 0.50 - 0.56$ | |

The drawn line is the prediction with equation 12.

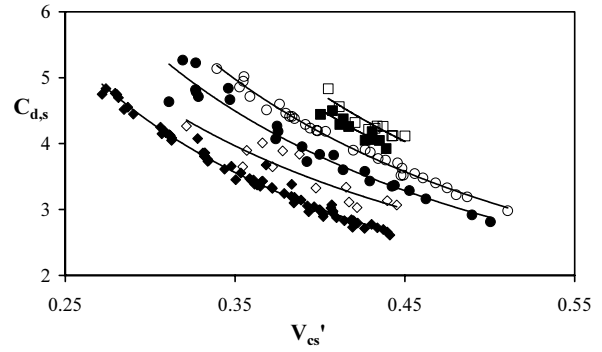


Figure 7b. Single gel bead drag coefficient in a 3-phase mixture of gel beads, dodecane droplets and 30 mM KCl as function of the dimensionless slip-velocity.

- | | |
|----------------------------|----------------------------|
| ◆ $\varepsilon_d = 0$ | ◇ $\varepsilon_d = 0.0125$ |
| ● $\varepsilon_d = 0.0275$ | ○ $\varepsilon_d = 0.0475$ |
| ■ $\varepsilon_d = 0.0725$ | □ $\varepsilon_d = 0.09$ |

A model was developed for the total drag coefficients of droplets and gel beads in a 3-phase mixture. This model used features demonstrated in Figure 7. Similar to Van der Wielen *et al.* (1996a), the model was based on force balances for a single droplet or gel bead in a mixture of droplets, gel beads and continuous liquid. Different correlations for the various total drag coefficients were used, however, as the correlations of Van der Wielen *et al.* (1996a) did not gave satisfactory predictions. The newly derived models for the drag coefficients were evaluated for predicting the various hold-ups.

Model for the droplet hold-up

In a 3-phase fluidized bed, the bed height is easily measured, and, from a known gel bead volume, the gel bead hold-up may be calculated directly. Therefore, the gel bead hold-up is assumed to be known in this paragraph. Figure 7a shows that the total drag coefficient for a single droplet in the 3-phase mixture may be described by a general equation:

$$C_{d,d} = c_1 (v_{cd}')^{c_2} = c_1 \left(\frac{v_{cd}}{v_{\infty,d}} \right)^{c_2} = C_{d,\infty,d} (v_{cd}')^{c_2} \quad 12$$

For $\varepsilon_s \rightarrow 0$ and $\varepsilon_d \rightarrow 0$, the slip velocity is equal to the terminal rise velocity of a single droplet ($v_{\infty,d}$). Consequently, parameter c_1 is equal to the drag coefficient for a single droplet rising in stagnant water ($C_{d,\infty d}$).

The drag coefficient ratio $C_{d,d}/C_{d,\infty d}$ (cf. equation 12) may also be derived from force balances. The force balance for a droplet in the 3-phase mixture (equation 7a) is divided by the force balance for a single droplet rising in stagnant water (an equivalent of equation 7a), which results in the drag coefficient ratio. Substituting this relation for the drag coefficient ratio in equation 12, and rewriting the resulting equation (with equation 8 for the mixture density), yields an implicit correlation for the droplet hold-up:

$$\varepsilon_s \frac{\rho_s - \rho_c}{\rho_c - \rho_d} + 1 - \varepsilon_d = \left(\frac{v_{cd}}{v_{\infty,d}} \right)^{c_2+2} \quad 13$$

In the next paragraph, it will be shown how parameter c_2 can be derived from a 2-phase droplet hold-up model.

Figure 7a shows that for $\varepsilon_s = 0$, i.e. a 2-phase droplet column, the total droplet drag coefficient in the droplet/water 2-phase mixture, can also be described by equation 12. An adequate model for the slip velocity between droplet and water in a 2-phase system has been presented by Van Zessen *et al.* (2003) for hold-ups below 0.13:

$$v_{cd} = v_{\infty,d} (1 - \varepsilon_d)^4 \quad 14$$

Substituting equation 14 in 13 and solving for parameter c_2 ($\varepsilon_s=0$), results in $c_2 = -1.75$. Although the droplet hold-up and drag coefficient (equation 12) for the 2-phase droplet water mixture are well described, the 3-phase experimental data (drag coefficient, and droplet hold-up) are systematically underestimated (data not shown). Therefore, parameter c_2 was fitted on the 3-phase droplet hold-up data, which resulted in $c_2=-2.06$. The total droplet drag coefficient for both a 2-phase and 3-phase system is now well described (Figure 7a). Apparently, the prediction of droplet drag coefficients in a 2-phase water/ droplet mixture is not very sensitive to parameter c_2 .

Up to a hold-up of about 0.06, the description of the data (equation 13, $c_2=-2.06$) is fair (Figure 8). The average deviation between data and model for hold-ups less than 0.06 is 16.5%; 81% of the model predictions show a deviation less than 25%. For hold-ups larger than 0.06 the prediction is not good (Figure 8).

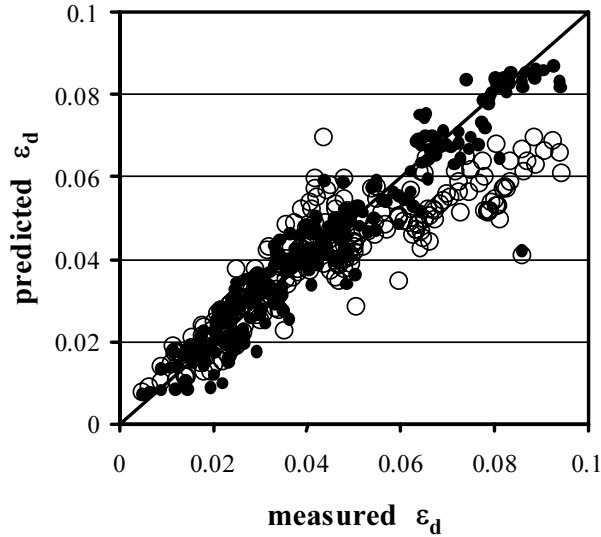


Figure 8. Parity plot for the droplet hold-up in a 3-phase fluidized bed. o the model fitted on the data is equation 12; • the model fitted on the data is equation 15.

In view of this partial inadequacy of the total droplet drag coefficient-based model (good description of the drag coefficient, but underestimation of the higher droplet hold-ups), an empirical model was tested as an alternative. A power-law dependency of the dimensionless slip-velocity on both the solvent phase velocity and its hold-up were assumed according to:

$$\frac{V_{cd}}{V_{\infty,d}} = v_{cd}' = c_3 \cdot U_d^{c_4} \cdot \epsilon_d^{c_5} \quad 15$$

A fit of this equation to the data in figure 5a yielded $c_3=5.4$, $c_4=0.88$ and $c_5=-0.76$. A parity plot between predicted and measured droplet hold-ups (Figure 8) shows that droplet hold-up is well described over the entire range of measured hold-ups. The average deviation between data and model is 13%; 89% of the model predictions show a deviation less than 25%. The prediction of the drag coefficient with this empirical model is fair; the average deviation is 17%, and 76% of the model predictions show a deviation less than 25%.

Model for droplet and gel bead hold-up

In the experimental set-up, the droplet hold-up was determined from the gel bead hold-up (equations 1-4). So, contrary to the preceding paragraph, in which a known gel bead hold-up was assumed, now both hold-ups were assumed unknown and will be predicted simultaneously. This overall model for hold-up prediction in a 3-phase fluidized bed is outlined in Figure 9, showing how physical parameters, nozzle geometry and liquid fluxes determine the three hold-ups.

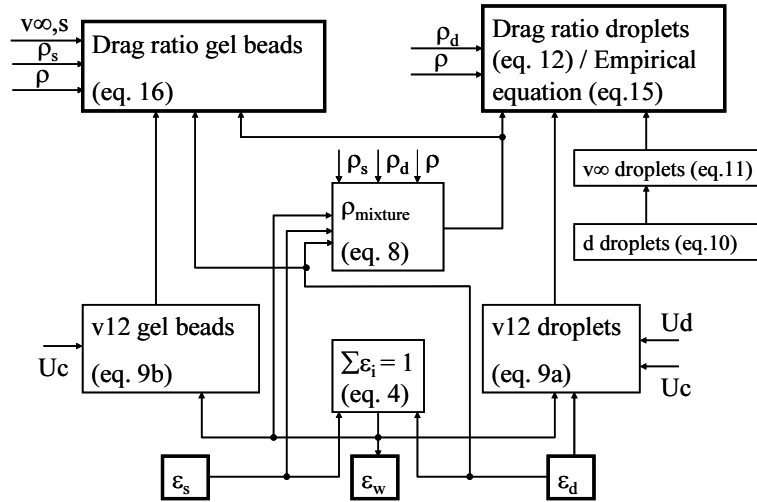


Figure 9. Hold-up calculations in a 3-phase fluidized bed.

Figure 7b suggests that the total drag coefficient of a single gel bead in mixture of gel beads, droplets and 30 mM KCl can be described by:

$$C_{d,s} = c_6 \left(\frac{v_{cs}}{v_{\infty,s}} \right)^{c_7} (1 - \varepsilon_d)^{c_8} = c_6 (v_{c,s}')^{c_7} (1 - \varepsilon_d)^{c_8} = C_{d\infty,s} c_9 (v_{c,s}')^{c_7} (1 - \varepsilon_d)^{c_8} \quad 16$$

For $\varepsilon_d \rightarrow 0$ and $\varepsilon_s \rightarrow 0$, the slip velocity (v_{cs}) is equal to the terminal settling velocity of a gel bead in stagnant water ($v_{\infty,s}$). So, parameter c_6 should be equal to the drag coefficient for a single gel bead settling in stagnant water ($C_{d\infty,s}$). The ratio of drag coefficients ($C_{d,s}/C_{d\infty,s}$) may be obtained by dividing the force balance for a single gel bead in the 3-phase mixture (equation 7b) with the force balance for a single gel bead settling in stagnant water (an equivalent of equation 7b). Using this drag coefficient ratio, together with equations 8 and 16, the gel bead hold-up may be predicted by:

$$\frac{\varepsilon_d \rho_d + \varepsilon_s \rho_s + \varepsilon_c \rho_c - \rho_s}{\rho_c - \rho_s} \left(\frac{v_{\infty, s}}{v_{cs}} \right)^2 = c_9 \cdot \left(\frac{v_{cs}}{v_{\infty, s}} \right)^{c_7} (1 - \varepsilon_d)^{c_8} \quad 17$$

In the next paragraph, it will be shown how parameters c_7 and c_9 can be derived from the 2-phase hold-up model of a liquid fluidized bed.

Van Zessen *et al.*, 2003 concluded that for a 2-phase fluidized bed of gel beads the slip velocity can be described by:

$$v_{cs} = \frac{U_c}{\varepsilon_c} = k \varepsilon_c^{1.35} \quad 18$$

where parameter k is not equal to the terminal settling velocity of a gel bead (5.12 cm s^{-1}) but equals 3.77 cm s^{-1} . Substituting equation 18 in equation 17, and solving for parameter c_7 ($\varepsilon_d=0$, $c_9=1$ and $c_8=0$) resulted in $c_7 = f(\varepsilon_c)$, and since $\varepsilon_c = f(U_c)$, also $c_7=f(U_c)$. However, Figure 7b suggests that parameter c_7 might have a single value. Therefore, it was fitted together with parameter c_9 to the solids hold-up data for a liquid-fluidized bed using equation 17 (data in figure 5b, $U_d=0 \text{ cm s}^{-1}$). This resulted in $c_7=-1.26$ and $c_9=1.24$. Figure 10b, a parity plot between measured and predicted gel bead hold-up, shows that the data are well described. Parameter c_9 had to be fitted on the data, as for $c_9=1$, there was a systematic underestimation of the higher solids hold-up, and the relative residuals were not randomly distributed, as they should be.

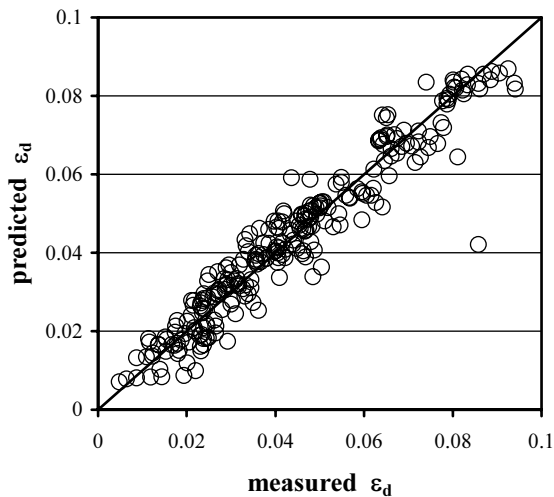


Figure 10a. Parity plot for droplet hold-up in a 3-phase fluidized bed. Models fitted on the data are equations 15 and 17.

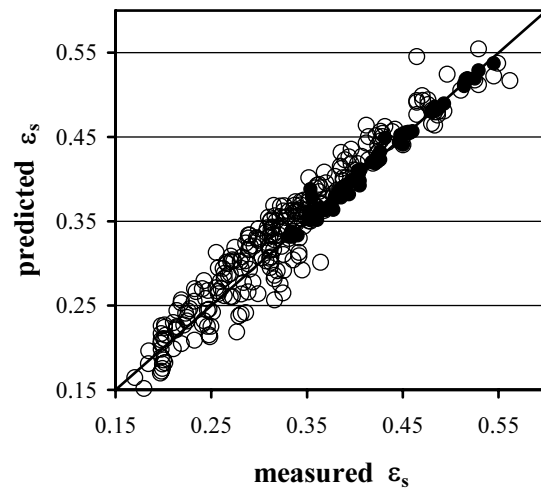


Figure 10b. Parity plot for gel bead hold-up in a 3-phase fluidized bed, ● 2-phase fluidized bed

As equation 15 was found adequate for the entire range of droplet hold-ups, this model was adopted as a part of the simultaneous prediction of all hold-ups. Equations 15 and 17 were now used to describe the droplet hold-up and gel bead hold-up simultaneously (cf. Figure 9). We used for c_7 and c_9 the parameter values of the 2-phase fluidized bed. Parameters c_3 , c_4 , c_5 and c_8 were obtained from fitting the model equations on the hold-up data (Figure 5); resulting in $c_3 = 6.15 \text{ s m}^{-1}$, $c_4 = 0.90$, $c_5 = -0.76$ and $c_8 = -6.51$. Our data are well described by this model (Figure 10). The average deviation between model and droplet hold-up data is 12% (89% of all data show a deviation less than 25%), for the gel bead hold-up data the average deviation is 7.2% (97% of all data show a deviation less than 25%).

Conclusion

The liquid analogue of a gas-liquid-solid fluidized bed, a liquid-liquid-solid (gel bead) fluidized bed was studied. Visual observations of the 3-phase fluidized bed showed how the behavior of the fluidized bed depended on the water and dodecane fluxes. Characterized by the gel beads flow, five flow patterns were discerned: two homogeneous regions, two heterogeneous regions and one unstable region in which droplets coalesced and gel beads were washed out from the fluidized bed. Gel bead hold-up and dodecane hold-up were measured. At a constant water velocity, the dodecane hold-up increased with the dodecane velocity. At a constant dodecane velocity, however, the droplet hold-up decreased with the water velocity, while at the same time gel bead hold-up decreased. For all fluxes, the dodecane hold-up was always higher than the droplet hold-up in a 2-phase droplet column.

Literature models for related 3-phase systems, a gas-liquid-solid 3-phase fluidized bed and a solid-solid-liquid fluidized bed, could not predict correctly the entire range of hold-ups in the present system. A new model, based on steady state force balances for both a single gel bead and a single droplet in a 3-phase mixture (gel beads, droplets and 30 mM KCl) was developed for predicting gel bead hold-up and dodecane droplet hold-up. The gel bead hold-up was well described for all data, but droplet hold-ups were described adequately for hold-ups up to 0.06 only. An empirical model for droplet hold-up was developed as an alternative. Its predictions were good for the entire range of measured droplet hold-ups.

Nomenclature

A	: cross-sectional column area	m^{-2}
c_1, c_2	: parameters in equation 12	-
c_3	: parameter in equation 15	s m^{-1}
c_4, c_5	: parameter in equation 15	-
c_{6-9}	: parameters in equation 16	-
C_{di}	: total drag coefficient for particle i	-
d	: diameter droplet	m
d_i	: diameter particle i	m
d_{noz}	: nozzle diameter	m
E_o	: Eötvös number, $g\Delta\rho d^2/\sigma$	-
$E_{o_{noz}}$: Eötvös nozzle number, $g\Delta\rho d_{noz}^2/\sigma$	-
g	: gravity acceleration (9.8)	$\text{m}^2 \text{s}^{-1}$
H_{bed}	: bed height	m
ΔP	: pressure drop	N m^{-2}
ΔP_{exp}	: measured pressure difference	N m^{-2}
U	: superficial velocity	m s^{-1}
V_s	: solids volume	m^3
v_∞	: terminal rise/settling velocity	m s^{-1}
v_{ci}	: slip velocity between water and component i	m s^{-1}
We_{noz}	: nozzle Weber number, $\rho_c v_{\infty, d}^2 d_{noz}/\sigma$	-
Δz	: height between two points	m

Greek

ε	: hold-up	-
η	: viscosity	Nm s^{-1}
ρ	: density	kg m^{-3}
$\Delta\rho$: density difference continuous and disperse phase	kg m^{-3}
σ	: interfacial tension	N m^{-1}

subscript

c	: continuous
d	: dispersed (organic solvent droplet)
mix	: mixture
s	: gel bead

Mixing of the continuous phase in a liquid-liquid-solid fluidized-bed bioreactor

Abstract

A liquid-liquid-gel bead (solid) fluidized bed is a new type of bioreactor to overcome biokinetic or solubility limitations present in different kinds of biotransformations. In this 3-phase fluidized bed both liquid phases (n-dodecane dispersed as droplets, and 30 mM KCl as the continuous phase) are separately introduced to the bioreactor. In this work the mixing of the continuous phase was studied by measuring the residence-time distribution for different superficial velocities of both liquid phases. A KCl-tracer was used. Due to mass transfer to the gel beads, the limitations using this tracer were studied as well. A pulse volume of 3 ml (4 M KCl) gave reliable results. An axial dispersion coefficient for the continuous phase was determined from inlet and outlet residence time distribution curves. The axial dispersion coefficient in the continuous phase (D_{ax}) increased with an increasing superficial n-dodecane velocity. For a superficial velocity of the continuous phase (U_c) smaller than $\sim 0.8 \text{ cm s}^{-1}$ the D_{ax} increased with an increasing U_c , whereas for U_c larger than $\sim 0.8 \text{ cm s}^{-1}$ the D_{ax} decreased with an increasing U_c . These results were easily explained by the isotropic turbulence theory of Baird and Rice (1975). The mixing of the continuous phase of this 3-phase fluidized bed was comparable with the mixing of either the continuous phase of a bubble column or the continuous phase in the main tube of a liquid-impelled loop reactor.

Introduction

The potentials of using an organic solvent as an extraction aid to overcome biokinetic or solubility limitations in different kinds of biotransformations have been shown by many authors (e.g. Adlercreutz, 2000; Vermuë, 1995). For a biotransformation in which the production rate is strongly reduced by the product itself, a new type of bioreactor has been studied: a liquid-liquid-solid 3-phase fluidized bed bioreactor. In this bioreactor there are three different phases: 1) the solid phase that consists of gel beads with biocatalyst, 2) one liquid phase, an organic solvent, which is dispersed as droplets, 3) another liquid phase which is continuous, and this phase is used for the supply of nutrients to the immobilized biocatalyst. This continuous phase fluidizes the gel beads, whereas the organic-solvent droplets, rising through the fluidized bed, extract the formed product.

The hold-ups of the different phases in a liquid-liquid-solid fluidized bed bioreactor have been studied before (Van Zessen *et al.*, 2003). In this paper the residence time distribution of the continuous phase is studied. A residence time distribution can be related to mixing characteristics of the bioreactor. As such, it serves as an important design parameter.

To measure a residence-time distribution, a tracer is injected and its concentration is followed in time at a fixed point in the bioreactor downstream from the point of injection. As mixing of the continuous phase is studied, this tracer must not be transferred to either of the two dispersed phases, i.e. the gel beads and the organic droplets. A suitable tracer can be a blue dextran solution (Gommers *et al.* 1986). In our experimental set-up, however, the concentration of the blue dextran comes close to the detection limit of the analysis equipment. Consequently, as the signal is full of noise, the interpretation of this signal can not be performed reliably. So, we chose a different tracer, viz. a KCl solution. This salt, however, can be transferred to the gel beads (Thompson and Worden, 1992) and this measuring method had to be validated.

In the first part of the results section the validation of this measuring method is discussed. In the second part of the results section this validated measuring method was applied for measuring the residence-time distribution of the continuous phase of the 3-phase fluidized bed. Different flow patterns regimes have been distinguished in the 3-phase fluidized bed (Van Zessen *et al.* 2003). Measurements have been performed in the structured solids flow and in the turbulent solids flow regimes.

A dispersion coefficient of the continuous phase is calculated from the

residence-time distribution curve, using a suitable flow model. Based on the magnitude of this dispersion coefficient it can be concluded that mixing of the continuous phase in a liquid-liquid-solid 3-phase fluidized bed bioreactor is more comparable to an ideally mixed flow pattern than to a plug flow pattern. It will be shown that the dispersion coefficient of the continuous phase is well described by the model of Baird and Rice (1975), using the energy-dissipation rate per unit mass for a 3-phase fluidized bed.

Theoretical aspects

Residence-time distribution represents the time-distribution of volume elements in a specific part of a device, in this case the continuous aqueous phase in the bioreactor. The shape of this time-distribution can be translated to flow characteristics of the bioreactor. To measure this distribution, a tracer is injected and its concentration is followed in time. The translation from tracer profile, $C(t)$, to a residence time distribution curve, $E(t)$, follows from (Levenspiel,1972):

$$E(t) = \frac{\Phi}{m} C(t) \tag{1}$$

with Φ is the flux of the continuous phase and m is the total amount of tracer injected. This amount is equal to:

$$m = \Phi \int_0^{\infty} C(t) dt \tag{2}$$

The shape of the distribution curve at the outlet is influenced by the tracer profile of the incoming fluid and the system itself, see Figure 1. Unless the shape of the inlet-tracer profile is known, this inlet-tracer profile should be measured. So, time-profiles of the tracer concentration at the outlet as well as time-profiles of the tracer concentration at the inlet have been measured.

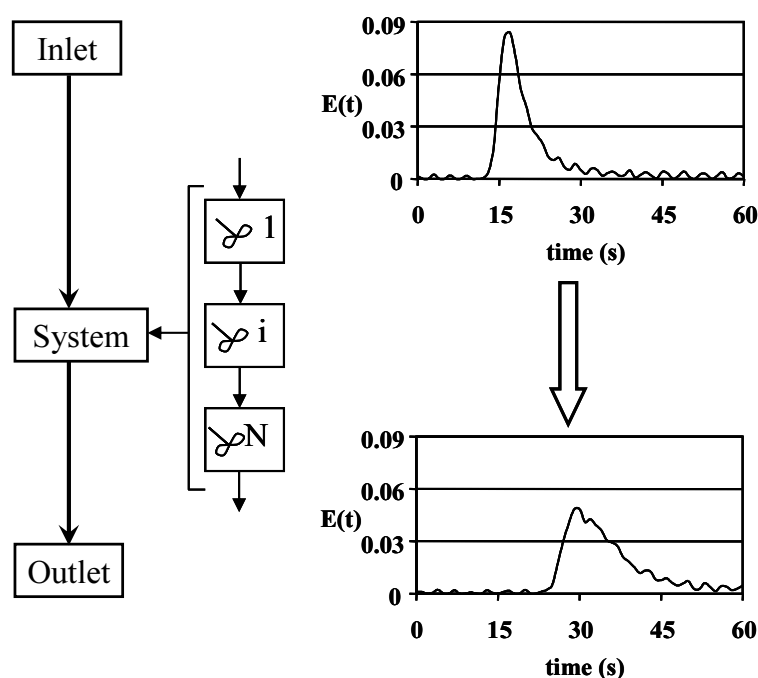


Figure 1. Transformation of the residence-time distribution curve at the inlet of a (reactor)system to the residence-time distribution curve at the outlet of a (reactor)system by the (reactor)system itself between the inlet and the outlet.

Fahim and Wakao (1982) presented a review on the parameter estimation from tracer-response measurements. Different methods were analyzed, e.g. methods based on 1) the moments of the distribution curve, 2) the application of transfer functions and 3) time-domain analysis. They concluded that the most reliable parameter values are obtained from the time-domain analysis. Thus in this paper, time-domain analysis is used for parameter estimation. To use time-domain analysis for parameter estimation, a dynamic model describing flow behavior of the continuous phase is needed.

Models for describing the flow behavior of the continuous phase can range from simple to highly complicated. Two of the most common and simple models are the tanks-in-series model and the plug-flow-with-dispersion model (axial dispersion model). The tanks-in-series model reads:

$$\begin{aligned}\frac{dC_1}{dt} &= \frac{1}{\tau}(C_{in}(t) - C_1) \\ \frac{dC_i}{dt} &= \frac{1}{\tau}(C_{i-1} - C_i) \quad \wedge \quad i = 2 \dots N-1 \\ \frac{dC_{out}}{dt} &= \frac{1}{\tau}(C_{N-1} - C_{out})\end{aligned}\tag{3}$$

in which C_{in} is the inlet tracer profile, C_{out} is the outlet tracer profile, C_i is the tracer profile in tank i , t represents time and τ is the mean residence time given by:

$$\tau = \frac{\varepsilon_c \Phi N}{V}\tag{4}$$

in which ε_c is the continuous phase hold-up, and V is the total volume of the bioreactor section considered in this analysis.

The axial dispersion model reads:

$$\frac{\partial C}{\partial t} = -\frac{U_c}{\varepsilon_c} \frac{\partial C}{\partial x} + D_{ax} \frac{\partial^2 C}{\partial x^2}\tag{5}$$

in which U_c is the superficial velocity of the continuous phase and the D_{ax} is the axial dispersion coefficient. The initial conditions are:

$$C(t=0, \forall x) = 0; \quad C(t>0, x=0) = C_{in}(t)$$

When U_c is given and ε_c is known, both models contain only one parameter; the number of tanks in the tanks-in-series model and the axial-dispersion coefficient in the latter model. For a flow pattern comparable to plug flow, i.e. a large number of tanks-in-series, or a small axial-dispersion coefficient, these parameters are related to each other, as pointed out by Levenspiel (1972):

$$D_{ax} = \frac{LU_c}{2N\varepsilon_c}\tag{6}$$

with L is the height of the bioreactor section.

For a flow pattern comparable to an ideally mixed tank, the basic idea of the axial dispersion model is violated. However, Gommers *et al.* (1986) showed the validity of applying the axial dispersion model to describe axial mixing for gas-liquid-solid fluidized beds. The axial dispersion model was also successfully applied to describe axial mixing in a liquid-liquid-solid fluidized bed (Kim *et al.*, 1989). Applying the axial dispersion model instead of the tanks-in-series models is tempting, as the axial dispersion coefficient can take continuous values, whereas the number of tanks can only be a discrete value. Especially for a small number of tanks, the limitation of using only discrete values might result in a less accurate description of the flow pattern. In this paper both models were used to describe the experimental data.

Materials and Methods

Two sets of different experiments were performed. The first set of experiments aimed at developing and validating the measuring method. In the second set of experiments this validated method was used to determine the mixing characteristics of the continuous phase of the 3-phase fluidized bed.

Materials

The gel beads used in all experiments were κ -carrageenan gel beads filled with 10% Celite®. The preparation of these gel beads can be found elsewhere (Van Zessen *et al.* 2003). The density of the gel beads was 1065.1 kg m^{-3} and the diameter was 2.76 mm. The density and diameter were determined as described by Van Zessen *et al.* (2001). A 30mM KCl solution was used as the continuous phase (density is 998.0 kg m^{-3}). The organic solvent used in the 3-phase fluidized bed was n-dodecane (Aldrich, 99%+ pure), density is 742.7 kg m^{-3} . As tracer solution a mixture of a blue-dextran solution and a KCl-solution was used.

Development and validation of the measuring method

The experimental set-up for developing and validating the measuring method is shown in Figure 2. A 30 mM KCl solution was pumped through the column with a flow rate high enough to establish a fluidized bed. A tracer pulse was introduced to the column by switching a three-way valve. Most of the liquid was purged, but a small part was pumped through a home-made flow-through conductivity cell connected to a conductivity meter (WTW). Next, the liquid flew through a flow-

through cuvette, in which the absorption at 280 nm was measured with a spectrophotometer (Ultrospec 2000, Pharmacia Biotech). The spectrophotometer and conductivity meter were connected to an A/D converter (Hewlett Packet) and a personal computer for data acquisition. Two different columns were used. One column was 20 cm high; the other was 130 cm high. Both columns had an internal diameter of 2 cm. At different flow rates tracer concentrations ranging from 40 mM up to 1 M and pulse volumes from 1 ml up to 7 ml were used to study whether mass transfer took place. To verify whether mass transfer took place in the 3-phase fluidized bed, the set-up for measuring absorption and conductivity, as described above, in combination with the experimental set-up of the 3-phase fluidized bed, see below, was also used.

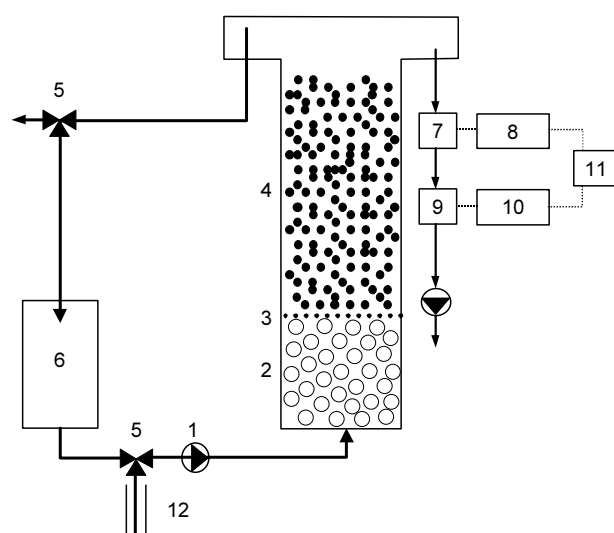


Figure 2. Experimental set-up for developing and validating the measuring method. 1 gear pump, 2 glass pearls to provide a good flow distribution, 3 sieve-plate, 4 fluidized bed of gel beads, 5 three-way valve, 6 storage vessel for 30 mM KCl, 7 flow-through conductivity cell, 8 WTW Conductivity Meter, 9 flow-through cuvette, 10 Ultrospec 2000 spectrophotometer, 11 A/D converter and personal computer, 12 tracer solution vessel.

Residence time measurements

Measurements were performed in an experimental set-up as shown in Figure 3. A detailed description of this set-up is given elsewhere (Van Zessen *et al.*, 2001). Water and n-dodecane flow co-currently upwards, and as both liquids were highly immiscible, they were easily separated with a one-stage gravity settler. The column was 2 m high with an internal diameter of 6 cm.

Figure 4 shows the set-up used for introducing a tracer pulse to the column. While a 30 mM KCl-solution was circulated over the column, a tube between two three-way valves was filled with the tracer solution. By adjusting the length of this tube, the tracer volume could be changed. In the residence-time experiments the tube length was 6 cm that resulted in a pulse volume of 3 ml (internal diameter of the tube is 0.8 cm). By switching both three-way valves simultaneously, the pulse was introduced to the column. The conductivity of the solution was measured at two different column heights: 25cm and 75cm. Residence-time distribution measurements were performed for the two (liquid-solid) and three phase (liquid-liquid-solid) fluidized bed.

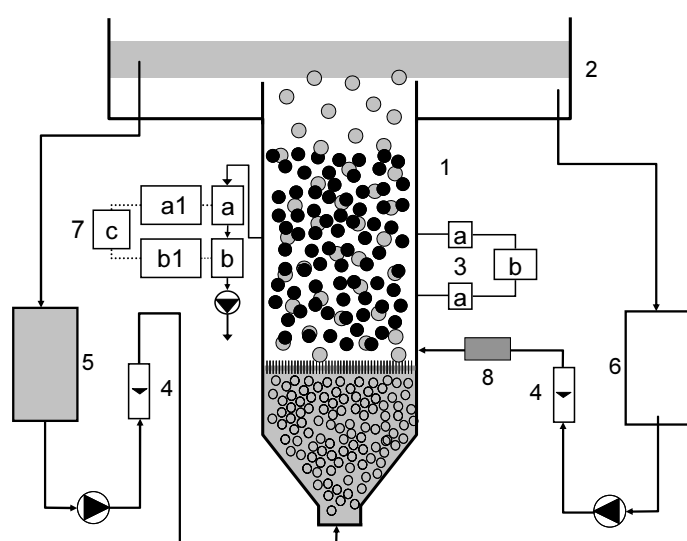


Figure 3. Experimental set-up of the 3-phase fluidized bed for measuring the residence time distribution. 1 3-phase fluidized bed, the gel beads, dodecane droplets, 2 separator for 30 mM KCl and dodecane, 3 conductivity measurement (a conductivity cells, b data acquisition device), 4 rotameter, 5 storage vessel for dodecane, 6 storage vessel for 30 mM KCl-solution, 7 absorbance measurement (a flow-through conductivity cell, a1 WTW conductivity meter, b flow-through cuvette, b1 Ultrospec 2000 spectrophotometer, c A/D converter and personal computer), 8 device for introducing the tracer solution.

Conductivity cell

The conductivity cell was home made. It consisted of two parallel placed platinum wires, 1 mm thick and 1 cm long. The distance between both wires was equal to the column diameter, i.e. 6 cm, see also Figure 5. The cell was connected to a conductivity meter (WTW). Using an A/D converter (Hewlett Packard) and a personal computer both conductivity signals were stored in time.

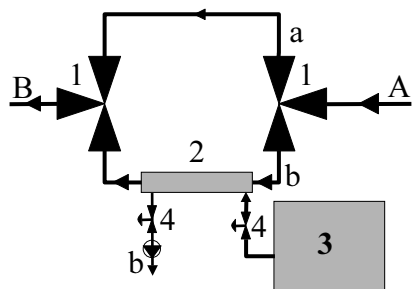


Figure 4. Set-up for the introduction of the tracer pulse. A) flow from the 30mM KCl-storage vessel, B) flow to the fluidized bed. a) By-passing the tracer pulse section, b) flow through the tracer pulse section. 1 three-way valve, 2 tube for tracer pulse (6 ml), 3 storage vessel tracer solution, 4 valve

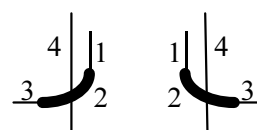


Figure 5. Home-made conductivity cell. 1 platinum wire, 2 (glass)-holder for platinum wire, 3 copper wire for connecting to a conductivity meter, 4 column wall.

Flow rates were measured with calibrated rotameters (Sho-Rate). The different flow rates applied in the experiments performed with either the 3-phase fluidized bed or the liquid fluidized bed are summarized below. U_c represents the superficial velocity of the continuous phase, and U_d represents the superficial velocity of the dodecane phase.

	U_c (cm s ⁻¹)	U_d (cm s ⁻¹)
3-phase fluidized bed		
Structured solids flow regime	0.55 – 0.8	0.1 – 0.4
Turbulent solids flow regime	1 – 1.8	0.05 – 0.7
Liquid fluidized bed	0.6 – 1.8	-

Fitting procedure

To obtain the parameters used by both presented flow models, the tracer concentration-profile has to be known. Although conductivity and UV-absorption are measured, these signals are linearly proportional with the KCl concentration and blue dextran concentration, respectively:

$$C(t) = k_i S(t) \quad 7$$

in which S is the measured signal and k_i is a proportionality constant for component i .

Implementing equation 7 into equation 1 and 2 gives the residence-time distribution based on a measured signal:

$$E(t) = \frac{S(t)}{\int S(t) dt} \quad 8$$

The measured outlet signal is transformed to a residence-time distribution using equation 8. Both models proposed for describing the mixing of the continuous phase, equation 3 and 5, are transformed in order to calculate a residence-time distribution. This was done by multiplying the respective equations with the water flux and by dividing the equations by the total mass of the injected tracer. For the tanks-in-series model the resulting set of equations is:

$$\begin{aligned} \frac{d E_1}{dt} &= \frac{1}{\tau} \left(\frac{S_{in}(t)}{\int S_{in}(t) dt} - E_1 \right) \\ \frac{d E_i}{dt} &= \frac{1}{\tau} (E_{i-1} - E_i) \quad \wedge \quad i = 2 \dots N-1 \\ \frac{d E_{out}}{dt} &= \frac{1}{\tau} (E_{N-1} - E_{out}) \end{aligned} \quad 9$$

For the axial dispersion model the resulting equation is:

$$\frac{\partial E}{\partial t} = -\frac{U_c}{\epsilon_c} \frac{\partial E}{\partial x} + D_{ax} \frac{\partial^2 E}{\partial x^2} \quad 10$$

The initial conditions are transformed as well

$$E(t=0, \forall x) = 0 ; E(t>0, x=0) = \frac{S_{in}(t)}{\int_0^{\infty} S_{in}(t)dt}$$

The hold-up of the continuous phase followed from a previous presented model predicting the different hold-ups in this type of fluidized bed (Van Zessen *et al.*, 2003), equations 14 and 15a-c. Equation 10 was then solved by discretization of the axial coordinate. To determine the number of ideally stirred tanks-in-series in equation 3 or the axial dispersion coefficient in equation 5, the calculated outlet profile ($E_{out,m}$) was compared with the measured outlet profile ($E_{out,exp}$). Both parameters were determined by minimizing the residual sum of squares as defined by equation 11:

$$SS_{res} = \sum_t (E_{out,m}(t) - E_{out,exp}(t))^2 \quad 11$$

Results and Discussion

First the results of the validation experiments are shown. These results are applied for performing reliable residence time distribution measurements in the 3-phase fluidized bed. Next, the results of these measurements are shown.

Development and validation of the measuring method

For a column without gel beads, the residence time distribution, determined with a KCl and blue dextran solution, is shown in Figure 6. As the molecular weight of blue dextran is $\sim 2,000,000 \text{ g mol}^{-1}$, diffusion of blue dextran into the gel beads can be neglected. In different experiments diffusion was indeed not observed. Figure 6 demonstrates that both tracers yield identical response curves. So, in order to evaluate whether mass transfer takes place, both response curves can be compared to each other. When mass transfer of KCl takes place, the salt- $E(t)$ curve will differ from the blue dextran $E(t)$ curve remarkably at two points: 1) the top of the salt-curve is lower and 2) the tail is elongated over a longer period of time. Consequently, the KCl-response curve crosses the blue dextran curve, see Figure 7.

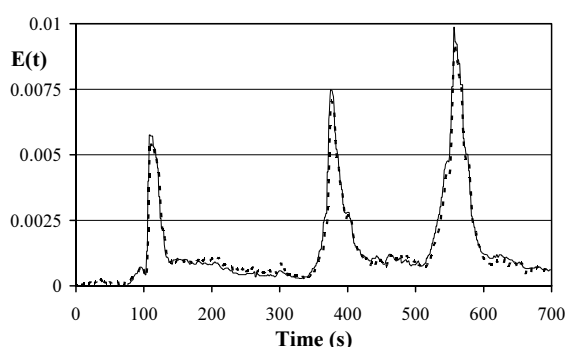


Figure 6. Residence time distribution curve of a 20 cm high column filled with water.
 blue dextran tracer; — KCl tracer.

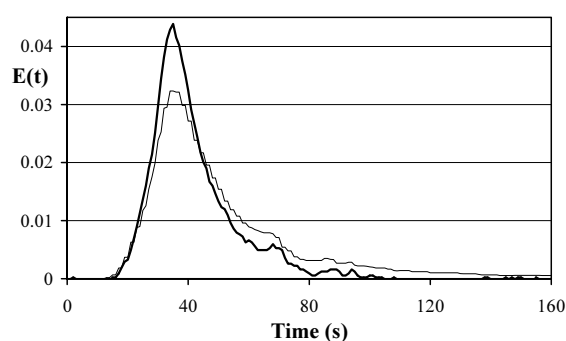


Figure 7. Residence time distribution curve for a 130 cm high column filled with gel beads. Pulse volume 2.9 ml (2 g/l blue dextran, 1 M KCl), . — blue-dextran tracer; KCl tracer.

From the experiments performed in the small column (20 cm high) it was observed that mass transfer was only important for a large pulse volume (6 ml) (data not shown). A better understanding whether mass transfer took place, was obtained from experiments in the larger column (130 cm). For a low flow rate (1 cm/s) mass transfer was absent for any salt concentration applied and each pulse volume used (data not shown). At a high flow rate (1.9 cm/s) mass transfer was observed for the

larger pulse volumes used, regardless of the salt concentrations applied (data not shown). By reducing the pulse volume, mass transfer almost disappeared (data not shown). So, a KCl-solution as tracer for $E(t)$ -measurements is well possible, provided the pulse volume is not too large.

For determining the $E(t)$ in a 3-phase fluidized bed, a pulse volume of 3 ml was used and a tracer concentration of 4 M KCl. This high concentration was used as experiments showed that a high salt concentration did not result in mass transfer, provided the pulse volume is small. Whether mass transfer took place, was verified by using the blue dextran/ KCl-salt tracer pulse for a dodecane flux of 0.1 cm s^{-1} and a water flux of 1.2 cm s^{-1} . Although the UV-absorption of the blue dextran was close to the detection limit, and consequently the signal is full of noise, it could be concluded that mass transfer was not significant (results not shown). Applying the same tracer pulse (3 ml, 4M KCl) in a 2-phase liquid-fluidized bed, it was concluded that even for high water fluxes mass transfer is not detectable (see Figure 8).

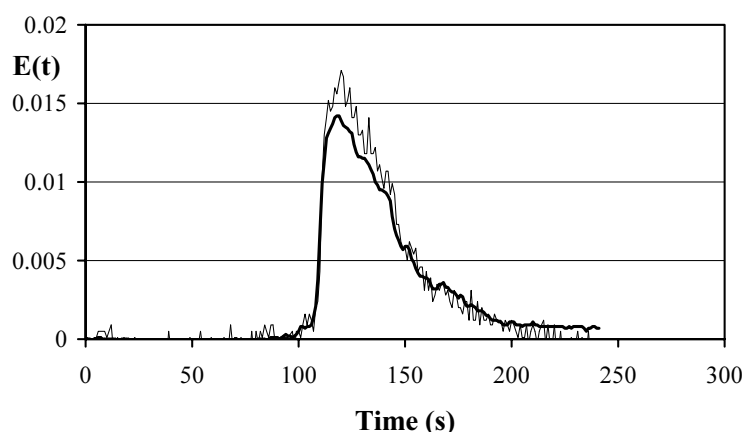


Figure 8. Residence time distribution curve for a liquid-solid (gel beads) fluidized bed. Puls volume 3 ml, — 4M KCl tracer, — 2 g l⁻¹ blue dextran tracer.

Residence time distribution experiments

First, a typical residence-time distribution curve for a 2-phase and a 3-phase fluidized bed will be shown. Thereafter, the dispersion coefficient derived from the residence time distribution curve, will be given as a function of the water and dodecane flux.

Figure 9 shows a typical measured $E(t)$ -curve at the inlet and the outlet of a liquid-solid fluidized bed (figure 9a), as well as of a liquid-liquid-solid fluidized bed (figure 9b). It appears that the inlet $E(t)$ -curve for a liquid-liquid-solid fluidized bed is much broader and the top is much lower. Regarding the outlet $E(t)$ -curves for both fluidized beds it can be said that the $E(t)$ -curve for the 3-phase fluidized bed is much broader. At equal superficial water velocity the differences between the $E(t)$ -curves of both fluidized beds shown in figure 9, were always observed.

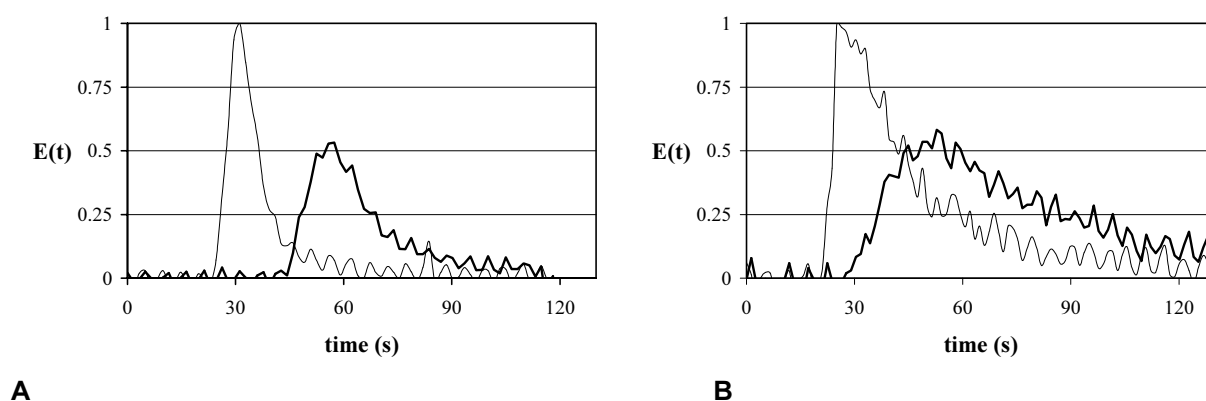


Figure 9. Residence time distribution for a liquid-solid fluidized bed (A) and a liquid-liquid-solid fluidized bed (B). 30 mM KCl-solution superficial velocity is 1.2 cm s^{-1} , dodecane flux is 0.4 cm s^{-1} . — inlet, — outlet.

Two different, but comparable models for describing the mixing of the continuous phase were used: the tanks-in-series model (eq. 9) and the axial dispersion model (eq. 10). Using the experimental data for a superficial continuous phase velocity of 1.4 cm s^{-1} and a superficial dodecane velocity ranging from 0.05 to 0.7 cm s^{-1} , the number of tanks-in-series and the axial dispersion coefficient were fitted. The number of tanks-in-series can be transformed to a dispersion coefficient using equation 6. Figure 10 shows the fitted dispersion coefficient, using the axial dispersion model, and the dispersion coefficient based on the tanks-in-series model. From this figure it can be concluded that both models give the same relationship between the superficial dodecane velocity and the dispersion coefficient.

From duplicate experiments (the same superficial dodecane velocity) it can be

concluded that the experimental method gives reproducible results (see Figure 10). Using the tanks-in-series model, the number of tanks-in-series can only take discrete values. As a result, for a liquid-liquid-solid fluidized bed, in which the number of tanks-in-series is between 2 and 9, the accuracy of the transformed dispersion coefficient is small: for $N=2$, D_{ax} is between 21 and 63 $\text{cm}^2 \text{s}^{-1}$; for $N=9$, D_{ax} is between 5.5 and 6.9 $\text{cm}^2 \text{s}^{-1}$. As the dispersion coefficient in the axial dispersion model can take any value, the axial dispersion model was used for fitting the dispersion coefficient on the other experimental data.

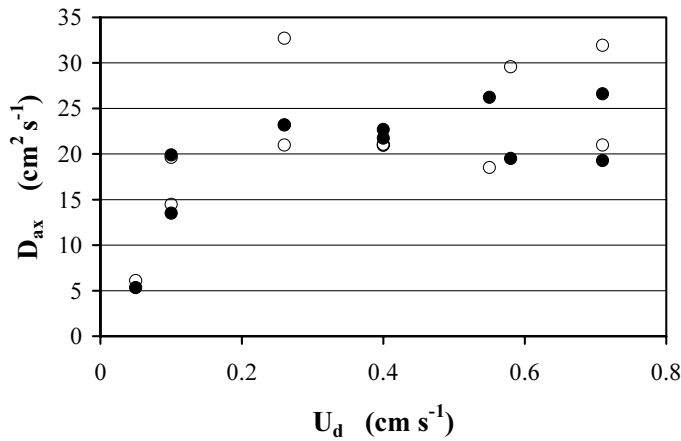


Figure 10. Dispersion coefficient as a function of the dodecane flux for a liquid-liquid-solid fluidized bed, 30 mM KCl-solution superficial velocity is 1.4 cm s^{-1} .

● dispersion coefficient fitted with the axial dispersion model, o dispersion coefficient based on the number of tanks-in-series fitted with the tanks-in-series model.

$U_d \text{ (cm s}^{-1}\text{)}$	0.05	0.1	0.1	0.26	0.26	0.4	0.4	0.55	0.58	0.71	0.71
N	9	4	3	3	2	3	3	4	2	2	3

In this type of liquid-liquid-solid fluidized bed different distinct flow regimes can exist (Van Zessen *et al.* 2003) depending on the superficial velocities of both phases. Measurements have been performed in the structured solids flow and turbulent solids flow regime. The transition from structured solids flow regime to turbulent solids flow regime occurred at a superficial velocity of the continuous phase of about 1 cm s^{-1} . For these two different flow regimes the dispersion coefficients of the continuous phase are discussed separately.

A clear characteristic of the structured solids flow regime is bed contraction: the bed height of the 3-phase fluidized bed is smaller than the bed height of the 2-phase fluidized bed at the same superficial water velocity. Another distinctive characteristic is the movement of the gel beads: the gel beads flow a short distance in upward

direction, and then they stop moving. Next they flow a short distance in downward direction – falling back - and they stop moving again. This cycle is continuously repeated in time. In flowing upwards the gel beads approach each other, so the solids are a little concentrated. In flowing downwards the gel beads are a little further apart, and the solids are a little diluted (Van Zessen *et al.* 2003).

A clear characteristic of the turbulent solids flow regime is bed expansion: the bed height of the 3-phase fluidized bed is always larger compared with the 2-phase fluidized-bed at the same water flux. The movement of the gel beads depends on the superficial water velocity; at a high velocity the gel beads move individually and randomly through the fluidized bed, at a lower velocity the gel beads move in small groups, and these small groups move randomly through the fluidized bed (Van Zessen *et al.* 2003).

Structured solids flow regime

In figure 11 the dispersion coefficient of the water phase fitted on the measured $E(t)$ -curve at the outlet, using the measured $E(t)$ -curve at the inlet and equation 10 and 11 is shown as a function of the superficial water velocity (U_c) for two superficial dodecane velocities (U_d) (0.1 cm s^{-1} and 0.2 cm s^{-1}). This figure clearly shows that up to an U_c of 0.7 cm s^{-1} the dispersion coefficient increases with an increase in both superficial velocities. At a higher U_c the dispersion coefficient decreases.

The structured solids flow regime is characterized by the flow of the gel beads (Van Zessen *et al.*, 2003). Large groups of gel beads move up and down the fluidized bed, but in such a large group the individual gel beads stick together. At higher U_d , the up-and-down movement of the large groups of gel beads intensifies, and hence the mixing of the continuous phase is better; the dispersion coefficient increases. At higher U_c , the movement of the individual gel beads inside the large groups of gel beads intensifies, and hence mixing of the continuous phase increases; the dispersion coefficient increases as well.

The decrease of the dispersion coefficient at an U_c higher than 0.7 cm s^{-1} follows the trends observed for the turbulent solids flow regime. At an U_c of about 1 cm s^{-1} , the flow pattern of the 3-phase fluidized bed is in turbulent solids flow. This transition from structured solids flow to turbulent solids flow regime is not sharp. Increasing U_c , the large groups of gel beads fall apart gradually into smaller groups and the mixing of the continuous phase becomes more comparable to mixing characteristics of the turbulent solids flow regime.

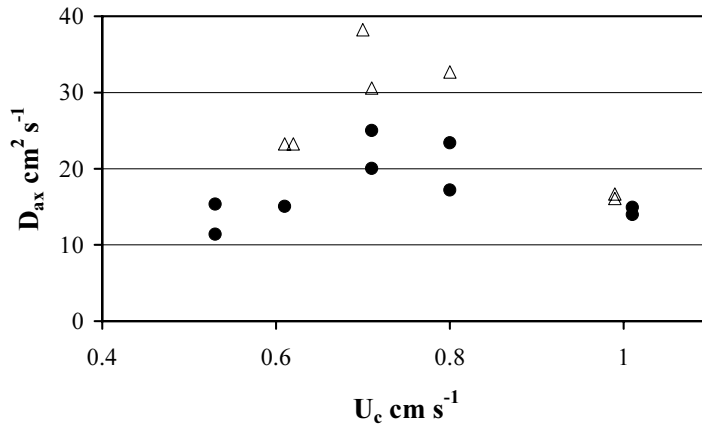


Figure 11. Axial dispersion coefficient as a function of the 30 mM KCl superficial velocity. Structured solids flow regime. ● $U_d = 0.1$ cm s⁻¹; Δ $U_d = 0.2$ cm s⁻¹.

Turbulent solids flow regime

Figure 12 shows the dispersion coefficient of the water phase fitted on the measured $E(t)$ -curve at the outlet, using the measured $E(t)$ -curve at the inlet and equation 10 and 11 as a function of U_c at different values of U_d . From figure 12 it follows that the dispersion coefficient of the continuous phase in a liquid-liquid-solid fluidized bed, regardless of the superficial water velocity applied, is always much larger than the dispersion coefficient of the continuous phase in a liquid-solid fluidized bed.

For a liquid-solid fluidized bed the dispersion coefficient increases with U_c (the dispersion coefficient at U_c is 1.8 cm s⁻¹ is 84% higher than the dispersion coefficient at U_c is 1 cm s⁻¹). However, for a liquid-liquid-solid fluidized the dispersion coefficient is virtually constant or decreases with an increasing U_c . This holds for all superficial dodecane velocities applied.

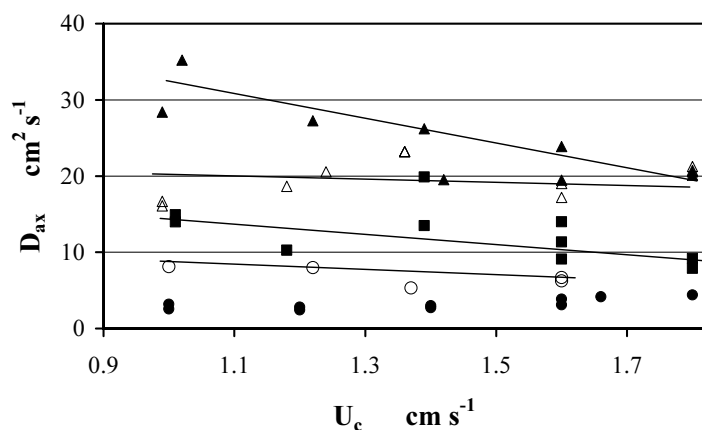


Figure 12. Axial dispersion coefficient as a function of the 30 mM KCl superficial velocity at different superficial dodecane velocity. ● $U_d = 0 \text{ cm s}^{-1}$ (liquid-solid fluidized bed), ○ $U_d = 0.05 \text{ cm s}^{-1}$, ■ $U_d = 0.1 \text{ cm s}^{-1}$, △ $U_d = 0.3 \text{ cm s}^{-1}$, ▲ $U_d = 0.6 \text{ cm s}^{-1}$.

In figure 13 the dispersion coefficient of the continuous phase for the 3-phase fluidized bed is shown as a function of U_d at different values of U_c . This figure 13 shows that at up to an U_d of 0.4 cm s^{-1} the dispersion coefficient increases with an increasing U_d . At U_d higher than 0.4 cm s^{-1} the dispersion coefficient is hardly increasing with an increasing U_d . These observations hold for all the different superficial water velocities applied.

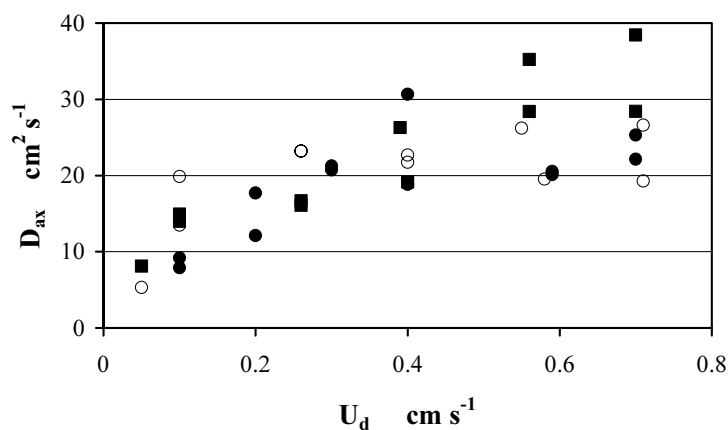


Figure 13. Axial dispersion coefficient as a function of the superficial dodecane velocity at different 30 mM KCl-solution superficial velocities. ■ $U_c = 1.0 \text{ cm s}^{-1}$, ○ $U_c = 1.4 \text{ cm s}^{-1}$, ● $U_c = 1.8 \text{ cm s}^{-1}$.

The experimental results (Figure 12 and 13) can be explained as follows. When dodecane droplets are introduced into a fluidized bed of gel beads, this will result in

a much more intense movement of the solids (visually, this change in behavior of the fluidized bed could be easily observed). The density of the gel beads is relatively low, and consequently they can be moved easily by the rising solvent droplets. Such an increase of the movement of the gel beads in comparison with a 2-phase (liquid- gel beads) fluidized bed results in a better mixing of the continuous phase of a 3-phase fluidized bed. Consequently, the dispersion coefficient of the continuous phase increases. A higher superficial dodecane velocity results in more dodecane droplets rising through the fluidized bed. The movement of the gel beads increases, and the mixing of the continuous phase increases as well. So, the dispersion coefficient increases with an increasing dodecane superficial velocity. An increase in U_d always results in an increase in the movement of the gel beads. Obviously, at a certain U_d the continuous phase is very well mixed, and a further increase in U_d will hardly result in better mixing of the continuous phase. As a result, the dispersion coefficient is constant, or it will increase only slightly.

A decrease in dispersion coefficient with an increasing superficial continuous phase velocity, at a constant U_d , can be explained by considering the energy dissipation rate per unit mass of the continuous phase, as will be shown in the next paragraph. This energy-dissipation rate decreases with an increasing superficial water velocity, and consequently the dispersion coefficient is lower.

The effect of the superficial dodecane velocity on the axial dispersion coefficient, found in this study is in complete agreement with the results of Kim *et al.* (1989), which is to our knowledge the only study on the dispersion coefficient for liquid-liquid-solid 3-phase fluidized bed. As 3-phase system these authors used water, kerosene and glass beads. For the relationship between U_c and the dispersion coefficient Kim *et al.* (1989) reported that the dispersion coefficient increases with an increasing U_c , which is in complete contradiction with our results. However, the density of the glass beads (2500 kg m^{-3}) differs very much from the density of the gel beads. This large difference in density can explain the different dependence of the dispersion coefficient on U_c . Kim *et al.* (1989) could well explain their data with the energy dissipation rate per unit mass (P_m). A higher U_c resulted for their system in a higher P_m . Our results could be explained in the same way, as will be shown below. Apparently, a general relationship between U_c and the dispersion coefficient does not exist; it depends on the physical constants of the 3-phase system.

Modeling the dispersion coefficient of the continuous phase

The isotropic turbulence theory (Baird and Rice, 1975) has been successfully applied to predicting the axial-dispersion coefficient for two- and 3-phase fluidized beds (Kim and Kim, 1983) as well as for liquid-impelled loop reactors (Van Sonsbeek *et al.*, 1992). The dispersion coefficient is given by:

$$D_{ax} = c_1 \cdot L^{4/3} \cdot P_m^{1/3} \quad 12$$

in which c_1 is a dimensionless constant, L is the length scale of the largest eddy (L equals the column diameter), and P_m is the energy-dissipation rate per unit mass. In analogy to Van Sonsbeek *et al.* (1992) the P_m for a liquid-liquid-solid 3-phase fluidized bed is given by, see also appendix A:

$$P_m = \left| g \frac{\rho_{mix} - \rho_c}{\varepsilon_c \rho_c} \cdot U_c + g \frac{\rho_{mix} - \rho_d}{\varepsilon_c \rho_c} \cdot U_d \right| \quad 13$$

in which g is the gravitational constant, ρ_c and ρ_d are the densities of the continuous and dodecane phase, and ε_c is the hold-up of the continuous phase. The mixture's density, ρ_{mix} , is given by:

$$\rho_{mix} = \rho_c \varepsilon_c + \rho_d \varepsilon_d + \rho_s \varepsilon_s \quad 14$$

in which ρ_s is the density of the gel beads, ε_s and ε_d are the hold-ups of the solid phase and dodecane phase. The hold-ups of the three different phases in a liquid-liquid-solid 3-phase fluidized bed are given by Van Zessen *et al.* (2003):

$$\frac{\rho_{mix} - \rho_s}{\rho_c - \rho_s} \left(\frac{v_{\infty,s}}{U_c / \varepsilon_c} \right)^2 = 1.24 \cdot \left(\frac{U_c / \varepsilon_c}{v_{\infty,s}} \right)^{-1.26} (1 - \varepsilon_d)^{-6.51} \quad 15a$$

$$\frac{U_d}{\varepsilon_d} - \frac{U_c}{\varepsilon_c} = 6.15 \cdot U_d^{0.9} \cdot \varepsilon_d^{-0.76} \cdot v_{\infty,d} \quad 15b$$

$$\varepsilon_c + \varepsilon_d + \varepsilon_s = 1 \quad 15c$$

in which $v_{\infty,s}$ is the terminal settling velocity of a single gel bead (5.12 cm/s), and $v_{\infty,d}$ is the terminal rise velocity of a single dodecane droplet. The rise velocity of a single droplet depends on the droplet diameter, and the droplet diameter depends on the superficial dodecane velocity and geometry of the sparger. For calculating the single rise velocity we used the Vignes' equation (Godfroy and Slater, 1994), and for the droplet diameter the equation of Kumar and Hartland (1996), see also Van Zessen *et al.* (2003).

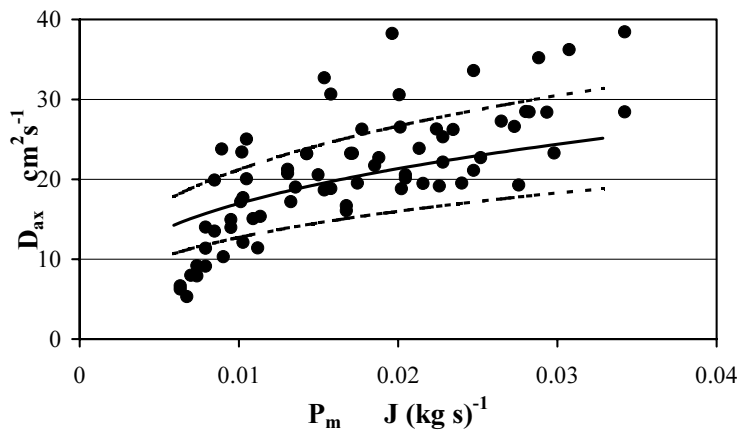


Figure 14. Axial dispersion coefficient as a function of the energy-dissipation rate per unit mass of the continuous phase. • data, — isotropic turbulence model with $c_1=0.33$, ---- 25% higher and lower predictions with the isotropic turbulence model.

Figure 14 shows the axial-dispersion coefficient as a function of the energy-dissipation rate per unit mass, calculated with equations 13, 14 and 15, for the different applied superficial velocities. An increase in P_m obviously results in a higher dispersion coefficient. It can be calculated that an increase in U_c at a constant U_d , results in a decrease of P_m ; the dispersion coefficient decreases with an increasing U_c . Figure 14 also shows equation 12 with the constant c_1 fitted on the experimental value of the axial dispersion coefficient: c_1 is equal to 0.330 ± 0.017 ($R=0.78$). The measured axial dispersion coefficients are well described by the model of Baird and Rice (1975), equations 12-15: the average deviation is 27.9%. A deviation less than 25% holds for 67.9 % of the data, see also Figure 15. It is shown in Figure 15 that most of the measured axial dispersion coefficients between $12.5 \text{ cm}^2 \text{ s}^{-1}$ and $30 \text{ cm}^2 \text{ s}^{-1}$ have a deviation less than 25%. A measured axial dispersion coefficient less than $12.5 \text{ cm}^2 \text{ s}^{-1}$ is found for $U_d=0.05 \text{ cm s}^{-1}$ and U_c between 1 and 1.6 cm s^{-1} , and for $U_d=0.1 \text{ cm s}^{-1}$ and U_c between 1.6 and 1.8 cm s^{-1} . At these flow conditions it could be visually verified that the fluidized bed of gel beads is only slightly disturbed by the rising

dodecane droplets. Apparently, at these conditions the relationship between energy dissipation rate and axial dispersion coefficient does not hold. For a measured axial dispersion coefficient larger than $30 \text{ cm}^2 \text{ s}^{-1}$, the deviation is always larger than 25%, see Figure 15. However, there is always a duplicate experiment (using the same superficial velocities of both phases) that gives an axial dispersion coefficient with a deviation less than 25%. So, the isotropic turbulence theory (Baird and Rice, 1975) describes well the relationship between axial dispersion coefficient and energy dissipation rate per unit mass for a liquid-liquid-solid fluidized bed, if those combinations of superficial velocities are excluded for which the solids flow in the 3-phase fluidized bed is not disturbed by the rising droplets.

For a bubble column (length/diameter ratio > 5) a c_1 value of ~ 0.35 was found in the absence of slugging, and for the main tube of a liquid-impelled loop reactor, at lab-scale (diameter 0.06m and length 0.44m), a c_1 value of 0.35 was also found (Van Sonsbeek, 1992). So, based on the theory of Baird and Rice (1974), it can be said that the mixing behavior of the continuous phase of a liquid-liquid-solid 3-phase fluidized bed is comparable with both the mixing behavior of the continuous phase of a bubble column and the mixing behavior of the continuous phase in the main tube of a liquid-impelled loop reactor.

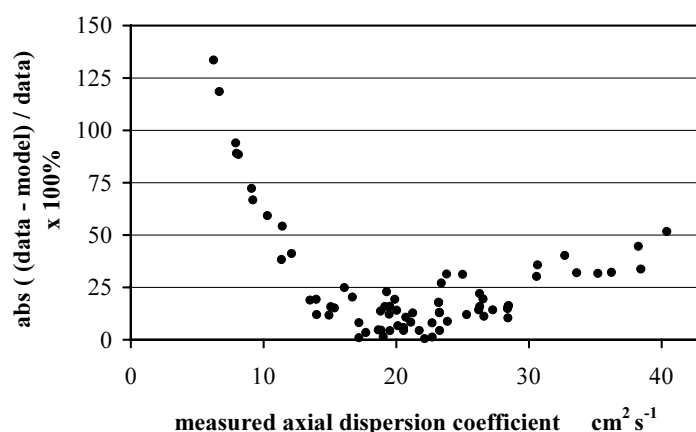


Figure 15. Absolute deviation between the measured axial dispersion coefficient and the predicted axial dispersion coefficient as a function of the measured axial dispersion coefficient.

Conclusion

A method to determine the residence time distribution of the continuous phase of a liquid-liquid-solid (gel beads) 3-phase fluidized bed bioreactor, using a KCl-tracer, was evaluated and validated. It is concluded that the use of a KCl-tracer gives a reliable residence-time distribution curve provided the pulse volume is not too large. For this study a pulse volume of 3 ml 4M KCl resulted in reliable results.

Using the residence-time distribution curves measured for different superficial velocities of the continuous phase (30 mM KCl) and dispersed phase (n-dodecane), two different but comparable models, the axial dispersion model and the tanks-in-series model, were applied to calculate the dispersion coefficient of the continuous aqueous phase. It is concluded that the dispersion coefficients determined with both models, show the same relationship between dispersion coefficient and superficial velocities of both phases. However, the accuracy of the dispersion coefficient calculated with the tanks-in-series model is much lower, because the number of tanks can only have discrete values.

The dispersion coefficient of the continuous phase increases with the superficial velocities of both phases, for flow conditions that belong in the structured solids flow regime. For flow conditions that belong in turbulent solids flow regime, the dispersion coefficient slightly decreases with an increasing continuous phase superficial velocity and increases with an increasing dodecane superficial velocity. These results are well explained by the energy dissipation rate per unit mass of the continuous phase (P_m); an increase in P_m results in a higher dispersion coefficient and a decrease in P_m results in a lower dispersion coefficient.

The relationship between dispersion coefficient and P_m as suggested by Baird and Rice (1975) describes the experimental dispersion coefficients of the continuous phase well, provided the dodecane superficial velocity is larger than 0.05 cm s^{-1} , and for a dodecane superficial velocity of 0.1 cm s^{-1} the continuous phase superficial velocity is smaller than 1.6 cm s^{-1} . With these restrictions the total deviation between experiment and model is 17.5%.

It is concluded that, regardless of the flow pattern, the mixing of the continuous phase in liquid-liquid-solid (gel beads) fluidized bed is comparable with the mixing of the continuous phase of either a bubble column or the main tube of a liquid-liquid impelled loop reactor.

Appendix A. Energy dissipation rater per unit mass for a 3-phase fluidized-bed bioreactor.

In analogy to Van Sonsbeek *et al.* (1992) we assume that the power input is totally dissipated in liquid motion of the continuous phase. The power input is equal to the difference between the gain in potential energy and loss in pressure energy:

$$E_{\text{disp}} = \Delta E_{\text{pressure}} - \Delta E_{\text{potential}} \quad \text{A.1}$$

The hydrostatic pressure gradient is given by

$$\Delta P_{\text{hydrostatic}} = g H \rho_{\text{mix}} \quad \text{A.2}$$

with the mixture's density given by:

$$\rho_{\text{mix}} = \rho_c \varepsilon_c + \rho_d \varepsilon_d + \rho_s \varepsilon_s \quad 14$$

For a liquid-liquid-solid fluidized bed, as described in the experimental part, both liquid phases loose energy when they flow through this pressure gradient:

$$\Delta E_{\text{pressure}} = A g H \rho_{\text{mix}} (U_c + U_d) \quad \text{A.3}$$

Both liquid phases gain potential energy

$$\Delta E_{\text{potential}} = A g H (\rho_d U_d + \rho_c U_c) \quad \text{A.4}$$

The energy dissipation rate per unit mass follows from implementing A.3 and A.4 in A.1 and dividing by the mass of the continuous phase ($\varepsilon_c \rho_c A H$). After rewriting the resulting equation for P_m is:

$$P_m = \left| g \frac{\rho_{\text{mix}} - \rho_c}{\varepsilon_c \rho_c} \cdot U_c + g \frac{\rho_{\text{mix}} - \rho_d}{\varepsilon_c \rho_c} \cdot U_d \right| \quad 13$$

Nomenclature

A	: area of the column	m^2
C	: concentration	mol m^{-3}
c_1	: constant	-
D_{ax}	: axial dispersion coefficient of the continuous phase	$\text{m}^2 \text{s}^{-1}$
E	: residence time distribution	s^{-1}
E_{disp}	: dissipated energy	J s^{-1}
ΔE	: change in energy	J s^{-1}
g	: gravitational constant	$\text{m}^2 \text{s}^{-1}$
H	: height of the fluidized bed	m
k_i	: proportionality constant	mol mA^{-1}
L	: length scale	m
m	: mass	mol
N	: total number of tanks-in-series	-
$\Delta P_{\text{hydrostatic}}$: hydrostatic pressure gradient	N m^{-2}
P_m	: energy dissipation per unit mass	$\text{J kg}^{-1} \text{s}^{-1}$
S	: signal	mA
t	: time	s
U_i	: superficial velocity of phase i	m s^{-1}
V	: volume of a section of the bioreactor	m^3
$v_{\infty, i}$: terminal rise velocity of phase i	m s^{-1}
x	: axial coordinate	m
<i>greek</i>		
Φ	: volume flux of the continuous phase	$\text{m}^3 \text{s}^{-1}$
ε_i	: hold-up of phase i	-
ρ_i	: density of phase i	kg m^{-3}
τ	: residence time	s
<i>subscript</i>		
c	: continuous phase	
d	: dodecane phase	
in, out	: inlet, outlet	
mix	: mixture of the different phases	
s	: solid (gel beads) phase	

Design of liquid-liquid-solid fluidized-bed bioreactors

Abstract

A liquid-liquid-solid 3-phase system is automatically formed, when in one apparatus an immobilized biocatalyst is used for a biotransformation and an organic solvent for extraction. The aim of this paper is to show that the application of such a 3-phase reactor system for biotransformations strongly inhibited by product, will result in a higher degree of conversion, compared to a conventional reactor system. For that, different reactor configurations are discussed. These include a simple 3-phase fluidized bed, but also more fancy options, like the different possibilities with a loop reactor. It is concluded that building and operating a 3-phase system is nothing more than a minor extension of conventional bioreactors. In the second part of this paper a simple reactor model was developed for a 3-phase liquid-liquid-solid fluidized-bed bioreactor. The influence of different parameters are discussed, e.g. the distribution coefficient of product over medium/organic solvent, the toxic product concentration, and the flux of the organic solvent. In the last part of this paper conditions have been established for which this 3-phase reactor performs better than a conventional 2-phase fluidized bed. At a given maximum substrate conversion rate, the distribution coefficient is determined for which the 3-phase fluidized bed performs equally well as the 2-phase fluidized bed. It appears that already a low distribution coefficient (larger than 1 but less than 2) suffices for a better operation. Provided *in situ* extraction is needed for such a biotransformation, a 3-phase fluidized bed, or less simple 3-phase bioreactors are a good choice.

published as: Erik van Zessen, Arjen Rinzema and Johannes Tramper. 2001. In Multi-phase bioreactor design. Chapter 12 Design of liquid-liquid-solid fluidized-bed bioreactors. Ed. Cabral JMS, Mota M and Tramper J, Taylor and Francis (London, New York). p 225-247.

Introduction

Advantages of using a liquid-liquid 2-phase system in biotransformations have been discussed (Van Sonsbeek *et al.* 1993; Vermuë and Tramper 1995a; Tramper *et al.* 1992; Adlercreutz 2000). Depending on the nature of the biotransformations, the reason for applying a liquid-liquid 2-phase system is different. Examples of different biotransformations carried out in a 2-phase system and the advantages of using such a system are given by Vermuë and Tramper (1995a). In general one can profitably choose for a liquid-liquid 2-phase system when:

- the substrate dissolves poorly in the medium; the organic solvent acts as a reservoir;
- there is product inhibition; by using an organic solvent the product concentration in the medium is lowered;
- the reaction equilibrium is unfavorable; the equilibrium products dissolve in the organic solvent and the degree of conversion can be enhanced.

Another reason for using *in situ* extraction, the combination of bioconversion with the first unit operation in the downstream processing, might be a facilitated product recovery.

Obviously, using an organic solvent in bioconversions also leads to disadvantages. For example, the toxicity of the solvent might reduce the biocatalytic activity and stability (Vermuë *et al.* 1995b). Furthermore, in any bioconversion with micro-organisms involved, surface active agents are present, whether excreted by the micro-organism, or present due to cell lysis. This can result in non-desirable, stable emulsions that are difficult to separate (Vermuë *et al.* 1995b).

Inhibition due to direct contact between micro-organisms and the organic solvent can be reduced by immobilizing the micro-organism. Immobilization may also reduce the amount of surface-active agents, and consequently prevent a stable emulsion (Vermuë *et al.* 1995b). Immobilization of micro-organism has been studied extensively (Wijffels *et al.* 1996). An elegant way of immobilizing micro-organisms is a method that uses a natural gel solution (e.g. κ -carrageenan, alginate). Broth is mixed with the gel solution and gel beads are made as described by for instance Hunik and Tramper (1993). Obviously, immobilization will only work when there is hardly any outgrowth of the micro-organisms, and little excretion of proteins.

In operating an extractive bioconversion one should decide whether to use a bioreactor with bioconversion and extraction integrated, or use a plant set-up with

both processes separated. In the latter case the medium has to be circulated between both apparatus at a high velocity, see also the section on loop reactors for more detail. Using in one apparatus immobilized cells for a bioconversion and an organic solvent for extraction, a 3-phase system is automatically formed. As apparatus, stirred tank reactors, although favorable for good mixing and a high interfacial area between medium and organic solvent, are not very useful; the harsh conditions in the tank will destroy the gel beads. A stronger immobilization matrix would be required than the natural gels mentioned above. Another option is using column reactors. For this purpose a liquid analogue of the air-lift loop reactor, the liquid-impelled loop reactor, was designed (Tramper *et al.* 1987) and hydrodynamically characterized by Van Sonsbeek (1992a). Different biotransformations have been executed in this type of reactor (Vermuë *et al.* 1995; Buitelaar *et al.* 1991; Van den Tweel *et al.* 1987; Mateus *et al.* 1996). The application of this type of reactor is discussed in the section on loop reactors. Another simple bioreactor is the liquid-liquid-solid 3-phase fluidized bed. The reactor is almost identical to a liquid-impelled loop reactor, but the water flow is controlled with a pump and not induced by a density difference. The hydrodynamics of this reactor have been studied: the hold-up of the different phases as a function of the fluxes of both phases (Van Zessen *et al.* 2003), as well as the mixing of the medium phase (Van Zessen *et al.* 2003). This type of reactor has good mixing characteristics, and seems promising for application in an *in situ* extraction bioprocess.

The aim of this chapter is to show that the application of a 3-phase reactor system for bioconversions strongly inhibited by product, will result in a higher degree of conversion, compared to a conventional reactor system. Not all conditions favor a 3-phase system, but it will be shown that with the right combination of operating conditions (fluxes of both liquids), and physical parameters (distribution coefficient and inhibition constant), a 3-phase system is always favorable.

Figure 1 summarizes different aspects looked upon in this paper. First, possible process lay-outs and different reactor configurations for a liquid-liquid-solid 3-phase system are discussed. Next, the focus is on one of the reactor configurations: a 3-phase fluidized-bed bioreactor. Then, a reactor model is developed, and characteristics of this model are discussed. Thereafter, the conditions for which a 3-phase fluidized-bed gives a better performance than a liquid-solid fluidized bed are demonstrated.

- *Reactor Configuration*
 - 3-phase liquid-liquid-solid fluidized-beds, both liquids flow co-currently
 - 3-phase liquid-liquid-solid fluidized-beds, water flow counter-currently
 - 3 Liquid-impelled loop reactors
- *Model derivation for reactor configuration 1*
 - Simulations for a batch operation
 - Profiles inside a gel bead
 - Different distribution coefficients
 - Different toxic product concentrations
 - Different fluxes of organic solvent
- *Comparison between a conventional reactor and reactor configuration 1*
 - Evaluation of the distribution coefficient for which reactor configuration 1 performs equally
 - Batch operation is studied extensively
 - Continue operation is briefly discussed

Figure 1. Short overview of different aspects looked upon

Process lay-out and operation

A schematic presentation of a possible plant is shown in Figure 2. The core of the plant is the bioreactor, i.e. a 3-phase fluidized bed. This column is fed by a continuous medium flow, introduced at the bottom of this column. This up-flowing stream is also used for fluidizing the biocatalytic particles. An immiscible solvent is pumped through a sparger, and the formed droplets rise through the fluidized bed. If coalescence of the droplets is easily achieved, which might be a prerequisite for good operation, both liquids are separated at the top of the column and sent back to their respective storage vessels. If separation between both liquids is not achieved by a simple one-stage gravity settler, the 2-phase mixture can be separated outside the column.

If the biocatalyst requires oxygen, than aeration of one or both storage vessels will be an adequate method. Temperature control of the bioreactor can be done by keeping the temperature of both storage vessels constant. pH is controlled by keeping the pH of the substrate storage vessel constant.

Operating the bioreactor in the above-described manner is a batch operation; accumulation of the product in the organic phase and depletion of the substrate will occur. A continuous operation with respect to the substrate phase can be achieved by adding a high substrate concentration to the storage vessel, keeping the substrate

concentration constant. To prevent overflow of the storage vessel part of the circulating medium flow has to be purged, see also Figure 2.

Operating the bioreactor with a continuous supply of substrate will still result in the accumulation of the product in the organic phase. Operating the organic phase continuously is easily done by sending the total out-flowing organic phase to the recovery section, and pumping purified organic phase into the column. This strategy will be disadvantageous when the product concentration in the organic phase is low; a large volume of organic solvent has to be clarified. A better strategy will be to allow accumulation of the product to a certain concentration, below the equilibrium concentration, and to send part of the out-flowing organic phase to the recovery section, see Figure 2.

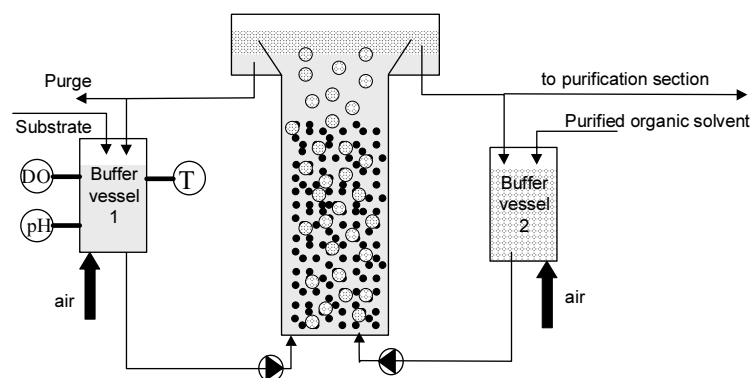


Figure 2. Process lay-out for a 3-phase fluidized-bed bioreactor

Above a plant lay-out and a process operation is discussed for a 3-phase fluidized-bed bioreactor. It is assumed that both liquid phases flow upward co-currently. This is true when the organic phase has a smaller density than the medium phase. When the organic-phase density is larger, this liquid has to be introduced at the top of the column, and both liquids have to be separated at the bottom of the column.

Another assumption is that the 3-phase fluidized-bed bioreactor is stable, which means that the fluidized bed is in a hydrodynamic equilibrium; particles remain in the column and the droplets do not coalesce in the fluidized bed. Experiments with different kinds of gel beads have shown that a stable fluidized bed exists, at least, for gel beads with a density of 1060 kg m^{-3} and a diameter of 2.3 mm. Applying gel beads with a density of 1010 kg m^{-3} and a diameter of 2 mm in a 3-phase fluidized bed resulted in the wash out of the beads at any organic flow rate larger than $10^{-4} \text{ m}^3 (\text{m}^2 \text{ s})^{-1}$. It can be concluded that a stable 3-phase fluidized bed is possible for particles with a settling velocity larger than 5.0 cm s^{-1} . Coalescence of droplets can be prevented by carefully adjusting both flows.

Alternatives

Below two different alternatives are given for operating a 3-phase liquid-liquid-solid system, see also Figure 1.

Counter-current water flow

A 3-phase fluidized bed with both liquids flowing co-currently is not possible for each type of particle. For particles with a terminal settling velocity larger than 5.0 cm s^{-1} a stable bed is possible, but for particles with a velocity smaller than 2 cm s^{-1} a stable bed could not be obtained (Van Zessen, unpublished). We do not know whether a stable fluidized bed is possible for particles with a terminal settling velocity between 2 and 5.0 cm s^{-1} .

A stable 3-phase fluidized bed is possible for those particles with a settling velocity smaller than 2 cm s^{-1} , if a different strategy is followed. In operating this strategy, droplets rise from bottom to top and medium flows counter-currently, i.e. from top to bottom, see Figure 3. A limit situation of this strategy is the case in which there is no medium flow. Firstly, this situation is shortly discussed. Thereafter, the counter-current operation is discussed.

For bubble columns, it is known that gel beads can be fluidized - kept in suspension - by the rising gas bubbles. As a liquid-liquid-solid 3-phase fluidized bed is the liquid analogue of a gas-liquid-solid 3-phase fluidized bed, it should be possible to create a droplet column with solids kept in suspension. Indeed, it was possible to keep two different kinds of κ -carrageenan gel beads in suspension in a droplet column (Van Zessen, unpublished). These gel beads had a density of 1007.4 kg m^{-3} and 1005.4 kg m^{-3} and a diameter of 1.97 mm and 3.12 mm . However, to maintain the gel beads in suspension a minimal solvent flux was required. Experimental data on hydrodynamic parameters, such as hold-up, were not determined; only visual observations were made on this operating strategy. Provided the solvent flux was higher than a minimal value, this 3-phase system was stable for at least 24 hours.

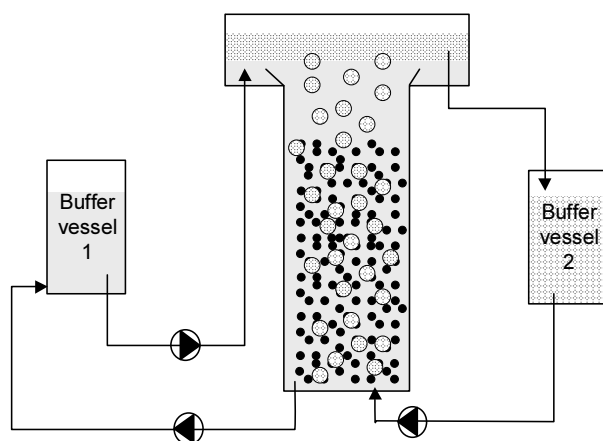


Figure 3. Alternative process lay-out: water flows counter-current with respect to the droplets flow

As the droplet column with suspended gel beads worked well without any water flow, we also tried to operate the set-up with water flowing counter-currently, see Figure 3. The water flux puts a downward directed force on the gel beads, whereas the force put on the gel beads by the organic solvent flux is directed upwards. Obviously, when the water flux becomes too high, the gel beads will settle. Again, we only made visual observations for this set-up. These observations can be summarized as follows:

- at a fixed water flux, the organic solvent flux has to have a minimal value in order to make this system work. Increasing the organic solvent flux resulted in a larger bed height, i.e. a lower gel-bead hold-up;
- at a fixed organic solvent flux, higher than the minimum flux required for stable operation, the water flux can be increased to a maximum value. At higher values the system will not work, i.e. gel beads settle, and droplets coalesce.

This operating strategy gives a couple of advantages over a co-current strategy. In extraction processes counter-current operation is always better than co-current operation, as there is always a higher driving force for mass transfer. In co-current operation the gel-bead hold-up decreases with an increasing medium flux, whereas in counter-current operation the gel-bead hold-up increases with an increasing medium flux. It is also observed that at a higher organic solvent flux a higher water flux can be applied; this means that the throughput of substrate can be higher in counter-current operation.

Loop reactors

Another type of bioreactors are the so-called loop reactors: these reactors consist of two tubes connected to each other; internal and external designs exist (Van 't Riet and Tramper, 1991). In order to function, there has to be a difference in density of the mixture in both tubes. A density difference results in a pressure difference and water will flow between both tubes: the direction of this water flow goes from a high to a low density.

This principle has been applied in air-lift reactors (Chisti, 1989). The liquid analogue, droplets instead of gas bubbles, the so-called liquid-impelled loop reactor, has been described by Van Sonsbeek (1992a). This type of reactor with particles, κ -carrageenan gel beads, has been used by Mateus *et al.* (1996) and Vermuë *et al.* (1995) for biotransformations.

Figure 4 shows four possible reactor configurations for the application of a 3-phase system in a loop reactor. First, it is assumed that the particles remain in one column, and are not circulating. Particles circulating between both tubes are discussed below. In parts A and B of this figure, a bed of biocatalytic particles and a spray extraction column are separated. In part C and D, conversion and extraction are fully integrated.

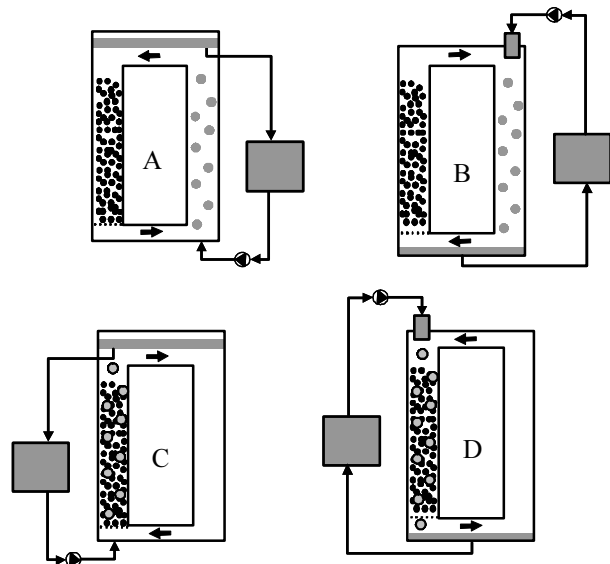


Figure 4. Loop reactors (see text for explanation)

In part A droplets of an organic solvent rise from the bottom to the top of the column as their density is lower than the water density. Consequently, pressure is lower in the spray column, and water flows from top to bottom in the column with particles.

If the density of the particles is higher than the water density, a packed bed will be formed. If the density of the particles is lower than the water density, and the water flux is larger than the rise velocity of the swarm of particles, a fluidized bed will be formed. This so-called inverse fluidization has been studied by Fan *et al.* (1982).

In part B, droplets of an organic solvent settle from the top to the column, as the density is higher than the medium density. Obviously, water flows from bottom to top in the column with particles. This set-up will work, if the particle density is higher than the water density. A fluidized bed will be observed, if the water flow is higher than the minimum fluidization velocity.

Part C of Figure 4 shows a 3-phase mixture in one column and medium in the other column of the loop reactor. The density of the organic solvent is less than the medium density and solvent droplets will rise. A 3-phase fluidized bed will only exist when the density of this mixture is less than the density of the medium in the other column. In that case water will flow from bottom to top in the 3-phase column. For example, in our laboratory experiments have been done on the hold-ups in a 3-phase system, i.e. water, dodecane and gel beads (density equals 1060 kg m^{-3}). At a water flux of $1.8 \times 10^{-2} \text{ m s}^{-1}$ and a dodecane flux of $0.91 \times 10^{-2} \text{ m s}^{-1}$, a gel bead hold-up of 0.20 and a dodecane hold-up of 0.08 was measured. This gives a mixture density of 992 kg m^{-3} . The density difference between both columns is in this case large enough to obtain this water flux of $1.8 \times 10^{-2} \text{ m s}^{-1}$ (Van Sonsbeek *et al.* 1990).

A different situation exists when the density in the 3-phase system is larger than the density of the medium in the other column, due to a higher solids hold-up or a lower organic solvent hold-up. In this case water will flow from top to bottom. Provided the density of the solids is close to water, this configuration can also work; see the preceding paragraph 'Counter-current water flow'.

The column with only medium can be aerated. However, aeration results in the decrease of the mixture density in this column, and the circulation velocity of the medium between both columns is changed. In order a 3-phase fluidized bed exists, the aeration must be carefully carried out. Aeration results in an air hold-up, and hence a smaller mixture density in the aerated column. Consequently, the density difference between both columns becomes less, and the circulation velocity decreases. At this smaller medium velocity a 3-phase fluidized bed must still exist.

Part D of Figure 4 is the same as part C, but in this case the density of the organic solvent is larger than the density of water, hence droplets settle. Water will always flow in the direction indicated in this figure; from top to bottom in the 3-

phase column. Only if the biocatalytic particles have a density smaller than water, i.e. they rise in the column, this configuration will work.

So far it is assumed that the particles remain in a fluidized state. However, the water circulation velocity can be so high, that it exceeds the terminal settling velocity of a single particle. In that case particles flow together with the water, and are present in both columns. This principle is widely used in air-lift bioreactors (Heijnen *et al.* (1997).

Performance of a conventional bioreactor and a 3-phase fluidized bed bioreactor

In the preceding section possible reactor configurations have been discussed. Whether such a 3-phase reactor will work better than a conventional reactor, is the topic of this section. We decided to compare a 2-phase fluidized-bed bioreactor, the conventional reactor, with a 3-phase liquid-liquid-solid fluidized-bed bioreactor. Comparing two different reactors, one should consider a fair comparison. This comparison can be based on cost, but in that case one should consider total cost, i.e. cost of a total production plant. Making a total process design and optimizing this design for both reactors, goes beyond the scope of this paper. One can also compare both reactors on their performance, i.e. degree of conversion of the substrate, or synthesis rate of product.

Before we go into a detailed comparison of both bioreactors, the model used for the calculations is described.

Model Derivation

Below, the model we used to calculate the performance of both bioreactors is briefly discussed. A general total model for the design of a reactor is schematically shown in Figure 5. This model consists of three major parts:

- hydrodynamics of the reactor
- kinetics of the bioconversion
- mass transfer of compounds between the different phases

Together with mass balances over each phase for the different components, the total model is complete.

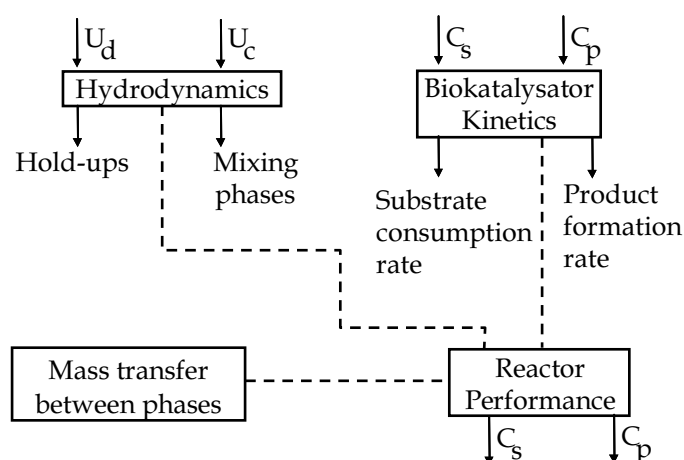


Figure 5. Model outline

Investigated system

In our laboratory hydrodynamic studies have been done on a 3-phase system consisting of water, dodecane and gel beads. This system is used as the model system. Obviously, highly complicated bioconversions can be involved in producing industrially interesting products, in which more than one substrate and product influence the kinetics. We have chosen a very simple one-to-one conversion: substrate S gives product P. It is further assumed that substrate is dissolved in the medium and insoluble in the organic solvent, transported to the gel bead and there converted to product. The product itself is transported out of the gel bead to the medium phase and subsequently to the organic solvent phase.

Hydrodynamics

This part of the model considers the hold-up and mixing of the different phases present. To model the medium flow, the fluidized bed is divided in a number of ideally mixed tanks. For a fluidized bed of 1 m high, and for medium fluxes between 0.5×10^{-2} and $2 \times 10^{-2} \text{ m s}^{-1}$, the number of tanks has been experimentally determined. It appears that for medium fluxes the number of ideally mixed tanks is equal to 13 for the 2-phase fluidized bed and 3 for the 3-phase fluidized bed.

In order to make the reactor model less complicated, it is assumed that gel beads remain in one tank and do not circulate between the different tanks.

A model has been developed for predicting the hold-ups in a 3-phase fluidized bed (Van Zessen, 2003), but we chose to use here the experimentally

determined hold-ups as they are more accurate. The dodecane hold-up and gel bead hold-up as a function of medium flux and dodecane flux is shown in Figure 6.

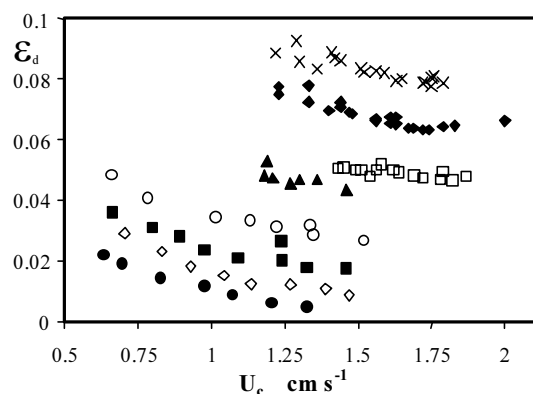


Figure 6a. Droplet hold-up as a function of the water and dodecane flux.

- $U_d = 0.05 \text{ cm s}^{-1}$ ◇ $U_d = 0.10 \text{ cm s}^{-1}$
- $U_d = 0.18 \text{ cm s}^{-1}$ ○ $U_d = 0.27 \text{ cm s}^{-1}$
- ▲ $U_d = 0.44 \text{ cm s}^{-1}$ □ $U_d = 0.54 \text{ cm s}^{-1}$
- ◆ $U_d = 0.73 \text{ cm s}^{-1}$ × $U_d = 0.91 \text{ cm s}^{-1}$

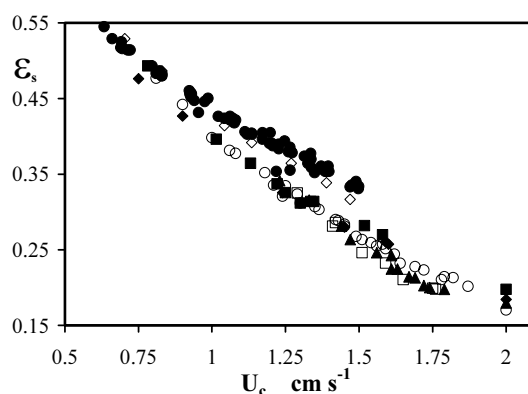


Figure b. Gel bead hold-up as a function of the water and dodecane flux.

- $U_c = 0.00 \text{ cm s}^{-1}$ ◇ $U_c = 0.10 \text{ cm s}^{-1}$
- $U_c = 0.29 \text{ cm s}^{-1}$ ◆ $U_c = 0.42 \text{ cm s}^{-1}$
- $U_c = 0.54 \text{ cm s}^{-1}$
- ▲ $U_c = 0.75 \text{ cm s}^{-1}$ □ $U_c = 0.91 \text{ cm s}^{-1}$

Table I gives an overview of the assumptions made and the models used for determining the hold-up and mixing characteristics of both reactors.

Table I. Hydrodynamic characteristics for a liquid-fluidized bed and a liquid-liquid-solid fluidized bed

	2-phase fluidized bed	3-phase fluidized bed
mixing		
water phase	number of tanks-in-series (15)	number of tanks-in-series (3)
gel bead phase	ideally mixed per tank	ideally mixed per tank
droplet phase	-	plug flow
hold-up	Richardson and Zaki model with experimentally determined parameters $U_c = v_\infty \varepsilon_w^n$	Experimentally determined, see Figure 6

Mass transfer

Mass transfer between the different phases in a 2- or 3-phase system can schematically be presented as shown in Figure 7. To describe mass transfer inside the gel bead we used Fickian diffusion of substrate and product. For describing the mass

transfer from gel bead interface to the bulk of the medium, we used the film model for substrate as well as product. The film model was also used for the mass transfer of the product from the bulk to the interface between medium and organic-solvent droplet. Mass transfer from this interface to the bulk of the organic-solvent droplet was also described by the film model. Further it is assumed that the distribution coefficient between gel bead and surrounding liquid is equal to one. Next, it is assumed that there is thermodynamic equilibrium at the interface between droplet and medium. The equilibrium distribution at the interface can be described with a constant distribution coefficient (m):

$$C_p^{o,int} = mC_p^{w,int}$$

The mass transfer rate between the different phases can be described with the equations given in Table II; the rates are a combination of mass transfer per gel bead or droplet, and the number of gel beads or droplets present, respectively. The resulting rates are given per volume reactor.

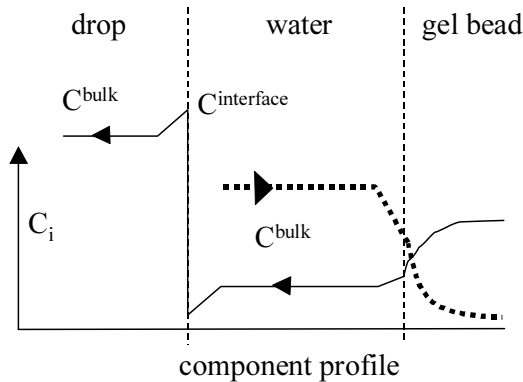


Figure 7. Profiles in a multi-phase system: — product profile, ... substrate profile

The mass transfer coefficient for the transfer of product from medium to organic phase (K) is a combination of the transfer coefficient from bulk to interface at both sides of the interface:

$$K = \left(\frac{1}{k_{drop,p}^w} + \frac{1}{mk_{drop,p}^o} \right)^{-1}$$

The mass transfer coefficients $k_{bead,s}$, $k_{bead,p}$, and $k_{drop,p}^w$ are calculated with the equation of Ranz and Marshall (1952); the mass transfer coefficient $k_{drop,p}^o$ is calculated with the equation of Newman (1931); see appendix A for equations. As

contact time in the latter equation, we used the residence time of a droplet ($t = H_{\text{bed}} \epsilon_o / U_d$).

Table II. Substrate and product transfer rates between the different phases

	medium / gel bead	medium / droplet
substrate	$k_{\text{bead},s} (C_s^{w,\text{bulk}} - C_s^{w,\text{int}}) \cdot \frac{6}{d_{\text{bead}} \epsilon_s}$	no transfer to the droplet
product	$-k_{\text{bead},p} (C_p^{w,\text{bulk}} - C_p^{w,\text{int}}) \cdot \frac{6}{d_{\text{bead}} \epsilon_s}$	$K \left(C_p^{w,\text{bulk}} - \frac{C_p^{d,\text{bulk}}}{m} \right) \cdot \frac{6}{d_{\text{drop}} \epsilon_o}$

Kinetics

Let us consider bioconversions carried out by either non-growing cells or enzymes immobilized in κ -carrageenan gel beads. It is further assumed that there is only one limiting substrate, which dissolves well in medium and not in the organic solvent. Medium is water containing all other essential nutrients. Straightforward Michaelis-Menten kinetics with first order product inhibition are considered:

$$-r_s = \frac{X v_{\text{max}} C_s}{K_m + C_s} \left(1 - \frac{C_p}{C_p^{\text{tox}}} \right)$$

When the product concentration reaches the toxic concentration (C_p^{tox}) the substrate consumption rate is zero. More complicated kinetics can be used, but this is the simplest model to demonstrate the benefits for *in situ* extraction.

Mass balances

Figure 8 shows how the liquid-liquid-solid 3-phase fluidized bed is divided in ideally stirred tanks to represent flow characteristics, see also Table 1.

The total 3-phase fluidized bed is divided in a number of tanks. In each tank the medium is ideally mixed. The gel beads remain in each tank. The organic-solvent phase is in each tank divided in 15 ideally mixed tanks-in-series to mimic plug flow behavior.

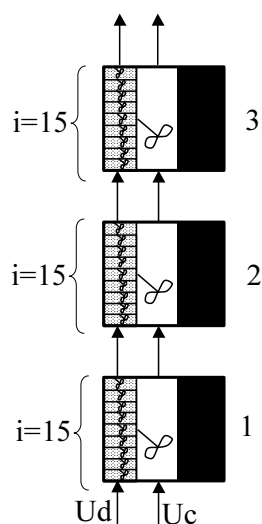


Figure 8. Schematic representation of the 3-phase fluidized bed

Mass balances are derived for single tanks. The total derivation of these balances is given in appendix A. The resulting dimensionless mass balances with the initial and boundary conditions are:

Within this model two different kinds of parameters can be discerned:

1. parameters that can be easily manipulated by the designer,
i.e. operating variables like the fluxes of the medium and organic solvent, and hence the hold-up of the different phases, initial concentration of substrate and product in the different phases, and reactor geometry.
2. parameters that are difficult to manipulate,
e.g. the physical parameters like density and viscosity of the pure liquids, the mass transfer coefficients, and the diffusion coefficients of the compounds.

Particle mass balances

substrate

$$\frac{\partial X_s^{p,n}}{\partial Fo} = \frac{\partial^2 X_s^{p,n}}{\partial z^2} + \frac{2}{z} \frac{\partial X_s^{p,n}}{\partial z} - (-r_s) \frac{r_p^2}{D_s C_s^{w,0}}$$

$$\forall t, z = 1, k_{\text{bead},s} (X_s^{w,n} - X_s^{w,\text{int},n}) = \frac{D_s}{r_p} \frac{dX_s}{dz} \Big|_{z=1}$$

$$\forall t, z = 0, \frac{dX_s}{dz} \Big|_{z=0} = 0$$

$$\forall z, t = 0, X = 0$$

product

$$\frac{\partial X_p^{p,n}}{\partial Fo} = \frac{D_p}{D_s} \frac{\partial^2 X_p^{p,n}}{\partial z^2} + \frac{D_p}{D_s} \frac{2}{z} \frac{\partial X_p^{p,n}}{\partial z} + (-r_s) \frac{r_p^2}{D_s C_s^{w,0}}$$

$$\forall t, z = 1, k_{\text{bead},p} (X_p^{w,n} - X_p^{w,\text{int},n}) = \frac{D_p}{r_p} \frac{dX_p}{dz} \Big|_{z=1}$$

$$\forall t, z = 0, \frac{dX_p}{dz} \Big|_{z=0} = 0$$

$$\forall z, t = 0, X_p = 0$$

Medium-phase mass balances

substrate

$$\frac{\partial X_s^{w,n}}{\partial Fo} = \frac{U_w}{\varepsilon_w H_t} \frac{r_p^2}{D_s} (X_s^{w,n-1} - X_s^{w,n}) - \frac{6}{d_{bead}} \frac{\varepsilon_s}{\varepsilon_w} k_{bead,s} \frac{r_p^2}{D_s} (X_s^{w,n} - X_s^{w,int,n})$$

batch operation

$t=0, X_s^w=1$ for each tank n

continuous operation

$t=0, X_s^w=0$ for each tank n

product

$$\begin{aligned} \frac{\partial X_p^{w,n}}{\partial Fo} = & \frac{U_w}{\varepsilon_w H_t} \frac{r_p^2}{D_s} (X_p^{w,n-1} - X_p^{w,n}) + \frac{6}{d_{bead}} \frac{\varepsilon_s}{\varepsilon_w} k_{bead,p} \frac{r_p^2}{D_s} (X_p^{w,int,n} - X_p^{w,n}) + \\ & - K \frac{6}{d_o} \frac{\varepsilon_o}{\varepsilon_w} \frac{r_p^2}{D_s} \left(X_p^{w,n} - \frac{\langle X_p^{w,n} \rangle_i}{m} \right) \end{aligned}$$

batch or continuous operation

$t=0, X_p^w=0$ for each tank n

Organic-solvent-phase mass balances

$$\frac{\partial X_p^{o,i}}{\partial Fo} = \frac{U_d}{\varepsilon_d H_{t,i}} \frac{r_p^2}{D_s} (X_p^{o,i-1} - X_p^{o,i}) + K \frac{6}{d_o} \frac{r_p^2}{D_s} \left(X_p^{w,n} - \frac{\langle X_p^{w,n} \rangle_i}{m} \right)$$

batch or continuous operation

$t=0, X_p^{o,i}=0$ for each tank i

Calculations

Before we compare a 3-phase fluidized-bed bioreactor with its 2-phase analogue, we will first show some typical results of the model. For these simulations we took a batch operation strategy for both liquids, and both liquids flew co-currently, see also Figure 2. Figure 1 gives a short overview of the different simulations done. First we show a typical time course of substrate and product concentration inside the gel bead. Next the influence of the distribution coefficient and toxic product concentration is shown. These parameters are system dependent; a toxic product concentration depends on the micro-organism used, and can hardly be influenced; the distribution coefficient depends on the two liquids used, but can be influenced by adding specific compounds to the organic solvent for enlarging the distribution coefficient. The influence of the dodecane flux is discussed at the end of this section. The parameters that were used throughout the simulations are summarized in Table III.

Table III Overview of parameters used in simulations

<i>Reactor Constants</i>		
# nozzles	209	
diameter nozzle	0.001	m
reactor height	1	m
reactor diameter	0.06	cm
<i>Physical parameters</i>		
density medium	998	kg m ⁻³
density dodecane	742.7	kg m ⁻³
density gel bead	1065.1	kg m ⁻³
viscosity medium	0.0009325	Nm s ⁻¹
viscosity dodecane	0.00135	Nm s ⁻¹
surface tension between water and dodecane	0.040	N m ⁻¹
diameter gel bead	2.76	mm
diffusion coefficient substrate	10 ⁻⁹	m ² s ⁻¹
diffusion coefficient product	10 ⁻⁹	m ² s ⁻¹
distribution coefficient	simulation depended	
<i>Hydrodynamics</i>		
hold-ups 3-phase fluidized bed	simulation depended	
Number of tanks per m reactor		
3-phase fluidized bed	3	
2-phase fluidized bed	13	
Richardson and Zaki constants 2-phase fluidization	2.35	
n	0.0377	m s ⁻¹
v_{∞}		
<i>Kinetics</i>		
Michaelis-Menten constant	1	mol m ⁻³
toxic product concentration	simulation depended	mol m ⁻³
maximum substrate conversion rate	simulation depended	mol (m ³ s) ⁻¹
<i>Operation parameters</i>		
medium flux	simulation depended	m s ⁻¹
dodecane flux	simulation depended	m s ⁻¹
initial substrate concentration	1000	mol m ⁻³
initial product concentration	0	mol m ⁻³

In Figure 9 a typical time course of substrate and product concentration inside the gel bead is shown. The maximum substrate conversion rate was $0.01 \text{ mol (m}^3 \text{ s)}^{-1}$, the toxic product concentration was 10 mol m^{-3} , and the distribution coefficient was 1000. We took a medium flux of $1.29 \times 10^{-2} \text{ m s}^{-1}$ and a dodecane flux of $0.91 \times 10^{-2} \text{ m s}^{-1}$, which resulted in gel bead hold-up of 0.32 and a dodecane hold-up of 0.093.

Figure 9a:

Substrate diffuses into the gel bead and gradually penetrates towards the centre of the gel bead. As time progresses the concentration increases, the profile flattens, and a maximum concentration is reached. At larger times the concentration decreases as result of consumption, until all substrate is converted into product. With the set of parameters used for calculating the profiles in Figure 9a, total conversion of substrate is reached. However, a combination of parameters is easily found, for which the substrate is not completely converted, hence substrate concentration inside the gel bead is not equal to zero. Substrate will be converted to product, as long as the product concentration at any place inside the gel bead is less than the toxic product concentration.

Figure 9b:

As substrate is converted, product is formed. Early in the process little product is present. Gradually product appears throughout the whole gel bead. As product is initially formed near the surface of the gel bead, product not only diffuses out of the gel bead but also towards the centre; consequently a maximum concentration is found inside the gel bead. This maximum concentration progresses towards the centre of the gel bead in time. Hence, after some time product concentration is highest in the centre. After some time also a maximum concentration profile is reached. If at this point of time, there is still mass transfer between the organic and medium phase, the product concentration inside the gel bead will decrease. This transfer of product will continue until equilibrium is reached between medium and organic phase.

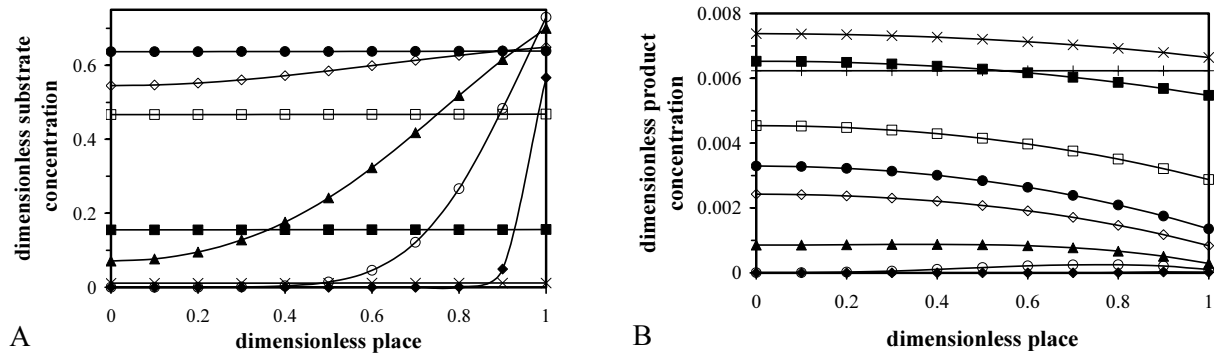


Figure 9. Profile of substrate (A) and product (B) concentration in a gel bead.

$U_c = 1.29 \text{ cm s}^{-1}$, $U_d = 0.91 \text{ cm s}^{-1}$, $\varepsilon_s = 0.32$, $\varepsilon_o = 0.0925$;

$Xv_{\max} = 0.01 \text{ mol (m}^3 \text{ s)}^{-1}$, $C_p^{\text{tox}} = 10 \text{ mol m}^{-3}$, $m = 1000$.

◆ $t = 0:0:3$ ○ $t = 0:0:33$, ▲ $t = 0:1:53$, ◇ $t = 0:6:40$, ● $t = 0:19:0$,
 □ $t = 19:6:0$ ■ $t = 66:0:0$, × $t = 98:0:0$, + $t = 111:0:0$.

Before discussing the influence of the distribution coefficient and toxic product concentration on the time course of the substrate concentration in the medium phase, and the time course of product concentration in the medium and organic phase, first some general remarks:

- The time course profile of the substrate concentration in the water phase shows two processes with a different time constant; the first process is completed after roughly 100 seconds, and is more or less independent of the distribution coefficient and the toxic product concentration. It can be seen in Figure 9b that around that point in time the gel bead is completely filled with substrate. The second process is the gradual conversion of substrate to product, and is dependent on the distribution coefficient and the toxic product concentration.
- Complete conversion of substrate can be reached with some combinations of distribution coefficient and toxic product concentration.
- If substrate is not completely converted, then the end-product concentration inside the gel bead and the medium phase is equal to the toxic product concentration.
- At the point in time where substrate is not longer converted, there is equilibrium for the product concentration between the medium phase and the organic phase.

The influence of the distribution coefficient (m) is shown in Figure 10a, 10b and 10c.

Figure 10a and 10b shows the concentrations in the medium phase, whereas Figure 10c shows the product concentration in the dodecane phase. The maximum substrate conversion rate was $0.01 \text{ mol (m}^3 \text{ s)}^{-1}$, and the toxic product concentration was 10 mol m^{-3} . We took a medium flux of $1.29 \times 10^{-2} \text{ m s}^{-1}$ and a dodecane flux of $0.91 \times 10^{-2} \text{ m s}^{-1}$, which resulted in a gel bead hold-up of 0.32 and a dodecane hold-up of 0.093. Figure 10a clearly shows that a larger m results in the end in a lower substrate concentration in the medium phase, hence substrate is converted to a higher degree. Naturally, when substrate is not converted totally, the product concentration in the medium phase is equal to the toxic product concentration, Figure 10b. As there is equilibrium between the medium and organic phase, the product concentration in the organic phase is higher for a higher m , Figure 10c. If the m is high enough, than at the end of the batch operation the product concentration in the medium phase will be lower than the toxic product concentration. Consequently, substrate is totally converted. This is observed for a distribution coefficient of 1000. The end of the batch operation is reached at an earlier time for a lower m .

The influence of the toxic product concentration (C_p^{tox}) is shown in Figure 11. Figures 11a and 11b show the concentrations in the medium phase, whereas Figure 11c shows the product concentration in the dodecane phase. Obviously, a higher C_p^{tox} results in a lower substrate concentration, hence a more complete conversion and the product concentration goes to C_p^{tox} . This concentration is reached earlier for a lower C_p^{tox} . At C_p^{tox} equal to 100, substrate is completely converted, and C_p^{tox} is not reached in the medium phase.

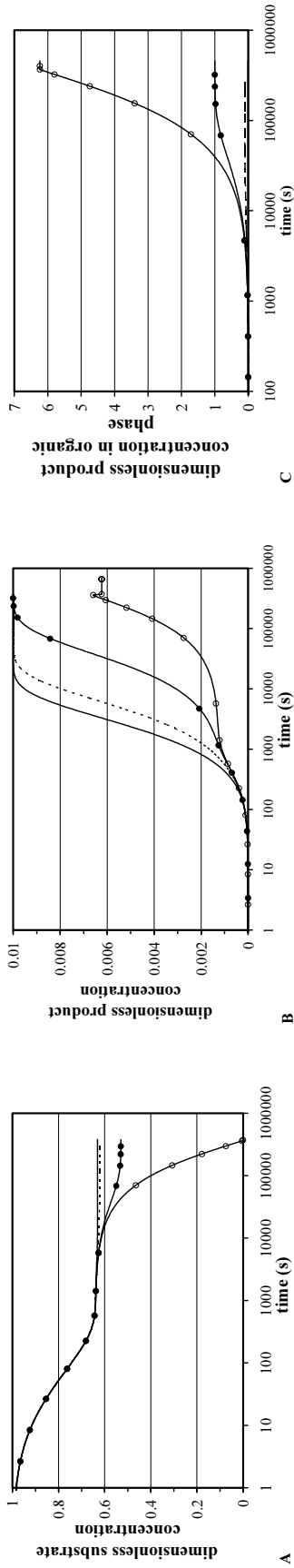


Figure 10. Profile of substrate (A) and product (B) concentration in the medium phase at different distribution coefficients. Profile of product concentration in the dodecane phase (C) at different distribution coefficients.

$U_c=1.29 \text{ cm s}^{-1}$, $U_d=0.91 \text{ cm s}^{-1}$, $\varepsilon_s=0.32$, $\varepsilon_o=0.0925$; $X_{V_{\max}}=0.01 \text{ mol m}^{-3} \text{ s}^{-1}$, $C_p^{\text{tox}}=10 \text{ mol m}^{-3}$, --- $m=1$, --- $m=10$, \bullet $m=100$, Δ $m=1000$

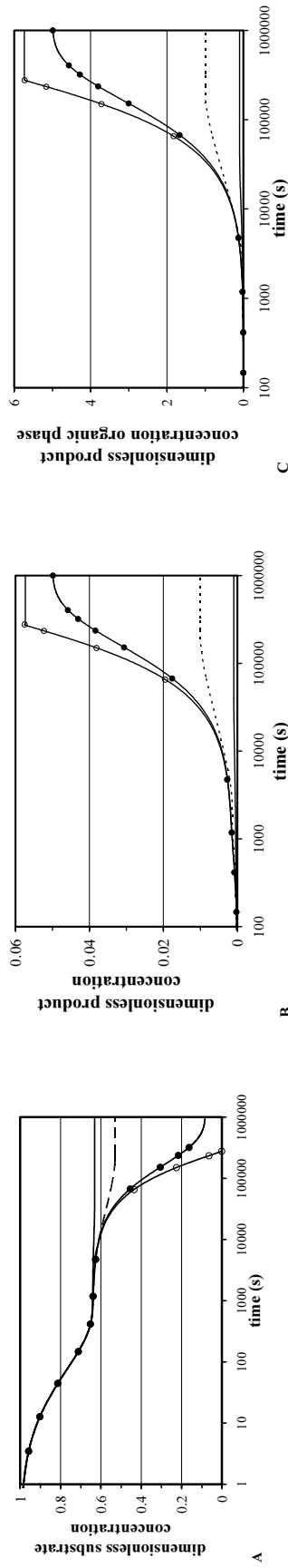


Figure 11. Profile of substrate (A) and product (B) concentration in the medium phase at different toxic product concentrations. Profile of product concentration in the dodecane phase (C) at different toxic product concentrations. $U_c=1.29 \text{ cm/s}$, $U_d=0.91 \text{ cm/s}$, $\varepsilon_s=0.32$, $\varepsilon_o=0.0925$; $X_{V_{\max}}=0.01 \text{ mol/m}^3 \text{ s}$, $m=100$, --- $C_p^{\text{tox}}=10 \text{ mol m}^{-3}$, \bullet $C_p^{\text{tox}}=50 \text{ mol m}^{-3}$, Δ $C_p^{\text{tox}}=100 \text{ mol m}^{-3}$

The influence of the organic solvent flux is shown in Figure 12. Figures 12a and 12b show the concentrations in the medium phase, whereas Figure 12c shows the product concentration in the dodecane phase. We kept the medium flux constant and changed the dodecane flux. The dodecane flux influences the hold-up of the different phases. At a constant medium flux, a higher dodecane flux gives a higher dodecane hold-up, but a lower gel bead hold-up. Figure 12a shows that complete conversion of substrate is reached for the highest U_d , although the gel-bead hold-up is the lowest ($U_d=0.75 \times 10^{-2} \text{ m s}^{-1}$, $\varepsilon_s=0.26$; $U_d=0.14 \times 10^{-2} \text{ m s}^{-1}$, $\varepsilon_s=0.30$). Obviously, at the highest dodecane flux, the product concentration in the medium phase is always below the toxic product concentration, Figure 12b. For the other dodecane fluxes applied in the simulations, the product concentration in the medium phase is equal to the toxic product concentration, Figure 12b. This concentration is reached at an earlier point of time for the lowest U_d . The time course of product concentration in the organic phase follows the time course for the product concentration in the medium phase.

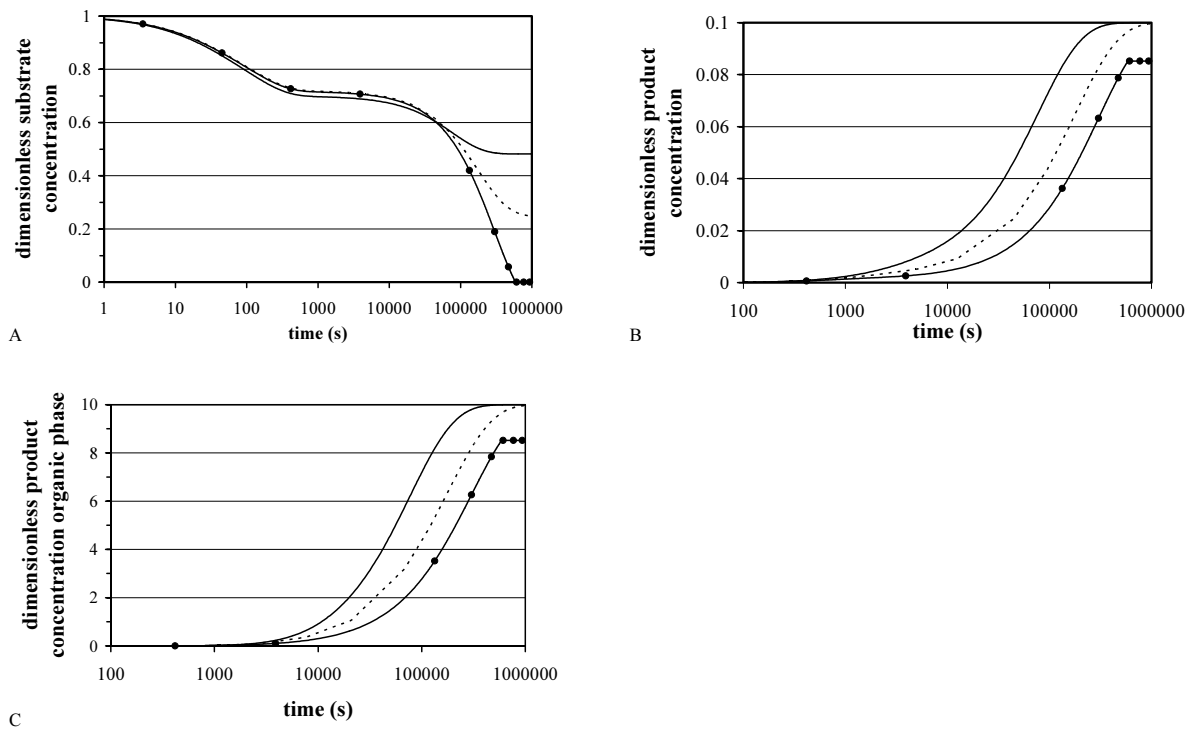


Figure 12. Profile of substrate (A) and product (B) concentration in the medium phase at different fluxes of the organic phase. Profile of product concentration in the organic phase (C) at different fluxes of the organic phase.

$U_c=1.49 \text{ cm s}^{-1}$, $X_{v_{\max}}=0.01 \text{ mol m}^{-3} \text{ s}^{-1}$, $m=100$, $C_p^{\text{tox}}=100 \text{ mol m}^{-3}$. — $U_d=0.14 \text{ cm s}^{-1}$, $\varepsilon_s=0.30$, $\varepsilon_o=0.012$; - - - $U_d=0.36 \text{ cm s}^{-1}$, $\varepsilon_s=0.27$, $\varepsilon_o=0.036$; • $U_d=0.75 \text{ cm s}^{-1}$, $\varepsilon_s=0.26$, $\varepsilon_o=0.069$.

We kept the medium flux constant and changed the dodecane flux. The dodecane flux influences the hold-up of the different phases. At a constant medium flux, a higher dodecane flux gives a higher dodecane hold-up, but a lower gel bead hold-up. Figure 12a shows that complete conversion of substrate is reached for the highest U_d , although the gel-bead hold-up is the lowest ($U_d=0.75 \times 10^{-2} \text{ m s}^{-1}$, $\varepsilon_s=0.26$; $U_d=0.14 \times 10^{-2} \text{ m s}^{-1}$, $\varepsilon_s=0.30$). Obviously, at the highest dodecane flux, the product concentration in the medium phase is always below the toxic product concentration, Figure 12b. For the other dodecane fluxes applied in the simulations, the product concentration in the medium phase is equal to the toxic product concentration, Figure 12b. This concentration is reached at an earlier point of time for the lowest U_d . The time course of product concentration in the organic phase follows the time course for the product concentration in the medium phase.

Comparison between a 2-phase and a 3-phase fluidized-bed bioreactor

In our comparison we did the simulations for batch operations:

substrate is circulated until a certain amount of substrate is converted. In a 2-phase fluidized bed substrate is not totally converted due to product inhibition. When the product concentration reaches the toxic product concentration in the medium phase the conversion stops. At this moment, the product concentrations inside the gel bead and in the medium phase are the same and equal to the toxic product concentration. So, the total amount of moles of product produced is equal to the toxic product concentration times the total reactor volume. In order to compare a 3-phase fluidized bed with a 2-phase fluidized bed we calculated the time necessary to reach 99% of the total amount that can be converted in a 2-phase fluidized bed. Obviously, there is a lot of freedom in totally or partly recirculating the organic solvent in the 3-phase fluidized-bed bioreactor, see Figure 2. We used in this strategy a total reflux as a fair comparison. An economic evaluation must show whether a total reflux yields the lowest cost, but this is not the topic of this paper.

At the end some remarks are made about operating the bioreactor continuously.

Batch operation

The comparison between both bioreactors was made for different combinations of medium and dodecane fluxes. Two different toxic product concentrations were used, i.e. 1 mol m^{-3} and 100 mol m^{-3} , and an initial substrate concentration of 1 kmol m^{-3} .

Introducing an organic solvent in a 3-phase fluidized bed, will in most cases result in a lower gel-bead hold-up. This means loss of biocatalytic activity per unit volume of bioreactor. This loss of activity has to be compensated for by lowering the product concentration in the gel beads, resulting in a higher substrate conversion rate. This is achieved by extracting the product into the organic solvent. The extraction rate is influenced by the distribution coefficient. As can be deduced from the equation in Table II, a higher distribution coefficient gives a higher transfer rate.

So, at a given maximum substrate conversion rate, the time to reach a certain degree of conversion can be manipulated by the distribution coefficient (m): a higher m results in a shorter time, see also Figure 10. Thus, to conclude whether a 3-phase fluidized bed performs better than a 2-phase fluidized bed, at a given maximum substrate conversion rate, a distribution coefficient is determined, that yields the same time to reach 99% of the total amount of moles converted in a 2-phase fluidized bed. A higher distribution coefficient results in a better performance, whereas a lower distribution coefficient gives a worse performance.

We chose to evaluate the performance of the bioreactor with two parameters, i.e. the maximum substrate conversion rate ($X \cdot v_{\max}$) and the distribution coefficient (m), and to keep the other parameters constant. The maximum substrate conversion rate can be influenced by using more or less biocatalyst, and the distribution coefficient might be influenced by adding specific compounds to the organic solvent for enlarging the distribution.

The distribution coefficient at a given maximum substrate conversion rate is thus calculated for which a 3-phase fluidized bed performs the same as 2-phase fluidized bed. This was done for a number of organic solvent fluxes and medium fluxes, and for different toxic product concentrations. The results are shown in Figures 13a-c.

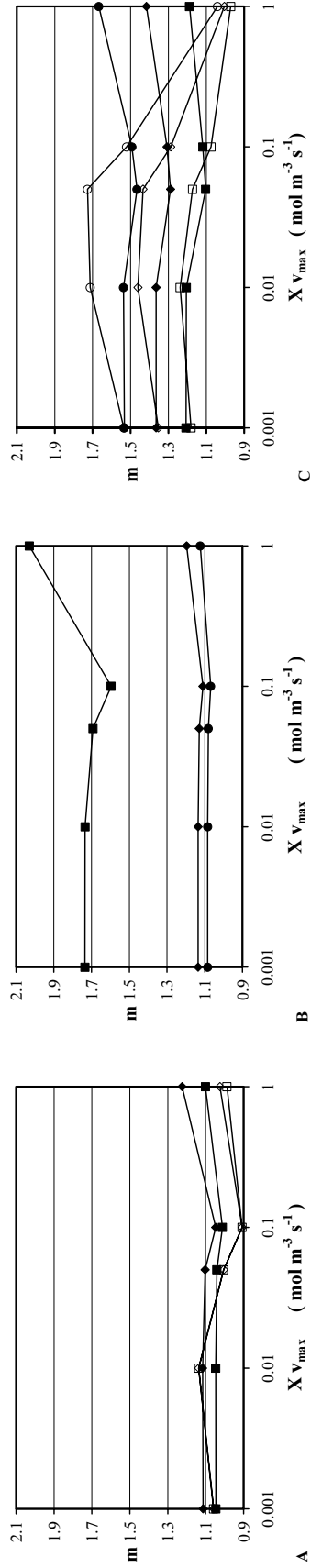


Figure 13. Distribution coefficient as a function of the maximum substrate conversion rate for which a 3-phase fluidized bed performs equally well as a liquid fluidised bed. Open symbols $C_p^{\text{tox}} = 1 \text{ mol m}^{-3}$, closed symbols $C_p^{\text{tox}} = 100 \text{ mol m}^{-3}$

A $U_c = 0.75 \text{ cm s}^{-1}$
 $U_d = 0.40 \text{ cm s}^{-1}$, $\blacklozenge U_d = 0.14 \text{ cm s}^{-1}$

B $U_c = 1.29 \text{ cm s}^{-1}$
 $U_d = 0.14 \text{ cm s}^{-1}$, $\blacklozenge U_d = 0.91 \text{ cm s}^{-1}$

C $U_c = 2 \text{ cm s}^{-1}$
 $U_d = 0.14 \text{ cm/s}$, $\blacklozenge U_d = 0.54 \text{ cm s}^{-1}$

$t_{\text{batch}} (99\%) \text{ (min)}$

$X v_{\text{max}} \text{ mol m}^{-3} \text{ s}^{-1}$	$C_p^{\text{tox}} = 1 \text{ mol m}^{-3}$	$C_p^{\text{tox}} = 100 \text{ mol m}^{-3}$	$C_p^{\text{tox}} = 100 \text{ mol m}^{-3}$
0.001	166.3	15545	355.8
0.01	22.13	1560	55.31
0.05	15.04	319.4	23.81
0.1	15.47	167.2	19.63
1	14.95	21.4	17.02
		20950	32504
		2108	3278
		435.5	699
		227.9	361.4
		32.3	55.94

A 3-phase fluidized bed performs better for combinations of the maximum substrate conversion rate ($X \cdot v_{\max}$) and distribution coefficient in the area above the lines in these figures.

The distribution coefficient at each $X \cdot v_{\max}$ in favor of the 3-phase fluidized bed is relatively low, see Figures 13a-c. Especially, when we consider the examples in Table IV, in which distribution coefficients for different solutes for different liquid-liquid 2-phase systems are given. Based on this table one might suggest that at any pre-set medium flux, a 3-phase fluidized bed performs better than a conventional 2-phase fluidized bed.

Table IV. Distribution coefficients for solute for different liquid-liquid 2-phase systems

Solute	2-phase system	distribution coefficient	reference
oxygen	FC40/ water	12	Sonsbeek <i>et al.</i> , 1992a
	octene/ water	11.4	Meer, 1993
propenoxide	toluene/ water	3.5	Brink and Tramper, 1985
	butylacetate/ water	4.6	Brink and Tramper, 1985
butanal	toluene/ water	6.9	Kawakami, <i>et al.</i> , 1992
	hexadecane/ water	1.52	Kawakami, <i>et al.</i> , 1992
tetraline	FC40/ water	120	Vermuë, <i>et al.</i> , 1994
	dodecene/ water	> 5000	Vermuë, <i>et al.</i> , 1994
<i>Steroids</i>			
Androstenolone-actate	Hexane/ water	1500	Boeren, <i>et al.</i> , 1992
4-Androstene-3,17-dione	Hexane/ water	8.5	Boeren, <i>et al.</i> , 1992
dehydro-epiandrosterone	Hexane/ water	24	Boeren, <i>et al.</i> , 1992
phenylalanine propyl ester	isobutyl methyl keton / water	123	Flaschel, <i>et al.</i> , 1992

Looking in more detail to Figure 13a to c, the results in Figure 13a and Figure 13b – a lower water flux applied – show that a lower dodecane flux requires a higher distribution coefficient, whereas the results in Figure 13c – the highest water flux

applied – show that a higher dodecane flux requires also a higher distribution coefficient. Although the latter observation might seem unexpected, both observations can be easily explained. In most cases the dodecane flux decreases the gel-bead hold-up and, as explained above, this decrease in gel-bead hold-up has to be compensated for with a high enough transfer rate to the dodecane phase. The transfer rate itself is influenced by the dodecane flux, as the dodecane flux determines largely the dodecane hold-up and the mass transfer coefficient, see also the equation in Table II. A higher dodecane flux results in a higher transfer rate. The transfer rate is also influenced by the distribution coefficient, a higher distribution coefficient gives also a higher transfer rate.

At the lower water fluxes, Figure 13a and Figure 13b, the decrease in gel-bead hold-up is not that large, less than 15% for all dodecane fluxes applied, and there is hardly any difference in gel-bead hold-up between the highest and lowest dodecane flux. Thus, the transfer rate in the 3-phase fluidized beds, necessary to perform equally well as the 2-phase fluidized bed, are more or less the same. So, at these water fluxes, a higher distribution coefficient is needed for the lower dodecane flux, to establish a high enough transfer rate.

For the highest water flux applied, Figure 13c, there is a significant decrease in gel-bead hold-up with an increasing dodecane flux (compared to the 2-phase fluidized-bed analogue, 39% for the highest dodecane flux and 7% for the lowest). Consequently, the transfer rate must be higher for the higher dodecane fluxes. When a lower distribution coefficient is used for the higher dodecane fluxes, as above for the lower water fluxes, the resulting transfer rate is not enough for establishing the required transfer rate, although dodecane hold-up is higher for a higher dodecane flux. Hence, the distribution coefficient has to be higher for the higher dodecane fluxes.

The open symbols in Figure 13a and c show the distribution coefficient as a function of the $X \cdot v_{\max}$ for which the 3-phase fluidized bed performs equally well for a low toxic product concentration (1 mol m^{-3} , i.e. 0.1 % of the initial substrate concentration). At the lower water flux, Figure 13a, the difference between both dodecane fluxes is almost insignificant. At the higher water flux, Figure 13b, this difference is a little more pronounced. A general remark about the difference between a high and low toxic product concentration can hardly be made: at $X \cdot v_{\max}$ the distribution necessarily for giving an equal performance is sometimes lower other times higher.

Continuous Operation

Executing a biotransformation continuously in a 2-phase fluidized bed without a recycle is highly inefficient, as the medium flux is high compared to the maximum substrate conversion rate. Consequently the residence time is short and the conversion rate is low. Only for fast conversions or high reactors, a high degree of substrate conversion is possible, and hence a fluidized bed might be attractive. As an example, a substrate conversion of 1 mol s^{-1} , a medium velocity of 0.02 m s^{-1} , and a reactor height of 1 m results in conversion of 50 mol , assuming zero-order kinetics. This is 50% of the attainable conversion at a toxic product concentration of 100 mol m^{-3} .

Otherwise one should use a set-up with a partial recycle and fresh substrate supply. The incoming substrate concentration is kept constant. The product concentration in the medium phase will accumulate until steady state is reached. As the product concentration increases with an increasing recycle, substrate will be less converted. Application of an organic solvent, i.e. using a 3-phase fluidized bed, will result in a higher conversion, as we calculated for the next case (the organic solvent was not recycled): medium flux $0.75 \times 10^{-2} \text{ m s}^{-1}$, dodecane flux $0.40 \times 10^{-2} \text{ m s}^{-1}$, hence $\varepsilon_s=0.48$, $\varepsilon_o=0.045$; $X \cdot v_{\max} = 0.01 \text{ mol s}^{-1}$, $C_{p}^{\text{tox}} = 100 \text{ mol m}^{-3}$, and $m=100$. The dimensionless concentrations for a 2-phase fluidized bed and 3-phase fluidized bed are calculated and given in Table V for different recycles.

Table V. Dimensionless substrate and product concentrations in a continuously operated fluidized bed

Recycle	2-phase fluidized bed		3-phase fluidized bed		
	<i>substrate</i>	<i>product</i>	<i>substrate</i>	<i>product</i>	<i>product organic solvent</i>
0.1	0.9993	6.50e-4	0.9994	6.07e-4	0.72e-4
0.9	0.9994	0.0061	0.9994	0.0019	2.98e-4
0.99	0.9996	0.0396	0.9994	0.005	8.5e-4

Obviously, little substrate is converted, and hence a small amount of product is made. The introduction of the organic solvent results in a smaller product concentration in the medium phase. In optimizing a continuous operation, there is lot of freedom, e.g. the initial substrate concentration, recycle of medium and/or organic solvent. So, whether a continuous operation is feasible depends on a total cost calculation of the plant.

Conclusion

Different aspects of liquid-liquid-solid 3-phase systems have been discussed. The benefits of such a system for typical biotransformations have been discussed in literature. However, the ideal reactor configuration can still be argued about. Different reactor configurations are discussed here, including a simple 3-phase fluidized bed, but also more fancy options, like the different possibilities with a loop reactor. It can be concluded that building and operating a 3-phase system is nothing more than a minor extension of conventional bioreactors.

For a liquid-liquid-solid 3-phase fluidized-bed bioreactor conditions have been established for which this reactor performs better than a conventional 2-phase fluidized bed. Keeping all parameters constant, changing the operation variables, medium flux and organic solvent flux, the distribution coefficient is determined, at given maximum substrate conversion rate, for which the 3-phase fluidized bed performs equally well. It appears that already a low distribution coefficient (larger than 1 but less than 2) suffices for a better performance.

So, it can be concluded that a 3-phase fluidized bed, or less simple 3-phase bioreactors, are good options for operating specific biotransformations, provided *in situ* extraction is needed for such a specific biotransformation.

Nomenclature

A_r	: area reactor	m^2
C_{ij}	: concentration component i in phase j	$mol\ m^{-3}$
$C_s^{w,0}$: substrate concentration in medium phase at $t=0$	$mol\ m^{-3}$
D_i	: diffusion coefficient component i	$m^2\ s^{-1}$
d_{bead}	: gel bead diameter	m
d_{drop}	: droplet diameter	m
d_{noz}	: nozzle diameter	m
Fo	: dimensionless time	-
g	: gravity constant	$m^2\ s^{-1}$
H_{bed}	: height fluidized bed	m
H_t	: height of one medium tank	m
$H_{t,i}$: height of disperse phase tank	m
K	: overall mass transfer coefficient water/droplet	$m^3\ (m^2_{int}\ s)^{-1}$
K_m	: michaelis-menten constant	$mol\ m^{-3}$
$k_{bead,i}$: mass transfer coefficient component i water/gel bead	$m^3\ (m^2_{int}\ s)^{-1}$
k_{drop}^o	: mass transfer coefficient interface droplet/bulk droplet	$m^3\ (m^2_{int}\ s)^{-1}$
k_{drop}^w	: mass transfer coefficient bulk water/interface droplet	$m^3\ (m^2_{int}\ s)^{-1}$
N_{dis}	: number of tanks in disperse phase per one medium tank	-
m	: distribution coefficient organic/water	-
R_p	: gel bead radius	m
r	: space-coordinate in gel bead	m
t	: time	s
U_c	: medium phase flux	$m^3\ (m^2s)^{-1}$
U_d	: organic solvent flux	$m^3\ (m^2s)^{-1}$
V_r	: reactor volume	m^3
v_∞	: terminal rise velocity droplet	$m\ s^{-1}$
v_{max}	: maximum substrate conversion rate	$mol\ (g_{cat}s)^{-1}$
v_{wp}	: slip velocity water particle	$m\ s^{-1}$
v_{wo}	: slip velocity water droplet	$m\ s^{-1}$
X	: concentration biocatalyst	$g_{cat}\ m^{-3}$
X_{ij}	: dimensionless concentration component i in phase j	-
z	: dimensionless space coordinate in gel bead	-

subscripts

p : product
s : substrate

superscripts

bulk : bulk phase
int : at the interface between two phases
n : tank number in medium phase
o : organic solvent phase
p : gel bead phase
tox : toxic
w : medium phase

greek

η_w	: viscosity medium phase	Nm s^{-1}
$\Delta\rho$: density difference	kg m^{-3}
ε_o	: organic solvent phase hold-up	-
ε_s	: gel bead phase hold-up	-
ε_w	: medium phase hold-up	-
ρ	: density	kg m^{-3}
σ	: interfacial tension	N m^{-1}
ϕ_{pw}^p	: mass transfer flux of product gel bead/water	mol s^{-1}
ϕ_{wo}^p	: mass transfer flux of product water/organic solvent	mol s^{-1}
ϕ_{wp}^s	: mass transfer flux of substrate water/gel bead	mol s^{-1}

Appendix A. Derivation of mass balances for a 3-phase fluidized-bed bioreactor

In a 3-phase fluidized bed three different phases are present. Mass balances are derived for the individual phases. As conversion we took one mole of substrate giving one mole of product. So, two components are present in the solid phase and the medium phase. Only product is present in the organic-solvent phase.

The total reactor is divided in a number of vertically stacked ideally stirred tank reactors, a tanks-in-series model (number of tanks is 3). We took a plug flow model for the organic-solvent phase. A tank-in-series model was applied with a large enough number of tanks to mimic plug flow. For simplicity reason we assumed that the gel beads did not circulate inside the reactor. Systematically the bioreactor looks as shown in Figure 8.

Mass transfer takes place from the medium phase to the gel beads for substrate. Product is transferred from the gel beads to the medium, and from medium to the organic solvent. Mass balances for one tank, including the boundary and initial conditions, read as follows:

The gel bead

Substrate

$$\frac{\partial C_s^{p,n}}{\partial t} = D_s \frac{\partial^2 C_s^{p,n}}{\partial r^2} + \frac{2}{r} \frac{\partial C_s^{p,n}}{\partial r} - (-r_s)$$

$$t=0, \forall r, C_s^{p,n}=0$$

$$r=0, \text{ centre of the gel bead} \quad \left. \frac{\partial C_s^{p,n}}{\partial r} \right|_{r=0} = 0$$

$$r=R_p, \text{ edge of the gel bead} \quad k_{\text{bead},s} (C_s^{w,n} - C_s^{w,\text{int},n}) = D_s \left. \frac{\partial C_s^{p,n}}{\partial r} \right|_{r=R}$$

Product

$$\frac{\partial C_p^{p,n}}{\partial t} = D_s \frac{\partial^2 C_p^{p,n}}{\partial r^2} + \frac{2}{r} \frac{\partial C_p^{p,n}}{\partial r} + r_p \quad \wedge \quad r_p = -r_s$$

$$t=0, \forall r, C_p^{p,n}=0$$

$$r=0, \text{ centre of the gel bead} \quad \left. \frac{\partial C_s^{p,n}}{\partial r} \right|_{r=0} = 0$$

$$r=R_p, \text{ edge of the gel bead} \quad k_{\text{bead},p} (C_p^{w,\text{int},n} - C_p^{w,n}) = -D_p \left. \frac{\partial C_p^{p,n}}{\partial r} \right|_{r=R_p}$$

The medium phase

Substrate

$$\varepsilon_w V_r \frac{dC_s^{w,n}}{dt} = U_c A_r (C_s^{w,n-1} - C_s^{w,n}) - \phi_{wp}^s$$

$t=0$, $C_s^{w,n} = 1$, batch operation

$C_s^{w,n} = 0$, continuous operation

Product

$$\varepsilon_w V_r \frac{dC_s^{w,n}}{dt} = U_c A_r (C_s^{w,n-1} - C_s^{w,n}) - \phi_{wp}^s$$

$t=0$, $C_p^{w,n} = 0$, batch operation and continuous operation

The organic solvent phase

Product

$$\varepsilon_d \frac{V_r}{No} \frac{dC_p^{o,i,n}}{dt} = U_d A_r (C_p^{o,i-1,n} - C_p^{o,i,n}) - \phi_{wo}^p$$

$t=0$, $C_p^{o,i,n} = 0$

The different transfer fluxes are represented by:

$$\phi_{wp}^s = k_{\text{bead},s} (C_s^{w,n} - C_s^{w,\text{int},n}) \frac{6}{d_{\text{bead}}} \varepsilon_s V_r$$

$$\phi_{pw}^p = k_{\text{bead},p} (C_p^{w,\text{int},n} - C_p^{w,n}) \frac{6}{d_{\text{bead}}} \varepsilon_s V_r$$

$$\phi_{wd}^{p,i} = \left(\frac{1}{k_{\text{drop},p}^w} + \frac{1}{mk_{\text{drop},p}^d} \right)^{-1} \left(C_p^{w,n} - \frac{C_p^{o,i,n}}{m} \right) \frac{6}{d_{\text{drop}}} \varepsilon_d \frac{V_r}{No}$$

The mass transfer coefficients $k_{\text{bead},s}$, $k_{\text{bead},p}$, and $k_{\text{drop},p}^w$ are calculated with the equation of

Ranz and Marshall (1952):

$$\frac{k_{\text{bead},i} d_{\text{bead}}}{D_i} = 2 + 0.57 \left(\frac{\rho_w v_{wp} d_{\text{bead}}}{\eta_w} \right)^{0.5} \left(\frac{\eta_w}{\rho_w D_i} \right)^{0.33}$$

$$\frac{k_{\text{bead},p} d_{\text{drop}}}{D_p} = 2 + 0.57 \left(\frac{\rho_w v_{wo} d_{\text{drop}}}{\eta_w} \right)^{0.5} \left(\frac{\eta_w}{\rho_w D_p} \right)^{0.33}$$

with v_{wp} the slip-velocity between water and gel bead, and v_{wo} the slip-velocity between water and organic phase. The droplet diameter is calculated with the equation of Kumar and Hartland

$$d = \frac{d_{\text{noz}}}{0.55 \text{Eo}_{\text{noz}}^{0.33} + 0.0393 \text{We}_{\text{noz}}^{0.73} \left(\frac{\rho_d g d_{\text{noz}}^2}{\sigma} \right)^{-0.315}}$$

$$\text{with } \text{Eo}_{\text{noz}} = \frac{g \Delta \rho d_{\text{noz}}^2}{\sigma}, \text{ and } \text{We}_{\text{noz}} = \frac{\rho v_{\infty}^2 d_{\text{noz}}}{\sigma}$$

The rise velocity of a single droplet is calculated with Vignes' equation:

$$v_{\infty} = \frac{d}{4.2} \left(\frac{g \Delta \rho}{\rho} \right)^{2/3} \left(\frac{\rho}{\eta} \right)^{1/3} \left(1 - \frac{\text{Eo}}{6} \right)$$

$$\text{with } \text{Eo} = \frac{g \Delta \rho d^2}{\sigma}$$

The mass transfer coefficient $k_{\text{drop},p}^d$ is calculated with the equation of Newman (1931).

$$k_{\text{drop},p}^d = -\frac{d_{\text{drop}}}{6t} \ln \left(\frac{6}{\pi \pi^2} \sum_{n=1}^{\infty} \frac{1}{n^2} \exp \left(-4n^2 \pi^2 D_{p,\text{drop}} \frac{t}{d_{\text{drop}}} \right) \right)$$

t represents the contact time and is equal to: $t = H_t \epsilon_o / U_d$

The mass balances are made dimensionless by dividing with the initial substrate concentration, the bead diameter, and with D_s/R_p^2 . The resulting dimensionless parameters are: dimensionless length inside the bead $z=r/R_p$, dimensionless concentration $C/C_s^{w,0}$, and a dimensionless time $\text{Fo}=D_s t/R_p^2$.

The resulting mass balances with the implementation of the transfer flux relations are:

$$\frac{\partial X_s^{p,n}}{\partial Fo} = \frac{\partial^2 X_s^{p,n}}{\partial z^2} + \frac{2}{z} \frac{\partial X_s^{p,n}}{\partial z} - (-r_s) \frac{r_p^2}{D_s C_s^{w,0}}$$

$$\frac{\partial X_p^{p,n}}{\partial Fo} = \frac{D_p}{D_s} \frac{\partial^2 X_p^{p,n}}{\partial z^2} + \frac{D_p}{D_s} \frac{2}{z} \frac{\partial X_p^{p,n}}{\partial z} + (-r_s) \frac{r_p^2}{D_s C_s^{w,0}}$$

$$\frac{\partial X_s^{w,n}}{\partial Fo} = \frac{U_w}{\epsilon_w H_t} \frac{r_p^2}{D_s} (X_s^{w,n-1} - X_s^{w,n}) - \frac{6}{d_{bead}} \frac{\epsilon_s}{\epsilon_w} k_{bead,s} \frac{r_p^2}{D_s} (X_s^{w,n} - X_s^{w,int,n})$$

$$\begin{aligned} \frac{\partial X_p^{w,n}}{\partial Fo} = & \frac{U_w}{\epsilon_w H_t} \frac{r_p^2}{D_s} (X_p^{w,n-1} - X_p^{w,n}) + \frac{6}{d_{bead}} \frac{\epsilon_s}{\epsilon_w} k_{bead,p} \frac{r_p^2}{D_s} (X_p^{w,int,n} - X_p^{w,n}) + \\ & - K \frac{6}{d_o} \frac{\epsilon_o}{\epsilon_w} \frac{r_p^2}{D_s} \left(X_p^{w,n} - \frac{\langle X_p^{w,n} \rangle_i}{m} \right) \end{aligned}$$

$$\frac{\partial X_p^{o,i}}{\partial Fo} = \frac{U_d}{\epsilon_d H_{t,i}} \frac{r_p^2}{D_s} (X_p^{o,i-1} - X_p^{o,i}) + K \frac{6}{d_o} \frac{r_p^2}{D_s} \left(X_p^{w,n} - \frac{\langle X_p^{w,n} \rangle_i}{m} \right)$$

The space co-ordinate in the gel bead mass balance is discretized, making the partial differential equation a set of ordinary differential equation (we took 31 grid points). To mimic the plug flow of the dispersed phase, we took 15 tanks per medium tank. Per medium tank $2 \times 30 + 2 + 15 = 77$ differential equations were solved simultaneously with a solver for stiff differential equations.

General discussion

The results presented in this thesis make it possible to design a liquid-liquid-solid 3-phase fluidized-bed bioreactor. This fluidized bed consists of 1) a solid phase, i.e. gel beads with an immobilized biocatalyst, 2) a continuous aqueous phase that was used for fluidizing the gel beads, and for supply of substrates essential for the biotransformation, and 3) an organic solvent, which rose through the fluidized bed of gel beads as organic droplets. This organic phase was also used as a sink for the biotransformation product. The design of this bioreactor for a specific biotransformation depends on knowledge of the biotransformation itself and various physical aspects of the bioreactor. Figure 1 summarizes the major topics to be considered for a conceptual process design.

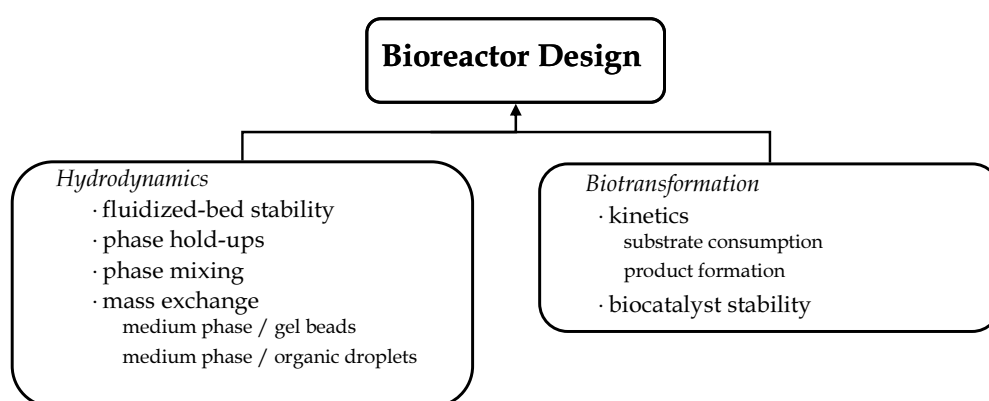


Figure 1. Major topics for designing a 3-phase fluidized-bed bioreactor.

In this study, we assumed the biotransformation data to be known. For the design of a 3-phase fluidized-bed bioreactor, the understanding of its hydrodynamic behavior is essential.

Hydrodynamics

For a 3-phase fluidized-bed bioreactor, both the aqueous phase as well as the organic solvent is recirculated with an external pump. This means that the hydrodynamics can be controlled with both the aqueous-phase velocity and the organic-phase velocity. Important hydrodynamic topics are:

- 1) Bed stability. Stability of the bed refers to stable operation, which means that the gel beads remain in the fluidized bed and are not washed out.

- 2) Phase hold-up. A phase hold-up is the fractional volume of a phase in the fluidized bed. The droplet hold-up thus determines largely the amount of extractive liquid present, and therefore the extraction potential. The gel-bead hold-up determines the height of the fluidized bed at a given total volume of gel beads. Hold-up determines also the specific area for mass exchange.
- 3) Phase mixing. Whether a phase shows plug-flow behavior or ideally mixed behavior can largely influence overall reactor performance. Besides, mixing characteristics also influence mass exchange.

In a 3-phase fluidized bed two distinct 2-phase systems are integrated: a liquid-solid fluidized bed and a spray column (a liquid-liquid extraction column). Hydrodynamic aspects of these constituent 2-phase systems were separately studied; Chapter 2 deals with the liquid-fluidized bed and Chapter 3 deals with the spray column. A 3-phase fluidized bed approaches a 2-phase system if either the amount of organic solvent present in the 3-phase system approaches zero (a liquid-solid fluidized bed), or the amount of gel beads present in the 3-phase system reduces to zero (a spray column). Being able to predict the hydrodynamic characteristics of the individual 2-phase systems, it was assumed that the two corresponding models could be combined to describe and predict hydrodynamic characteristics of the 3-phase fluidized bed. In Chapter 4, it is shown that this idea is only partly valid for predicting the different phase hold-ups. With respect to mixing of the continuous phase, it is shown in Chapter 5 that models predicting the axial dispersion coefficient in a spray column can be reliably used for predicting the axial dispersion coefficient in a liquid-liquid-solid 3-phase fluidized bed.

In the following paragraphs, the hydrodynamics of the individual 2-phase systems and the integrated 3-phase system will be discussed in some detail. For the 2-phase systems we will focus on hold-up. Operational stability of both 2-phase systems was good, provided the water velocity did not exceed the settling velocity of a single gel bead. Mixing characteristics of the separate 2-phase system were not determined. For the integrated 3-phase system, we will discuss stability, hold-up and mixing below.

2-phase systems

In Chapter 2, experimental results on gel-bead hold-up in a 2-phase liquid-solid (gel bead) fluidized bed are presented. Increasing the aqueous velocity was found to result in a decreasing gel-bead hold-up. It was found that this hold-up could not be

predicted with the well-established slip-velocity model of Richardson and Zaki (1954), if standard parameter values were used. However, the experimental hold-up data could be well described by the Richardson and Zaki equation if standard parameter values were adopted to fit the experimental data. Further analysis showed that the drag force between the continuous flowing phase (the medium) and gel beads, either present in a group or as single particle, was much lower than for more conventional solids such as glass pearls. Hence, the slip-velocity was much higher. Gel beads consist over 95% of water, and obviously their surface properties are different from those of conventional solids. Apparently, these differences resulted in a lower drag force. The drag force is largely determined by a drag coefficient. In Chapter 2, a more mechanistic model, based on the model of Foscolo *et al.* (1983), is presented for the prediction of the drag coefficient of a single gel bead in a packed or fluidized bed. This drag coefficient can successfully be used to predict pressure drop and gel-bead hold-up in a liquid-fluidized bed.

Chapter 3 shows the influence of sparger lay-out, mode of operation (counter-current or co-current operation) and both liquid velocities on the droplet hold-up. The droplet hold-up in a liquid-liquid extraction spray column can be well predicted with a Richardson and Zaki type of slip-velocity equation, featuring as model parameters an exponent n , and a rise velocity of a single droplet. An established literature model for rise velocities is used; for the exponent n a new model was derived. With this new model for n , the experimental data can be well described. In Chapter 3, it is also shown in which way the droplet hold-up can be manipulated by means of the sparger lay-out (number of nozzles and nozzle diameter).

3-phase fluidized beds: stability

A liquid-liquid-solid (gel bead) fluidized bed is created by introduction of an organic disperse solvent into a 2-phase liquid-solid fluidized bed. Single droplets rising through this 3-phase fluidized bed of gel beads will hardly disturb the fluidized bed, and wash-out of gel beads does not occur.

Through collisions, rising droplets will transfer momentum to the gel beads. If the amount of rising droplets is substantial, gel beads will be washed out from the bioreactor by these rising droplets. Whether this phenomenon took place depended on the density (i.e. inertia) of the gel beads. In this study, gel beads were used with densities of $1006 - 1065 \text{ kg m}^{-3}$. Wash out was indeed observed for gel beads with a density of 1010 kg m^{-3} and a diameter of 2 mm, at a superficial solvent velocity of

0.01 cm s⁻¹. Wash out of the heavier gel beads (1065 kg m⁻³) was not observed at any flux, and stable operation of the 3-phase fluidized bed at all practical solvent velocities was possible.

Practical water velocities were between 0.5 and 2 cm s⁻¹, while practical organic solvent velocities were between 0.05 and 0.9 cm s⁻¹. For gel beads of 1065 kg m⁻³, a flow diagram is presented in Chapter 4. By means of the superficial velocities of both liquid phases, this flow diagram demarcates five areas with characteristic flow patterns: two homogeneous patterns, two heterogeneous patterns (in these four areas, gel beads remained in the fluidized bed, and a freeboard of solids was hardly formed), and an unstable area in which the organic droplets coalesced and gel beads were washed out. In a 2-phase fluidized bed, the solids were homogeneously distributed over the bed, and they moved very slowly through it. At very low organic solvent velocities (much lower than 0.05 cm s⁻¹), this flow pattern of the solids was not disturbed. Also at relatively high water velocities, the solids were homogeneously distributed. Their motion through the bed, however, was much more rapid and more chaotic. A structured heterogeneous flow pattern of the solids was observed at intermediate organic solvent velocities (< 0.35 cm s⁻¹) and water velocities less than 0.8 cm s⁻¹. Axial concentration waves of gel beads along the column were present throughout the fluidized bed. For this flow pattern, a radial concentration distribution of the gel beads was not observed. An irregular chaotic heterogeneous flow pattern of the gel beads was present at high organic solvent velocities and intermediate water velocities. There were significant axial and radial distributions of gel beads and these distributions rapidly and randomly changed with time without a repetitive pattern. Coalescence of the organic solvent droplets occurred at relatively high organic solvent velocities (> 0.35 cm s⁻¹) and relatively low water velocities (< 0.6 cm s⁻¹).

So far, it was assumed that the organic solvent and medium flowed co-currently. For gel beads with a very low density (1010 kg m⁻³), however, co-current flow does not yield a stable bed, except at extremely low velocities of the organic solvent. At practically all organic solvent velocities, the organic droplets push the gel beads up, and before they can fall back again, they are pushed once more. This way, the gel beads are transported out of the fluidized bed. For a fluidized bed of low density gel beads (1010 kg m⁻³), the gel beads could be retained in the fluidized bed without wash-out only if the water flux was zero. Thus, stable operation of this 3-phase system with low density gel beads is possible. Stable operation of the analogue of

this system, a 3-phase bubble column, filled with gel beads, is described in literature (Santos *et al.* 1997). Obviously, the net upward velocity of the aqueous phase in a co-currently operated 3-phase liquid-liquid-solid fluidized bed is, among other things, responsible for wash out of low density gel beads. Apparently, in a 3-phase system without external recirculation of the aqueous phase, internal circulation of the aqueous phase (upward and downward flow) prevents the wash-out of the gel beads.

Although a stable 3-phase fluidized bed was possible if only the organic solvent was pumped to the fluidized bed, a gel-bead concentration gradient along the column height was observed. This concentration gradient could be strongly reduced by applying a downward countercurrent aqueous flow. A stable operation of this 3-phase system was possible. The gel beads were kept in suspension, a packed bed was not formed, and coalescence of the organic droplets was not observed. It was observed that an increase in both flow velocities did not affect the height of the fluidized bed. This opens the way to a really interesting 3-phase fluidized bed; if both velocities are increased in the same way, the volume of the bioreactor and the bioreactor activity remain the same, while the extractive power increases.

Hold-ups in a co-current 3-phase fluidized bed

For high density gel beads (1065 kg m^{-3}), the influence of the organic-solvent and medium velocities on the gel bead and droplet hold-ups is described in Chapter 4. As the amount of gel beads in these experiments was fixed, the bed height was depending on the two phase velocities. At water velocities below 0.75 cm s^{-1} , the bed height was smaller than in a liquid-solid fluidized bed at the same water velocity (bed contraction occurred); at water velocities above 0.75 cm s^{-1} it was larger (bed expansion). It was also shown that at any phase velocity, the droplet hold-up was always larger than in a 2-phase droplet column at the same phase velocity. So, the individual models for both 2-phase systems are not additive, and a new model was needed.

The new model for gel-bead and organic-droplet hold-up is based on the drag forces for a gel bead and a droplet present in the 3-phase mixture (Chapter 4). The gel-bead hold-up is well described by the model. The prediction of droplet hold-up, however, is only fair for hold-ups below 0.06; at higher hold-ups, the droplet hold-up is strongly underestimated. As an alternative, an empirical model was derived; it gives a good description for the whole range of measured hold-ups ($0.005 \rightarrow 0.09$).

To calculate the drag forces, a drag coefficient is needed. Models for drag coefficients for the individual 2-phase systems were extended to model the drag coefficients of a gel bead and a droplet in the 3-phase fluidized bed. When the parameters of the individual 2-phase models are used, the gel bead hold-up is very well described, but the droplet hold-up is systematically underestimated.

Mixing

Mixing of the continuous phase in a 3-phase fluidized bed was studied with high-density gel beads (Chapter 5). It is much more turbulent than mixing in a 2-phase fluidized bed, which was easily verified on sight. Indeed, the axial dispersion coefficient is much higher for a 3-phase fluidized bed and can be very well predicted with the isotropic-turbulence theory of Baird and Rice (1975). It is concluded that mixing of the continuous phase in a 3-phase fluidized bed is comparable with mixing of the continuous phase of either a bubble column or the main tube of a liquid-impelled loop reactor (Van Sonsbeek *et al.*, 1992).

Mixing characteristics of the gel beads, i.e. the circulation velocity of individual gel beads through the fluidized bed, were not determined. Also the mixing of the organic solvent droplets was not determined, but a preliminary indication may be obtained from predictions of solvent hold-up. To predict droplet hold-up, a single droplet diameter was assumed. The successful prediction of solvent hold-up was in support of the assumption of a single droplet diameter. Since droplets with the same diameter will have an equal rise velocity through the 3-phase fluidized bed, plug flow of the droplet phase may be concluded.

As stated above, mixing characteristics of the gel beads in a 3-phase fluidized bed were not studied. For the design of the 3-phase fluidized bed, we assumed the gel beads not to move. Obviously, this is a simplification. Future work should elucidate the movement of gel beads throughout the bed and its impact. It may be monitored with radio-active labeling and appropriate sensors. The results can be transformed to generic flow patterns of the gel beads in the fluidized bed.

Mass transfer

Besides hold-up and mixing, mass exchange of substrates and products between the different phases of the 3-phase fluidized bed is vital for the design of the bioreactor. Mass transfer in the fluidized bed takes place at two different levels: 1) transfer in the

continuous phase through a droplet or gel bead boundary layer, and 2) transfer within a droplet or gel bead. The same transfer path holds for gel beads. Mass transfer within particles or droplets has already been studied extensively in literature and may be adequately predicted from established equations. Mass transfer through the outer boundary layer of gel beads or droplets in a 3-phase fluidized bed, on the contrary, has not been studied yet; also in this study, such mass transfer experiments have not been done. In the next paragraph we will focus on these mass transfer phenomena.

In the design of the 3-phase fluidized bed (Chapter 6), we used the well-known equation of Ranz and Marshall (1950) for calculation of mass transfer coefficients from the bulk liquid to the surface of either a droplet or a gel bead. This equation uses the slip velocity between the different phases, which can be determined with the hold-up model given in Chapter 4. It is questionable, however, whether the empirical constants in this mass transfer correlation may be applied also for mass transfer in the liquid-liquid-solid (gel bead) fluidized bed bioreactor.

Other models use the energy dissipation rate in the fluidized bed for determination of mass transfer coefficients (Kikuchi *et al.*, 1994). This method is also widely used for the determination of mass transfer in stirred tanks and bubble columns (Van 't Riet and Tramper, 1991). The energy input determines the mixing of the aqueous phase, and mixing determines the extent of the boundary layer. The size of the boundary layer, finally, determines the external mass transfer coefficient. So, it is expected that the energy-input determines the external mass transfer coefficient. In Chapter 5 it is shown that mixing of the 3-phase fluidized bed can be adequately described with the well-established model of Baird and Rice (1975) using the energy dissipation rate. So, external mass transfer coefficients may be adequately determined using established correlations based on the energy dissipation rate.

Further research should substantiate this idea, as for gel beads mass transfer in 3-phase systems (gas-liquid-solid or liquid-liquid-solid) has not been elucidated. Experiments should yield the external mass transfer coefficients for the transfer from the continuous liquid phase to either a droplet or a gel bead surface. In a 3-phase fluidized bed there is simultaneous transfer from the aqueous phase to both the organic droplet and the gel bead; one would like to determine the external transfer coefficients independently. To determine the mass transfer coefficient from bulk liquid to gel bead surface one could use a tracer component that is exchanged between the bulk liquid and the gel beads, but, at the same time, does not dissolve in the organic solvent.

Determination of the external transfer coefficient from the continuous aqueous phase to the droplet surface can use a similar set-up (Van Sonsbeek *et al.*, 1991). However, a tracer component that is not transferred to the gel beads might be hard to find, as the gel beads consist for over 95% of water. An alternative would be to use a component that is exchanged between the continuous aqueous phase and both the gel beads and the organic droplets. Transfer experiments with such a component would thus involve two simultaneous transfer coefficients. Nevertheless, the coefficient for transfer into the organic phase may be calculated from experimental data if the value for the coefficient of transfer into the gel beads would be available from preceding experiments as described above.

Summary and Future prospects

The work in this thesis aimed at design rules for a 3-phase liquid-liquid-solid (gel bead) 3-phase fluidized-bed bioreactor. A full design of such 3-phase fluidized bed bioreactors is only partially possible with the results presented in this thesis. Operational stability of the fluidized bed, hold-up of the different phases, and mixing of the continuous phase as a function of operational variables (superficial velocities of the organic solvent and medium) are well understood, and reliable models have been derived. For mass transfer and mixing of the organic solvent phase, educated guesses can be made, based on our experience with the fluidized bed. Mixing behavior of the gel beads is still unknown. In our design, given in Chapter 6, we assumed that the gel beads did not move. The other extreme would be an ideally mixed bed of gel beads. The actual mixing of the bed will be in-between both extremes. Future work should address the mixing characteristics of the gel beads, and the correlations for mass transfer coefficients.

To elucidate the hydrodynamic behavior of the 3-phase fluidized bed, a specific type of gel bead was used. A generalization of the behavior can thus not be given. However, with respect to stability of the fluidized bed we concluded that to prevent wash-out of the gel beads, their terminal settling velocity should exceed 5.0 cm s^{-1} . The model for the hold-up in the 3-phase fluidized bed contains empirical constants, which, in principle, have to be measured for each type of gel beads. Experimental methods for determination of these constants are given. It is also shown that if an

energy dissipation rate is available, mixing of the continuous phase may be straightforwardly determined.

In Chapter 6, it is shown that the performance of the 3-phase fluidized-bed bioreactor is influenced by the distribution coefficient of the product over the organic solvent and medium phase. It appeared that a distribution coefficient larger than 2 suffices for a better performance of this 3-phase fluidized bed. In order to demonstrate that the newly developed bioreactor does also perform better for practical systems, a bioconversion hindered by strong product inhibition should be performed with this bioreactor.

In future, one could consider using a 3-phase fluidized bed bioreactor for performing substrate or product inhibited biotransformations, as this thesis elucidated the most important physical aspects, and showed the operational suitability of the bioreactor.

References

- Adlercreutz P. 2000. In Applied Biocatalysis. Biocatalysis in non-conventional media. Ed. Straathof AJJ and P. Adlercreutz, 2nd edn Harwood Academic Publishers. (Singapore). p 295 - 316.
- Almering JHJ (Ed.). 1988. Analyse. Delftse Uitgevers Maatschappij (Delft). p 356 - 359.
- Baird MHI and Rice RG. 1975. Axial dispersion in large unbaffled columns. Chem Eng J 9:171-174.
- Bird RB, Stewart WE and Lighthfoot EN. 1960. Transport Phenomena. John Wiley & Sons (Singapore). p 200.
- Boeren S, Laane C and Hilborst R. 1992. In Biocatalysis in Non-conventional media. The effect of alkanes on viability, enzyme induction and enzyme activity in *Flavobacterium dehydrogenans*. Ed Tramper J, Vermuë MH, Beeftink HH and Von Stockar U, Elsevier Science Publ (Amsterdam). p 637 - 643.
- Boon MA, Van 't Riet K and Janssen AEM. 2000. Enzymatic synthesis of oligosaccharides: product removal during a kinetically controlled reaction. Biotechnol Bioeng 70:411-420.
- Brink LES and Tramper J. 1985. Optimization of organic solvent in multiphase biocatalysis. Biotechnol Bioeng 27:1258 - 1269.
- Bruggink A (ed). 2001. Synthesis of beta-lactam antibiotics. Chemistry, biocatalysis & process integration. Kluwer Academic Publishers. (Dordrecht).
- Duijn G and Rietema K. 1982. Segregation of liquid-fluidized solids. Chem Eng Sci 39:365-368.
- Buitelaar RM, Langenhoff AAM, Heidstra R and Tramper J. 1991. Growth and thiophene production by hairy root cultures of *tagetes patula* in various two-liquid-phase bioreactors. Enzym Microb Techn 13:487 - 494.

Chen Y-M and Fan L-S. 1990. Drift flux in gas-liquid-solid fluidized systems from the dynamics of bed collapse. Chem Eng Sci 45:935-945.

Chisti MY (ed.). 1989. Air-lift Bioreactors. Elsevier Science Publishers BV (London).

Collins AM, Woodley JM and Lidell JM. 1995. Determination of reactor operation for the microbial hydroxylation of toluene in a two-liquid phase process. J Ind Microbiol 14:382-388

Coutouly, <http://gerard.coutouly.free.fr/fr/Origine/cdindetf.html>

Dalingaros W, Kumar A and Hartland S. 1986. Effect of physical properties and dispersed-phase velocity on the size of drops produced at a multi-nozzle distributor. Chem Eng Process 20:95-102.

Dakshinamurty P, Veerabhadrarao K and Venkatarao AB. 1979. Bed porosities in 3-phase (liquid-liquid) fluidized beds. Ind Eng Chem Proc Des Dev 18:638 – 640.

Dakshinamurty P, Subrahmanyam V, Prasada Rao RV and Vijayasradhi P. 1984. Liquid-liquid mass transfer in 3-phase fluidized beds. 3. Measurement of individual fluid-phase resistances. Ind Eng Chem Proc Des Dev 23:132 – 137

Dallavalle JM. 1948. Micrometrics: the technology of fine particles. 2nd Edn. Pitman (London).

Davison BH and Thompson JE. 1993. Continuous direct solvent extraction of butanol in a fermenting fluidized-bed bioreactor with immobilized *Clostridium acetobutylicum*. Appl Biochem Biotech 39/40: 415-426.

De Bont JAM. 1998. Solvent-tolerant bacteria in biocatalysis. Trends Biotechnol 12:493-499

Di Felice R. 1995. Hydrodynamics of liquid fluidisation. Chem Eng Sci 50(8): 1213-1245.

- Krab-Hüsken LE. 2002. Production of catechols: microbiology and technology. PhD thesis, Wageningen Agricultural University, Wageningen, The Netherlands.
- Fahim MA and Wakao N. 1982. Parameter estimation from tracer response measurements. *Chem Eng J* 25:1-8.
- Fan L-S. Muroyama K. and Chern S-H. 1982. Hydrodynamic characteristics of inverse fluidization in liquid-solid and gas-liquid-solid systems. *Chem Eng J* 24:143 – 150.
- Flaschel E, Crelier S, Schulz K, Huneke F-U and Renken A. 1992. In Biocatalysis in non-conventional media. Process development for the optical resolution of phenylalanine by means of chymotrypsin in a liquid-liquid-solid 3-phase reaction system. Ed Tramper J, Vermuë MH, Beeftink HH and Von Stockar U. Elsevier Science Publishers BV. (Amsterdam). p 637 – 643.
- Foscolo PU, Di Felice R and Gibilaro IG. 1987. An experimental study of expansion characteristics of gas fluidized beds of fine catalysts. *Chem Eng Process* 22:69-78.
- Foscolo PU, Gibilaro LG and Waldram SP. 1983. An unified model for particulate expansion of fluidized beds and flow in fixed porous media. *Chem Eng Sci* 38:1251-1260.
- Garside J and Al-Dibouni MR. 1977. Velocity-voidage relationships for fluidization and Sedimentation in solid-liquid Systems. *Ind Eng Chem Process Des Dev* 16:206-214.
- Gòdia F and Solà S. 1995. Fluidized-bed bioreactors. *Biotechnol Prog* 11:479-497.
- Gòdia F, Casas C and Solà C. 1987. A survey of continuous ethanol fermentation systems using immobilized cells. *Process Biochem* 4:43-48.
- Godfrey JC and Slater MJ. 1991. Slip velocity relationships for liquid-liquid extraction columns. *Trans IchemE* 69:130-141.

- Godfrey JC and Slater MA (Ed.) 1994. Liquid-liquid extraction equipment. John Wiley and Sons (New York).
- Gommers PJF, Christoffels LP, Kuenen JG and Luyben KChAM. 1986. Gas-phase influence on the mixing in a fluidized bed bio-reactor. *Appl Microbiol Biotechnol* 25:1-7.
- Grbavcic ZB, Garic RV, Hadzismajlovic DZE and Jovanvic S. 1991. Variational model for prediction of the fluid-particle interphase drag coefficient and particulate expansion of fluidized and sedimenting beds. *Powder Technol* 68:199-211.
- Hartman M, Havlin V, Trnka O and Carsky M. 1989. Predicting the free-fall velocities of spheres. *Chem Eng Sci* 44:1743-1745.
- Heijnen JJ, Hols J., Van der Lans GJM, Van Leeuwen HLJM, Mulder A. and Weltevrede R. 1997. A simple hydrodynamic model for the liquid circulation velocity in a full scale two- and 3-phase internal airlift reactor operating in the gas recirculation regime. *Chem Eng Sci* 52:2527 - 2540.
- Hidaka N, Kakoi K and Matsumoto T. 1994. Correlation of solid hold-up in liquid-solid fluidized bed. *J Chem Eng Jpn* 27:563-570.
- Hiemenz PC (Ed). 1986. Principles of colloid and surface chemistry. 2nd Marcel Dekker Inc (New York). p 288-293.
- Hulst AC, Tramper J, Van 't Riet K and Westerbeek JMM. 1985. A new technique for the production of immobilized biocatalyst in large quantities. *Biotechnol Bioeng* 27:870-876.
- Hunik JH and Tramper J. 1993. Large Scale production of κ -carrageenan droplets for gel bead production: theoretical and practical limitations of size and production rate. *Biotech Progress* 9:186-192.
- Hunik JH, Tramper J and Wijffels RH. 1994. A strategy for scale-up of nitrification processes with immobilized nitrifying cells. *Bioprocess Eng.* 11:73-82.

- Hüsken LE, Oomes M, Schroën CHGP, Tramper J, De Bont JAM and Beeftink HH. 2002. Membrane-facilitated bioproduction of 3-methylcatechol in an organic/water 2-phase system. *J Biotechnol* 96: 281-289.
- Hüsken LE, Dalm MCF, Tramper J, Wery J, De Bont JAM and Beeftink HH. 2001. Integrated bioproduction and extraction of 3-methylcatechol. *J Biotechnol* 88:11-19.
- Kahn RA and Richardson JF. 1987. The resistance to motion of a solid sphere in a fluid. *Chem Eng Commun.* 62:135-150.
- Kawakami K and Yosida T. 1992. In *Biocatalysis in Non-conventional media*. Kinetic study of enzymatic reaction in aqueous-organic 2-phase systems – an example of enhanced production of aldehydes by alcohol oxidase. Ed Tramper J, Vermuë MH, Beeftink HH and Von Stockar U. Elsevier Science Publishers BV. (Amsterdam). p. 637 – 643.
- Kikuchi K, Itoh E, Takahashi H and Sugawara T. 1994. Mass transfer between particles and liquid in dilute fluidized beds containing small particles. *Chem Eng J* 27:674-677.
- Kim SD and Kim CH. 1983. Axial dispersion characteristics of 3-phase fluidized beds. *J Chem Eng Japan* 16:172 – 178.
- Kim SD, Han PW and Yu YH. 1988. Phase holdups and liquid-liquid mass transfer in three phase fluidized beds. *Chem Eng Commun* 68:57-68.
- Kim SD, Lee MJ and Han JH. 1989. Axial dispersion characteristics of three (liquid-liquid-solid) phase fluidized beds. *Can J Chem Eng* 67:276 – 282.
- Kim SD, Kim DY and Han JH. 1994. Dispersed phase characteristics in 3-phase (liquid-liquid-solid) fluidized beds. *Can J Chem Eng* 72: 222-228
- Kim SD and Kang Y. 1997. Heat and mass transfer in 3-phase fluidized-beds reactors – an overview. *Chem Eng Sci* 52:3639 – 3660.

- Kim SD, Kim JS, Nam CH, Kim SH and Kang Y. 1999. Immersed heater-to-bed heat transfer in liquid-liquid-solid fluidized beds. *Chem Eng Sci* 54:5173 – 5179.
- Kumar A and Hartland S. 1985. Gravity settling in liquid/liquid dispersions. *Can J Chem Eng* 63:368-376.
- Kumar A and Hartland S. 1995. A unified correlation for the prediction of dispersed-phase hold-up in liquid-liquid extraction columns. *Ind Eng Chem Res* 34:3925-3940.
- Kumar A and Hartland S. 1996. Unified correlations for the prediction of drop size in liquid liquid extraction columns. *Ind Eng Chem Res* 35:2682-2695.
- Leenen EJTM. 2001. In *Immobilized Cells. Mechanical Stability of the Support*. Ed. Wijffels RH, Springer Lab Manual (Berlin).
- Leenen EJTM. 2001. In *Immobilized Cells. Support Material Stability at the Process Conditions Use*. Ed. Wijffels RH, Springer Lab Manual (Berlin).
- Levenspiel O (Ed.). 1972. *Chemical reaction engineering*. John Wiley (New York).
- Marshall CT and Woodley JM. 1995. Process synthesis for multi-step microbial conversions. *Bio/Technology* 13:1072-1078.
- Mateus DMR, Alves SS and Da Fonseca MMR. 1996. Model for the production of L-tryptophan from L-serine and indole by immobilized cells in a 3-phase liquid-impelled loop reactor. *Bioprocess Eng* 14:151 – 158.
- Michielsen MJF, Wijffels RH, Tramper J and Beeftink HH. 2001. In *Multi-phase bioreactor design*. Chapter 8 Solid-to-solid bioconversions: batch or continuous?. Ed. Cabral JMS, Mota M and Tramper J, Taylor and Francis (London, New York). p 225-247.
- Muroyama K and Fan L-S. 1984. *Fundamentals of gas-liquid-solid fluidization*. *AIChE J* 31:1-34.

- Nelder JA and Mead R. 1965. A simplex method for function minimization. *Computer J* 7: 308-313.
- Newman AB. 1931. The drying of porous solids: diffusion and surface emission equations. *Trans Am Int Chem Engrs* 27:203 – 220.
- Paireau O and Bonn D. 1999. Drag reduction in liquid-liquid friction. *Physical Review Letters* 83:5591-5594.
- Qureshi N and Maddox IS. 1995. Continuous production of Acetone-butanol-ethanol Using Immobilized Cells of *Clostridium acetobutylicum* and Integration with product removal by liquid-liquid extraction. *J Ferment Bioeng* 80:185-189.
- Ranz WE and Marshall WR. 1950. Evaporation from drop I + II. *Chem Eng Progr* 48: 141 – 146, 173 – 180.
- Riba JP and Couderc JP. 1977. Expansion de couches fluidisées par des liquides. *Can J Chem Engng* 55:118-121.
- Richardson JF and Zaki WN. 1954. Sedimentation and fluidization. Part 1. *Trans Inst Chem Eng* 32:35-53.
- Roszak J and Gawronski R. 1979. Cocurrent liquid-liquid extraction in fluidized beds. *Chem Eng J* 17:101-109.
- Rowe PN. 1987. A convenient model empirical equation for estimation of the Richardson-Zaki exponent. *Chem Eng Sci.* 43:2795 – 2796.
- Schmid A, Dordick JS, Hauer B, Kiener A, Wubbolts M and Witholt B. 2001. Industrial biocatalysis today and tomorrow. *Nature* 409:258-268.
- Stieglitz B, Dicosimo R and Fallon RD. 1996. Formation of aliphatic ω -cyano-carboxamide(s) from α,ω -dinitrile(s) – using biocatalyst having regioselective nitrile hydratase activity derived from *Pseudomonas putida*. US Patent US 5728556.

Thompson VS and Worden RM. 1992. The effect of tracer diffusion on liquid dispersion in a three phase fluidized bed bioreactor. Chem Eng Sci 47:3435 – 3441.

Tramper J, Wolters I and Verlaan P. 1987. In Biocatalysis in organic media. The liquid-impelled loop reactor: a new type of density-difference-mixed bioreactor. Ed. Laane C, Tramper J and Lilly MD, Elsevier Science Publishers BV (Amsterdam). p 311 – 316.

Tramper J, Vermuë MH, Beeftink HH and Von Stockar U (Eds.). 1992. Progress in Biotechnology 8. Biocatalysis in non-conventional media. Elsevier Science Publishers BV (Amsterdam).

Turton R and Levenspiel O. 1986. A short note on the drag coefficient for spheres. Powder Technol 47:83-86.

Turton R and Clark NN. 1987. An explicit relationship to predict particle settling velocity. Powder Technol 53:127-129.

Ueyama K and Miyauchi T. 1979. Properties of recirculating turbulent 2-phase flow in gas bubble columns. AIChE J 15:258-266.

Van den Tweel WJJ, Marsman EH, Vorage MJAW, Tramper J and De Bont JAM. 1987. In Bioreactors and biotransformations. The application of organic solvents for the bioconversion of benzene to *cis*-benzene glycol. Ed. Moody GW and Baker PB, Elsevier Science Publishers BV (London). p. 231 – 241.

Van der Meer AB. 1993. Multi-phase fermentation: reaction engineering models for the production of optically active 1,2-epoxyoctane from 1-octene by free and immobilized *Pseudomonas oleovorans* cells. PhD thesis, University of Groningen, Groningen, The Netherlands.

Van der Wielen LAM, Van Dam MHH and Luyben KChAM. 1996. On the relative motion of a particle in a swarm of different particles. Chem Eng Sci 51:995-1008.

- Van der Wielen LAM, Van Dam MHH and Luyben KChAM. 1996a. Trickle flow of dense particles in a fluidized bed of others. *Chem Eng Sci* 52: 553-565
- Van der Wielen LAM, Diepen PJ, Houwers J and Luyben KChAM. 1996b. A countercurrent adsorptive reactor for acidifying bioconversions. *Chem Eng Sci* 51:2315-2325.
- Van der Wielen LAM. 1997. A countercurrent Adsorptive Fluidized Bed Reactor for Heterogeneous Bioconversions. PhD thesis, Technical University Delft, Delft, The Netherlands.
- Van Sonsbeek HM, Beeftink HH and Tramper J. 1993. Two-Liquid-phase bioreactors. *Enzyme Microb Technol* 15:722 – 729.
- Van Sonsbeek HM, Verdurmen REM, Verlaan P and Tramper J. 1990. Hydrodynamic model for liquid-impelled loop reactors. *Biotech Bioeng* 36: 940 – 946.
- Van Sonsbeek HM, Gielen SJ and Tramper J. 1991. Steady state method for $k_L a$ measurements in model systems. *Biotech Techn* 5:157-162.
- Van Sonsbeek HM. 1992a. Physical aspects of liquid-impelled loop reactors. PhD thesis, Wageningen Agricultural University, Wageningen, The Netherlands.
- Van Sonsbeek HM, De Blank H and Tramper J. 1992b. Oxygen transfer in liquid-impelled loop reactors using perfluorocarbon liquids. *Biotechnol Bioeng* 40:713 – 718.
- Van 't Riet K and Tramper J. (Ed.). 1991. *Basic Bioreactor Design*. 2nd edn. Marcel Dekker Inc (New York).
- Van Zessen E, Rinzema A and Tramper J. 2003. Fluidized-bed and packed-bed characteristics of gel beads. submitted (Chapter 2).
- Van Zessen E, Rinzema A and Tramper J. 2003. Phase hold-ups in a water-dodecane 2-phase system. submitted (Chapter 3)

Van Zessen, E., Dierendonck, F. van, Rinzema A. and Tramper J. (2003) Solid and droplet phase hold-ups in a liquid-liquid-solid 3-phase fluidized bed bioreactor. submitted (Chapter 4).

Van Zessen, E, Keijzer, T., Rinzema A. and Tramper J. (2003) Residence time distribution of the water phase in a liquid-liquid-solid 3-phase fluidized bed bioreactor. submitted (Chapter 5).

Van Zessen E, Tramper J and Rinzema A. 2001. In Immobilized Cells. Measurement of density, particle size and shape of support. Ed Wijffels R, Springer Lab Manual, Springer-Verlag (Berlin).

Vermuë MH, Sikkema J, Bakker R, Janssen G and Tramper J. 1995. Strategy for selection of a suitable solvent for extractive biocatalysis in a liquid-impelled loop reactor. Vermuë MH. In Biocatalysis in non-conventional media thermodynamic and kinetic aspects. PhD thesis, Wageningen Agricultural University, Wageningen, The Netherlands.

Vermuë MH and Tramper J. 1995. Biocatalysis in non-conventional media; medium engineering aspects – a review. Pure & Applied Chem 67:345-373.

Vermuë MH, Tacken M and Tramper J. 1994. Tetralin and oxygen transfer in the liquid-impelled loop reactor. Bioprocess Eng 11:224 – 228.

Wallis GB (Ed.). 1969. One-dimensional 2-phase flow. McGraw-Hill (New York).

Wang H, Seki M and Furusaki S. 1994. Characteristics of immobilized *Lactobacillus Delbrueckii* in a liquid-solid fluidized bed bioreactor for lactic acid production. J Chem Eng Jpn 28:198-203.

Weast RC. 1979. Handbook of Chemistry and Physics. 59th Edition. CRC Press Boca Raton.

Wilhelm RH and Kwauk M. 1948. Fluidization of solid particles. Chem Eng Prog 44:201-217.

Willaert RG, Van Baron G and De Backer L. 1996. In Immobilized living cell systems modeling and experimental methods. Immobilized cell systems. John Wiley & Sons (New York). p. 67-97.

Wijffels RH, Buitelaar RM, Bucke C and Tramper J (Ed.). 1995. Immobilized Cells: Basics and Applications. Elsevier (Amsterdam).

Yu H and Rittmann BE. 1997. Predicting bed expansion and phase holdups for 3-phase fluidized bed reactors with and without biofilm. Wat Res 31: 2604 – 2616.

Zigang DJ and Silvester ND. 1981. An explicit equation for particle settling velocities in solid-liquid systems. AIChE J 27:1043-1044.

Summary

If a batchwise bioconversion and subsequent (*i.e.* serial) downstream processing are adopted as a standard production strategy, a low overall productivity may result for certain types of biotransformations. Examples may be found among reactions that are kinetically inhibited by a substrate or a product, transformations featuring an unfavorable thermodynamic equilibrium, and bioconversions involving poorly soluble substrates or products.

An alternative to sequential processing would be the integration of bioconversion and downstream processing by controlled supply of substrate to the reaction *in situ*, or by controlled removal of product from the reaction *in situ*. Such integration involves a multi-phase reactor in which a helper phase may serve as substrate reservoir or as product sink.

To facilitate integration of reaction and product removal or substrate supply, a new type of multi-phase bioreactor was developed, containing a continuous liquid phase, a dispersed liquid phase, and a dispersed solid phase; it may be conceived of as a 3-phase liquid-liquid-solid fluidized bed. The solid reaction phase were biocatalytic gel beads that were fluidized by the continuous medium phase; through this fluidized bed, organic droplets rose and served as a helper phase (extracting the product or acting as a substrate sink).

This thesis focuses on the hydrodynamic aspects of such a 3-phase fluidized bed; a general design strategy was developed. Within this 3-phase system, two 2-phase sub-systems may be identified: a liquid-solid fluidized bed consisting of biocatalytic gel beads in a continuous medium phase, and a liquid-liquid extraction column or spray column, consisting of organic droplets in a continuous medium phase. The hydrodynamic characteristics of these constituent 2-phase systems were studied separately (Chapters 2 and 3). Once good descriptions and predictions of the hydrodynamics of these individual 2-phase systems were obtained, it was assumed that the two corresponding models could be combined to describe and predict the hydrodynamic characteristics of the 3-phase fluidized bed. For the phase hold-ups in the 3-phase system, this assumption was only partly valid (Chapter 4). The continuous-phase axial dispersion coefficient of the 3-phase fluidized bed, however, could be reliably predicted from a model for this dispersion coefficient in a 2-phase droplet column (Chapter 5).

The physical behavior of gel beads was studied; they were either settling as single beads, or present in a packed or fluidized bed (Chapter 2). For five types of gel beads of different diameter and density, three related characteristics were analyzed that all involved the drag force between a particle and its surroundings: the terminal settling velocity of a single gel bead, the pressure drop over a packed bed, and the voidage in a liquid-fluidized bed. Although gel beads showed similar characteristics as conventional solids, established models did not quantitatively predict. It is concluded that the drag force between the gel beads and liquid was lower than for conventional solids. Two hypotheses were put forward to explain this. The first one attributes the drag reduction to small amounts of dissolved polymer. The second one attributes the smaller drag force to the nature of the gel beads; gel beads contain over 95% of water and can in that sense be regarded as 'rigid' water droplets. Hence, the gel bead surface might show waterlike properties. A new model was presented that correctly predicted the drag coefficient of a single gel bead in a packed or fluidized bed. It was used to predict the pressure drop over a packed bed of beads and the voidage in a fluidized bed of beads.

Droplet hold-ups in a liquid/liquid 2-phase spray column were studied with different sparger geometries (Chapter 3). The continuous phase (water) and the dispersed phase (dodecane droplets) were fed into the column co-currently and counter-currently. Although water and dodecane superficial velocities were within the same order of magnitude, the water velocity had only a minor influence on the dodecane hold-up. The number of nozzles, however, influenced the dodecane hold-up to a large extent: at the same dodecane superficial velocity, the sparger with the lowest number of nozzles showed the highest hold-up. The droplet hold-up could be well described using a model based on the slip velocity between the continuous phase and dispersed phase. The slip velocity obeyed a Richardson and Zaki type equation. It features a parameter n , for which a new model was presented. Up to a hold-up of 0.13, this parameter was found constant ($n=4$); for higher hold-ups, a decrease in n was found. The validity of this model was demonstrated by extending it to a 2-phase system differing in surface tension (60 mM KCl / dodecane).

The integration of a solid (gel bead)-liquid fluidized bed with a droplet spray column results in a liquid-liquid-solid 3-phase fluidized bed reactor. Integration of the models for a solid/liquid 2-phase system (a fluidized bed) and a liquid/liquid 2-phase system (a droplet spray or extraction column) was assumed to yield a potential

description of a liquid-liquid-solid 3-phase fluidized bed reactor. The different phase hold-ups of this 3-phase fluidized bed were studied as well as the flow behavior of the fluidized bed (Chapter 4). The reactor featured a bed of Celite™-enforced κ -carrageenan gel beads as solid phase (density 1065 kg m^{-3}). The bed was fluidized by a continuous aqueous phase (30 mM KCl, 'water'); a disperse organic phase (n-dodecane droplets) rose through the bed of particles. At various velocities of water and n-dodecane, the flow characteristics of the gel beads in the fluidized bed were characterized; in addition, the various phase hold-ups were studied. From visual observation of the fluidized bed, five flow regimes were defined for the gel beads: two stable homogeneous regimes, two stable heterogeneous regimes, and an unstable regime in which gel beads were washed-out from the bed. Literature models for existing 3-phase systems were tried to predict phase hold-ups. The more fundamental literature models for existing 3-phase systems rely on parameters valid for the individual 2-phase systems. Unfortunately, the prediction with these models was poor using parameters derived for the individual 2-phase systems. Prediction with other literature models was also poor. Consequently, a new model for a fluidized bed with gel beads and dodecane droplets had to be derived, based on stationary force balances. To this end, drag-force models for a single gel bead and for a single droplet in a 3-phase suspension were set up. All data for gel bead hold-up and the data for droplet hold-ups below 0.06 were well described. For the description of the entire range of droplet hold-ups, an empirical model was adopted.

The study of the continuous phase mixing in the 3-phase fluidized bed is described in Chapter 5. Mixing was characterized by an axial dispersion coefficient that was determined from residence-time distribution measurements with a KCl-tracer. Because of KCl mass transfer into the gel beads, the inherent limitations of this tracer had to be studied as well. A pulse with a small volume was found to give reliable results. The continuous-phase axial dispersion coefficient was found to increase with the superficial n-dodecane velocity, while its dependency on the continuous-phase superficial velocity showed a maximum. These results reflect the increase in continuous-phase dispersion coefficient with the energy dissipation rate per unit mass of continuous phase. A literature relationship for this dependency was found to yield good predictions of the dispersion coefficient with some minor exceptions. It is concluded that the mixing of the continuous phase in a liquid-liquid-solid 3-phase fluidized bed is comparable with the mixing of the continuous phase of either a bubble column or the main tube of a liquid-impelled loop reactor.

A simple process design for a 3-phase liquid-liquid-solid fluidized bed bioreactor was made (Chapter 6). It was based on the results from the preceding chapters, on educated guesses for mass exchange and flow behavior of both dispersed phases (gel beads and droplets); a simple product-inhibited reaction was assumed. It was demonstrated that application of a 3-phase reactor system resulted in a higher degree of conversion than 2-phase liquid-solid fluidized bed reactors. From a practical viewpoint, it was concluded that implementation of a 3-phase system would require minor adaptations only as compared to a 2-phase fluidized bed bioreactor. On the basis of the model for the 3-phase fluidized-bed bioreactor, the influence of different parameters was discussed, such as the distribution coefficient of the product over the medium and solvent phases, the product toxicity, and the solvent flux. Operational conditions were established at which the 3-phase reactor would outperform a conventional 2-phase fluidized bed. Already at quite modest values of the distribution coefficient, the 3-phase fluidized bed performs better than the 2-phase fluidized bed. For conversions that would benefit from *in situ* extraction, therefore, a 3-phase fluidized bed would be the apparatus of choice.

The thesis finally reviews the current status of the newly developed 3-phase liquid-liquid-solid fluidized-bed bioreactor; it outlines additional research to be performed for a full understanding of its hydrodynamic behavior. Additional steps that have to be taken for practical implementation of the 3-phase fluidized bed as a new type of bioreactor are emphasized.

Samenvatting

Indien voor een aantal typen fermentaties een normale productiestrategie wordt toegepast, dat wil zeggen eerst een batchgewijze fermentatie en vervolgens de opwerking van het gewenste product, dan zal dit resulteren in een lage productiviteit voor het gehele proces. Voorbeelden van dergelijke fermentaties zijn: 1) substraat of product geremde reacties, 2) bioconversies die sterk beperkt worden door een ongunstige evenwichtsligging, en 3) fermentaties die gepaard gaan met een slechte oplosbaarheid van het substraat of het product.

Een alternatief voor de normale productiestrategie kan de directe integratie in één apparaat van bio-conversie en opwerking zijn. Hierbij is dan sprake van enerzijds een *in situ* gecontroleerde toevoer van substraat naar de fase waar de reactie plaatsvindt, of anderzijds de gecontroleerde afvoer van product vanuit de reactiefase. Voor een dergelijke integratie is een meerfase reactor noodzakelijk, waarbij een hulpfase gebruikt wordt als substraatreservoir of als productafvoer.

Een nieuw soort meerfasenreactor was ontwikkeld om de integratie van reactie en productafvoer of substraattoevoer te vergemakkelijken. Deze meerfasenreactor bestond uit een continue vloeistoffase, een disperse vloeistoffase en een disperse vaste fase. De reactor kan worden gezien als een 3-fase vloeistof-vloeistof-vast gefluïdiseerd bed bioreactor. De vaste fase bestaat uit biokatalytische gel deeltjes, die worden gefluïdiseerd door de continue vloeistoffase. Door dit gefluïdiseerde bed stijgen druppels organisch oplosmiddel op. Deze druppels treden op als de hulpfase; zij extraheren het product of zij dienen als substraatreservoir.

In dit proefschrift worden hydrodynamische aspecten van een dergelijk 3-fase gefluïdiseerd bed onderzocht. Daarnaast is een algemene ontwerpstrategie voor een 3-fasen gefluïdiseerd bed bioreactor ontwikkeld. In een 3-fase systeem zijn er twee 2-fasen systemen te onderscheiden: een vast-vloeistof gefluïdiseerd bed, dat bestaat uit de biokatalytische deeltjes in een continue vloeistoffase, en een vloeistof-vloeistof extractie kolom, die bestaat uit druppels van een organisch oplosmiddel in een continue vloeistoffase. Van deze twee afzonderlijke 2-fase systemen werden de hydrodynamische karakteristieken onderzocht (Hoofdstuk 2 en 3). Nadat een goede beschrijving en voorspelling van het hydrodynamische karakter van deze twee afzonderlijke 2-fase systemen was verkregen, werd er verondersteld dat de corresponderende modellen konden worden gecombineerd om het hydrodynamische karakter van het 3-fase gefluïdiseerd bed te kunnen beschrijven en

voorspellen. Deze veronderstelling was gedeeltelijk waar voor het voorspellen van de verschillende fasen hold-ups in het 3-fasen systeem (Hoofdstuk 4). De voorspelling voor de axiale dispersiecoëfficiënt van de continue vloeistoffase was goed, indien een model gebruikt werd dat deze dispersie coëfficiënt voorspelde in een 2-fase druppelkolom (Hoofdstuk 5).

Het fysische gedrag van gel deeltjes werd bestudeerd: een gel deeltje bezonk als enkel deeltje in stilstaand water, of was aanwezig in een gepakt bed of gefluïdiseerd bed (Hoofdstuk 2). Voor vijf verschillende soorten gel deeltjes (verschillend in diameter en dichtheid) werden drie verwante karakteristieken bestudeerd. Deze karakteristieken hadden te maken met de weerstandskracht tussen het deeltje en zijn omringende omgeving: de eindige valsnelheid van één enkel deeltje, de drukval over een gepakt bed van deze deeltjes, en de deeltjes fractie in een vloeistof-gefluïdiseerd bed. Hoewel deze karakteristieken dezelfde trends lieten zijn zoals deze worden waargenomen voor conventionele deeltjes (glas knikkers), bleek dat gerenommeerde modellen deze karakteristieken niet kwalitatief konden voorspellen. Er werd geconcludeerd dat de weerstandskracht tussen gel deeltje en vloeistof lager was vergelijken met conventionele deeltjes. Twee verschillende hypothesen werden voorgesteld. De eerste hypothese veronderstelde dat de vermindering in weerstand veroorzaakt wordt door de aanwezigheid van een kleine hoeveelheid opgeloste polymeer. De tweede hypothese ging uit van de aard van de gel deeltjes. Gel deeltjes bestaan voor meer dan 95% uit water, en in dat licht gezien kunnen gel deeltjes worden beschouwd als 'vaste' water druppels. Vandaar dat het oppervlak van het gel deeltje waterachtige eigenschappen kan vertonen, met als gevolg dat de weerstandskracht lager is. Een nieuw model dat de weerstandskracht van één gel deeltje in een gepakt of gefluïdiseerd bed correct beschrijft, werd gepresenteerd. Dit model werd gebruikt voor de voorspelling van de drukval over een gepakt bed en de deeltjes hold-up in een gefluïdiseerd bed.

Voor verschillende spargerontwerpen werd de druppel hold-up in vloeistof-vloeistof sproeikolom bestudeerd (Hoofdstuk 3). De continue waterfase en de disperse fase (dodecaan druppels) werden zowel in mee- als in tegenstroom door de kolom geleid. Hoewel de superficiële watersnelheid en dodecaansnelheid van dezelfde orde grootte waren, had de watersnelheid slechts een zeer geringe invloed op de dodecaan hold-up. Het aantal pijpjes had echter wel een grote invloed op de dodecaan hold-up: bij een gelijke superficiële dodecaan snelheid werd de hoogste

hold-up waargenomen voor die sparger met het laagste aantal pijpjes. De druppel hold-up kon goed worden beschreven met een model dat gebaseerd was op het snelheidsverschil tussen de continue fase en de dodecaan fase. Dit snelheidsverschil volgde een Richardson en Zaki-achtige vergelijking. Deze vergelijking maakt gebruik van een parameter n , waarvoor een nieuw model werd gepresenteerd. Tot een hold-up van 0.13 werd gevonden dat deze parameter constant was ($n=4$); voor hogere hold-ups nam deze parameter af. Dit model werd succesvol toegepast voor de voorspelling van de hold-up van een ander 2-fase systeem, dat verschilde in oppervlaktespanning (60 mM KCl/ dodecaan).

De integratie van een vast-vloeistof gefluidiseerd bed met een druppel sproeikolom heeft als resultaat een vloeistof-vloeistof-vast 3-fase gefluidiseerd bed. Er werd verondersteld dat de integratie van de modellen voor een vloeistof/vast 2-fasen systeem (een gefluidiseerd bed) met een vloeistof/vloeistof 2-fasen (een druppel sproeikolom), een goede beschrijving zou kunnen opleveren voor het 3-fasen systeem. De verschillende fasen hold-ups van dit 3-fasen systeem en het stromingsgedrag van de gel deeltjes werden bestudeerd (Hoofdstuk 4). Als vaste fase (dichtheid 1065 kg m^{-3}) werden κ -carrageen deeltjes gevuld met Celite™ gebruikt. Deze deeltjes werden gefluidiseerd door een continue waterfase (30 mM KCl, 'water'). De disperse organische fase (dodecaan druppels) steeg op door het gefluidiseerd bed van gel deeltjes. Voor verschillende water en dodecaansnelheden werden de stromingskarakteristieken van de gel deeltjes beschreven. Daarnaast werden de verschillende fasen hold-ups bestudeerd. Op basis van visuele waarneming van het gefluidiseerde bed konden vijf verschillende stromingsregimes worden onderscheiden: twee stabiele homogene stromingsregimes, twee stabiele heterogene stromingsregimes, en één instabiel stromingsregime, waarbij uitspoeling van de deeltjes uit het bed optrad. Verschillende literatuurmodellen voor bestaande 3-fasen systemen werden geprobeerd om de verschillende fase hold-ups te voorspellen. Hierbij gebruiken de meer fundamentele modellen parameters, die afgeleid zijn voor de afzonderlijke 2-fasen systemen. Helaas was de voorspelling met deze modellen slecht, indien de parameters, afgeleid voor de afzonderlijke 2-fasen systemen, werden gebruikt. De voorspelling met empirische literatuur modellen was ook niet goed. Dus een nieuw model voor een gefluidiseerd bed van gel deeltjes en dodecaan druppels moest worden afgeleid. Dit model was gebaseerd op stationaire krachtenbalansen. Daartoe werden modellen opgesteld voor de weerstandskrachten voor zowel een gel deeltje als een dodecaan druppel aanwezig in de 3-fasen

suspensie. Alle data voor de deeltjes hold-up en druppel hold-up werden goed beschreven voor een druppel hold-up kleiner dan 0.06. Voor de beschrijving van de gehele data set werd een empirisch model opgesteld.

Het onderzoek naar de mening van de continue fase van een 3-fase gefluïdiseerd bed is beschreven in hoofdstuk 5. Menging wordt gekenmerkt door een axiale dispersie coëfficiënt. Deze coëfficiënt werd bepaald op basis van metingen aan de verblijftijdspreiding, waarbij gebruik werd gemaakt van een KCl-merkstof. KCl kan de deeltjes in diffunderen, en daarom werden de beperkingen van het gebruik van deze merkstof ook bestudeerd. Er werd gevonden dat een puls met een gering volume betrouwbare resultaten gaf. Het bleek dat de axiale dispersiecoëfficiënt van de continue fase toenam met de superficiële dodecaansnelheid, terwijl de afhankelijkheid van deze dispersiecoëfficiënt met de superficiële watersnelheid een maximum liet zien. Deze resultaten weerspiegelen de toename van de continue fase dispersiecoëfficiënt met de energiedissipatie per massa-eenheid. Een model uit de literatuur voor het verband tussen dispersiecoëfficiënt en energiedissipatie werd, op kleine uitzonderingen na, met succes toegepast voor de voorspelling van de dispersiecoëfficiënt. Er werd geconcludeerd, dat de menging van de continue fase van een 3-fase gefluïdiseerd bed vergelijkbaar was met de menging van de continue fase van zowel een bellenzuil als de hoofdbuis van een 'liquid-impelled loop reactor'.

Een eenvoudig procesontwerp voor een 3-fase vloeistof-vloeistof-vast gefluïdiseerd bed bioreactor werd gemaakt (Hoofdstuk 6). Dit ontwerp maakte gebruik van de resultaten van de voorafgaande hoofdstukken, en weloverwogen schattingen voor stofoverdracht en stromingsgedrag van beide disperse fasen (de gel deeltjes en de dodecaan druppels). Een eenvoudige productgeremde reactiekinetiek werd verondersteld. Er werd aangetoond, dat bij gebruik van een 3-fase reactor een hogere conversiegraad wordt bereikt vergeleken met een 2-fase vloeistof-vast gefluïdiseerd bed bioreactor. Er werd geconcludeerd dat, uit praktisch oogpunt, voor de inzet van een 3-fase systeem er slechts geringe aanpassing aan een 2-fase vloeistof-vast gefluïdiseerd bed nodig zijn. Met behulp van het procesontwerp werd de invloed van verschillende modelparameters onderzocht, zoals 1) de verdelingscoëfficiënt van het product over de waterfase en de organische oplosmiddelfase, 2) de toxiciteit van het gevormde product, en 3) het debiet van het organische oplosmiddel. Operationele voorwaarden werden opgesteld, waarvoor de prestatie van het 3-fasen systeem beter is dan de prestatie van het 2-fasen systeem. Het bleek dat al voor

bescheiden waarden van de verdelingscoëfficiënt het 3-fasen gefluïdiseerd bed beter presteerde dan het 2-fasen gefluïdiseerd bed. Dus voor die bioconversies, waarvoor *in situ* extractie gunstig is, is de 3-fasen gefluïdiseerd bed bioreactor een zeer geschikt apparaat.

Dit proefschrift wordt afgesloten met een overzicht van de huidige status van deze nieuw-ontwikkelde 3-fasen gefluïdiseerd bed bioreactor. Er wordt aangeven welk extra onderzoek noodzakelijk is voor een volledig begrip van het hydrodynamische gedrag van deze bioreactor. Daarnaast wordt benadrukt welke stappen ondernomen moeten worden voor de praktische inzet van dit nieuwe type bioreactor.

Nawoord

Nog een paar woorden schrijven en dan is het boekje echt af. Terugdenkend aan de afgelopen jaren bekruipt mij een gevoel dat veel lijkt op een gevoel nadat ik gefinisht ben na een lange, zware hardlooppwedstrijd. Euforische gevoelens overheersen, maar gedachten gaan ook terug naar de onderweg veelvuldig voorkomende zware momenten, momenten van overgave en opgave.

Allereerst wil ik jou, Hans, bedanken voor het feit dat je vertrouwen in mij had en de mogelijkheid hebt gegeven om op jouw vakgroep mijn promotie te kunnen uitvoeren. Hoewel we de deur bij elkaar plat niet liepen, was je wel aanwezig als ik om raad en advies vroeg. Arjen, als co-promotor en directe begeleider zagen wij elkaar vaker; bedankt voor je inzet en goede adviezen. Rik, in het begin was je betrokken bij dit project en vervolgens was je lange tijd uit beeld. In de laatste fase was je echter weer prominent aanwezig. Bedankt voor je inzet en het helpen gereed komen van mijn proefschrift.

Gedurende de eerste 4 jaren, heb ik veel hulp gehad van vier studenten, Wouter, Jenke, Francine en Timo. Wouter, met veel plezier denk ik terug aan onze discussies. Hoewel van jouw werk en resultaten niets is terug te vinden in dit proefschrift, zijn een aantal gedachten toch teruggekomen in verschillende hoofdstukken. Jenke, jij had de pech om met een meetmethode te moeten werken, waarvan het signaal nauwelijks boven de ruis uitkwam. Jouw resultaten hebben echter wel bijgedragen aan het tot stand komen van hoofdstuk 5 over verblijftijdspreiding. Francine, veel heb je gemeten, geklust aan de opstelling en goede pogingen ondernomen om de hold-up van die deeltjes te voorspellen. Je zult je resultaten terugvinden in hoofdstuk 4. Timo, na eerst veel gestoeid te hebben met grafiekjes om de juiste instelling te achterhalen voor het doen van goede verblijftijdspreidingsmetingen, heb je daarna de ontwikkelde meetmethode toegepast om het menggedrag te meten. Jouw resultaten zul je terugvinden in hoofdstuk 5.

Promoveren is vaak een eenzame zaak. Echter er zijn altijd wel mensen, waarmee je met gedachten kan wisselen of die je simpelweg aansporen. (Ex)-vakgroepgenoten, als toeschouwers langs de kant was jullie aandacht en aansporingen zeer welkom. Promoveren naast een volledige aanstelling bleek haast onmogelijk. ECN, Hans, Johan en Huibert, bedankt dat jullie mij de ruimte hebben gegeven om het proefschrift af te kunnen ronden.

Op deze plaats wil ik nog een groep mensen, van origine hardloopmaatjes, maar tegenwoordig goede vrienden, bedanken voor hun interesse in mijn promotieperikelen. Tijdens mijn studie in Delft begonnen als hardloophvrienden, nu een vriendenclub die elkaar geregeld ziet. In het begin waren er jullie oprechte vragen, hoe staat het met het *boekje?*, en mijn standaardantwoord was: het gaat goed, maar de voortgangssnelheid is niet zo hoog (type duuratleet). De laatste tijd verstomde jullie vragen, wellicht in de overtuiging dat de voortgangssnelheid tot nul was gereduceerd. In elk geval bedankt voor de oprechte interesse. Het boekje is nu af, en is er weer volop tijd voor trainen en mooie hardlooppuitjes.

Familie, pa, Stefan, vaak hebben jullie je afgevraagd of dat boekje er nog zou komen en misschien nog wel belangrijker, komt dat feest er nog? Het boekje ligt er nu en dat feestje komt er ook. Bedankt voor vooral de mentale steun in de afgelopen jaren.

Als laatste bedank ik jou, Imke, vooral voor je geduld en begrip als ik weer in het weekeinde achter de PC kroop. Toen wij elkaar leerden kennen had dit boekje immers al af moeten zijn. De afgelopen periode is veel van onze spaarzame tijd opgegaan aan werken achter jouw PC-tje. Het is nu af en dus veel tijd over om samen leuke dingen te gaan doen.

Erik

Curriculum vitae

Erik van Zessen werd geboren op 1 december 1969 in Zoetermeer. Na het behalen van het Gymnasium diploma aan het Stedelijk Gymnasium te Schiedam in 1988 werd in datzelfde jaar begonnen met zijn studie Chemische Technologie aan de Technische Universiteit Delft. In november 1994 studeerde hij af in de richting bioprocestechnologie bij het Kluverlaboratorium.

Vervolgens begon hij in februari 1995 als AIO bij de vakgroep proceskunde aan de Wageningen Universiteit. Het onderzoek dat hij hier heeft uitgevoerd, heeft geresulteerd in dit proefschrift.

Vanaf oktober 2000 tot oktober 2003, is hij werkzaam geweest bij het Energie onderzoek centrum Nederland (ECN).

